Fabrication of Ferrite Thin Film using Low Pressure Metalorganic Chemical Vapor Deposition

BY

YI YANG
B.S., Nanjing University, 2005

THESIS

Submitted as partial fulfillment of the requirements
for the degree of Doctor of Philosophy in Chemical Engineering
in the Graduate College of the
University of Illinois at Chicago, 2014

Chicago, Illinois

Defense Committee:

Christos G. Takoudis, Chair and Advisor

Sohail Murad

Alan Feinerman, Electrical and Computer Engineering

Gregory Jursich, Bioengineering and Chemistry

Kebin Low, Research Resources Center

DEDICATION

I dedicate this thesis to my husband, my daughters and my parents who supported me with their deep love all these years.

ACKNOWLEDGEMENTS

First and foremost, I am heartily thankful to my advisor and dissertation chair, Prof. Christos G. Takoudis, whose continuous encouragement, patient guidance and generous support from the initial to the final level enabled me to develop a profound understanding of this research study. I would also like to thank my committee members, Dr. Sohail Murad, Dr. Gregory Jursich, Dr. Alan Feinerman and Dr. Kebin Low for taking time out of their busy schedules to serve as my defense committee. Thank National Science Foundation (NIRT-NSF Grant) for funding this research work.

I owe my deepest gratitude to Dr. Manish Singh who trained and instructed me from the beginning of my PhD research, especially for the training of operating the deposition system and characterizations of thin films. Some part of the research work would not have been possible without his insightful guidance and ideas. I also need to sincerely thank Dr. Gregory Jursich for TGA training and analysis of iron precursors. I am grateful to Dr. Ke-Bin Low at Research Resource Center (UIC east campus) for his training and several interpretations with XPS analysis. I greatly appreciate the help from Dr. Qian Tao and Dr. Mauro Sardela who analyzed my samples with GAXRD, and Dr. Doug Jeffers for RBS training at Frederick Seitz Materials Research Laboratory Central Facilities, University of Illinois, Urbana. Thanks a lot to Dr. Alan Feinerman for helping solve the Ellipsometry problems. Also, thanks a lot to Dr. Gopalan Srinivasan who helped provide the substrates and carried out the magnetization measurement.

Especially thanks to Lukasz Zientara who impressed us by his great ideas and technical support on several electrical and mechanical installation which helped construct

and upgrade the deposition system to a more outstanding design. Also, I owe my thanks to Eric Schmidt (Engineering Machine Shop) for his technical expertise with design and work of some metal parts for the experiments.

In addition, a thank you to IMSA student Max Mckittrick and REU student Mark Kimbell who assisted me in fabrication of ferrite materials and provided valuable feedback on my research study.

Finally, I would like to express my wholeheartedly gratitude to all the AMRel members who have been greatly supportive in many aspect, especially for Lin Jiang who offered me a lot of good suggestions and Runshen Xu who helped me a lot at the end of my PhD study. Also, the deepest thanks to my parents and my husband, who always love me and back me when I need them.

YY

CONTRIBUTION OF AUTHORS

Chapter 1 is an introduction to the background information of the PhD research topic I worked on. Chapter 2 is a literature review that covers recent research progress in this area, the common techniques scientists used and the topic I was focusing on. In this chapter, some portions have been published previously in a paper in Coordination Chemistry Reviews in which I contributed as the second author. In Chapter 4, the figure 22, 25, 26 were done by Dr. Manish Singh in our published paper in Journal of The Electrochemical Society. Figure 31, was done by Dr. Manish Singh, and figure 33, 34, 35, were done by Dr. Tatarenko, Dr. Srinivasan, Dr. Kharel and Dr. Lawes in our published paper in Electrochemical and Solid-State Letters. I am also the second author of this paper and contributed to the samples fabrications and the characterizations of their chemical compositions. The other portions of the work were based on my own unpublished experiments and results. I anticipate that the work in Chaper 4.4 will be published soon and I am the first author in this manuscript.

TABLE OF CONTENTS

TABLE OF CONTENTS (continued)

LIST OF TABLES

TABLE **PAGE**

LIST OF FIGURES

LIST OF FIGURES (continued)

FIGURE **PAGE**

LIST OF FIGURES (continued)

LIST OF FIGURES (continued)

LIST OF ABBREVIATIONS

AACVD	aerosol assisted chemical vapor deposition
ALD	atomic layer deposition
APCVD	atmosphere chemical vapor deposition
BE	binding energy
BFO	$BiFeO_3$
BLT	$Bi_{4-x}La_xTi_3O_{12}$
BNT	$(Bi,Nd)_4Ti_3O_{12}$
BSCCO	Bi-Sr-Ca-Cu-O
BSTO	$Ba_{0.7}Sr_{0.3}TiO_3$
CSD	chemical solution deposition
CVD	chemical vapor deposition
DLICVD	direct liquid injection chemical vapor deposition
EDX	energy dispersive X-ray spectroscopy
GAXRD	glancing-angle X-ray diffraction
HWCVD	hot wire chemical vapor deposition
ICDD	international center for diffraction data
KE	kinetic energy
LPCVD	low pressure chemical vapor deposition
LSMO	$(La, Sr)MnO_3$
ME	magnetoelectric
MOCVD	metalorganic chemical vapor deposition
NFO	$NiFe_2O_4$
PDF	powder diffraction files
PECVD	plasma enhanced chemical vapor deposition

LIST OF ABBREVIATIONS (continued)

PLD	pulsed laser deposition
PMN-PT	$(1-x)[Pb(Mg_{1/3}Nb_{2/3})O_3]-x[PbTiO_3]$
PZT	$Pb(Zr_xTi_{1-x})O_3$
RBS	Rutherford backscattering spectrometry
RPCVD	rapid thermal chemical vapor deposition
SBT	$SrBi_2Ta_2O_9$
SEM	scanning electron microscopy
TEM	transmission electron microscopy
TGA	thermogravimetric analysis
UHVCVD	ultrahigh vacuum chemical vapor deposition
XPS	X-ray photoelectron spectroscopy
XRD	X-ray diffraction

SUMMARY

This thesis is based on the research work on the multiferroic material fabrications using low pressure metalorganic chemical vapor deposition (MOCVD). Multiferroic material refers to the ones who have two or more ferroic properties, like ferroelectricity, ferromagnetism, ferroelasticity and ferrotoroidicity. Extensive research findings focused on pure nano scale thin films and composites those were related to presenting both ferroelectricity and ferromagnetism coupling within the material.

$BiFeO_3$ (BFO) was known to be the only single phase multiferroic material which exhibited magnetoelectric (ME) coupling effect at room temperature. This coupling effect provided an extra degree of freedom for designs of whole new devices and applications never thought to be possible before. Recently, large ME effect was found in its thin epitaxial-strained films. However, very few papers reported the CVD techniques for depositing BFO thin films so far. Most of these reports used direct liquid injection method to deliver the organometallic reactants during the CVD process (ie. DLICVD). Here, we introduced a novel liquid iron precursor, n-butylferrocene, delivered into the reactor by heating the precursor canisters at certain temperatures for growing BFO thin films. Other crucial MOCVD conditions (reactor's pressure, reactor's temperature, substrates…) were also discussed and optimized. Characterizations for the film composition, crystallinity, ferroelectricity, ferromagnetism and the magneto-dielectric coupling effect were analyzed in detail. The results confirmed that BFO film had multiferroic properties and could be potentially used in future tunable high-frequency devices.

Although single-phase BFO exhibited ME effect, this suffered from problems such as current leakages, weak ME coupling and low ordering temperatures. Doping or ion substitution was a limited way to enhance the ME property since the compounds had definite compositions. Therefore, heterostructures such as bilayered/multilayered thin films, nanoparticles/nanopillars embedded in different materials and nanowires became more promising for the future on-chip integration applications because the coupling in such structures was many orders of magnitude stronger. Another research scientists interested in was the heterostructural magnetostrictive NiFe2O4 (NFO) with piezoelectric materials. NFO was a promising magnetic phase for ME heterostructures due to its low anisotropy, high permeability with high resistivity, low eddy current losses and smaller coercive field. In this study, the nickel ferrite thin films had been deposited using computer controlled MOCVD setup in both co-deposition mode and cyclic-deposition mode. Conditions for CVD process were discussed and optimized for growing NFO thin film. The thin films showed NFO composition, uniformity in chemical states and thickness, trevorite crystalline form, free from carbon contamination and similar magnetic property as other literature reported.

1. INTRODUCTION

In recent years, multiferroic materials have been interested and focused by scientists and industry due to its promising applications for the electronic devices in the future. According to the definition of multiferroics, these materials refer to the ones which have two or more ferroic properties like ferroelectricity, ferromagnetism, ferroelasticity and ferrotoroidicity. Of particular interest are the magnetoelectric multiferroics which have the coupling effect caused by (anti) ferroelectric and (anti) ferromagnetic domains existing in the same phase. [1] Such materials are defined in the overlapped area between multiferroic and magnetoelectric materials. [2] Because of the advantage of this coupling effect, electronic and magnetic functionalities can be combined together in a single device component to make further microelectronic device miniaturization. This coupling provides an extra degree of freedom for designs of whole new devices and applications. Potential applications include high speed low power electrically controlled magnetic memory elements, electrically tunable microwave devices and highly sensitive magneto sensors. [3] This coupling effect between electric and magnetic fields was speculated in 1894. [4] It took few decades before magnetoelectric (ME) coupling was first predicted and later observed in Cr_2O_3. [5], [6] Interest in ferroelectric ferromagnets began mainly with the innovative research studies of Smolensky in 1958 on the perovskite family materials. Recent developments in the field of materials research have led to renewed interest in multiferroic materials. From the improvements in first-principles theoretical calculations which led to identification of new mechanisms, we had a better understanding of the underlying multiferroic phenomena. [7], [8] Besides, the progress

of thin film deposition techniques provided new approaches to fabricate novel multiferroics in the form of horizontal multilayer or vertical superstructures. [9]

In this thesis, ferrite thin films for the multiferroic material study were fabricated by the metalorganic chemical vapor deposition (MOCVD) due to its conformal coverage with high throughput, production of high film quality, viability in the future industrial production. The experimental parameters related to process optimization and film characterization results will be discussed in the later paragraphs.

1.1.Nano Scale Multiferroic Material

Just like the Moore's Law presented, the miniaturization of devices for computer hardware, communication technology and sensor technology made a dramatic progress in the past. Limitations can be broken by introducing novel materials for building various electronics. In integrated circuits and related electronic devices, thin films, multilayered thin films, super lattice, nanoarrays or other nanostructures are required. The properties of nano scale materials are very different from their bulk form. Some properties may be enhanced remarkably by reducing the materials' dimensions to the nano scale.

Some single-phase thin films exhibit ME effect, for example, the pure $BiFeO_3$, however, it may also suffer from problems such as current leakages, weak ME coupling and low ordering temperatures.[10-12] Doping or ion substitution can be an approach to enhance the ME property. Heterostructures such as bilayered/multilayered thin films, nanopillars and nanowires are more promising for the future on-chip integration applications since the coupling in such structures is stronger based on calculation and experimental results.[13] One of the most promising

approaches is to synthesize composites of magnetostrictive and piezoelectric materials. In such composites the mechanical strain between the two materials is employed to induce the magnetoelectric effect. However, the ME effect in this case may be non-linear unlike the behavior in the case of single-phase materials. Also, the interfacial mechanical strain should be transferred between the components with minimal losses.

1.2.$BiFeO_3$

Among the several known single-phase magnetoelectrics, $BiFeO_3$ (BFO) was known to be the only material that exhibited ferro electromagnetism at room temperature (T_C=810 °C, T_N=380 °C). BFO had a degradation of ferroelectric behavior and a low polarization in its bulk polycrystalline form.[14] In contrast, thin film samples were demonstrated to exhibit a large polarization that was an order of magnitude higher than its single crystal or polycrystalline counterparts.[15] However, there was a small window in which impurity-free single phase $BiFeO_3$ thin films can be grown. It was observed that insufficient oxygen partial pressure during deposition processing could cause valence fluctuations of Fe ions leading to oxygen vacancies which contribute to the result of high leakage currents. [16] The electromagnetism was weak in the BFO film alone, so for recent two years scientists start to work on the doped BFO films or complex nanostructures of other materials.

1.3.$NiFe_2O_4$

This inverse spinel structural ferrite thin film caught scientists' attentions for its applications in high-frequency devices. Compared with metal films and garnet-structure materials, it provided high resistivity and high saturation

magnetization (50 emu/g in bulk form).[17]

For the ME heterostructure, $NiFe_2O_4$ (NFO) is a promising magnetostrictive phase due to its low anisotropy, high permeability with high resistivity, low eddy current losses and smaller coercive field, for exhibiting better ME coupling effect than single phase ME material.[18-21]

2. LITERATURE REVIEW

2.1. Single Phase Multiferroic Materials

The major breakthrough for the understanding of the magnetoelectric effect happened when Landau and Lifshitz demonstrated the pioneering work wherein it meant that the ME response needed a time-asymmetric media [22]. The experiments on Cr_2O_3 that was predicted to show the violation of time-reversal symmetry, established another major step forward in later research [6, 23], including the identification of several more ME compounds[24]. However, the ME coupling in single-phase materials was found to be weak for device applications, and could only be observed at low temperatures due to their low Néel (T_N) and Curie (T_C) temperatures. Also, the rarity of the single-phase magnetoelectric multiferroic materials had been elaborated in recent theoretical investigations [7]. The conventional mechanisms shows that driven ferroelectricity required empty transition metal orbitals in the material, while driven ferromagnetism in the material required partially filled transition metal orbitals. Both of them were mutually exclusive. However, there was an alternate mechanism for driving either of the ferroic properties leading to find magnetoelectric behavior in a single phase material [8, 25, 26]. A number of single-phase multiferroics which has been discovered can be classified into several families—(i) perovskites such as $BiMnO_3$, $BiFeO_3$, (ii) hexagonal rare earth manganites ($RMnO_3$, R=Y, Sc, In, Ho, Er, Dy, Tm, Yb, Lu), (iii) cuprates [27], (iv) other compounds such as 3d metal boracites family, $BaMnF_4$ [28], $Ni_3B_7O_{13}I$ [24], and (v) rare earth molybdates like $Tb_2(MoO_4)_3$ and $TbGd(MoO_4)_3$. Among these, $BiFeO_3$ deserved a special mention as it was the only known single-phase magnetoelectric material that had electric and magnetic ordering

temperatures above room temperature (T_C~1100 K and T_N~650 K) [29].

2.1.1. Perovskites and Hexagonal Rare Earth Manganites

The perovskite structure has the chemical formula ABO_3. It is stabilized by the 6 coordination of the B-cation in the corner, 12 of the A-cation in the middle of the cube, and O anions in the center of the face edge. The different atomic radius of A and B ions can alter the cubes to distorted ones. Rare earth manganites (R=Y, Ho, Er, Tm, Yb, Lu, Sc) have hexagonal crystallographic structures, while other rare earth elements with larger ionic radius have orthorhombic structures. The hexagonal $RMnO_3$ are both ferroelectric under the temperature T_{FE} 800-1000 K and antiferromagnetic under the T_N 70-100 K. Among these manganites, $YMnO_3$ was the most studied one because it was a new candidate for use in nonvolatile memory devices. A.A. Bosak[30] reported using low-pressure chemical vapor deposition method to grow $RMnO_3$ (R=Dy, Ho, Tm, Lu, Y) thin films. All the films had perovskite phase.

$YMnO_3$

Choi et al used MOCVD to deposit $YMnO_3$ films on Y_2O_3 buffered p-type Si(100) substrates at 500 ºC and 3 Torr for FeRAM applications [31]. Organometallics $Y(thd)_3$ and methylcyclopentadienylmanganese tricarbonyl ($(CH_3C_5H_4)Mn(CO)_3$) kept in individual bubblers were used as sources for Y and Mn, respectively. The $Y(thd)_3$ and $(CH_3C_5H_4)Mn(CO)_3$ bubblers were kept at 162 ºC and 20 ºC, respectively. The deposited films annealed for 60 min in 100 mTorr vacuum at 750 ºC were observed to have superior properties (crystallinity, ferroelectricity and low leakage) compared to

films annealed in oxygen. Magnetic behavior was not reported for these films.

Bosak et al deposited single-phase epitaxial $YMnO_3$ films on $LaAlO_3$ (001) and $SrTiO_3$ (001) substrates using $Y(thd)_3$ and $Mn(thd)_3$ [30]. The MOCVD used a single-source band-flash evaporation method was used for precursor delivery [32]. The films were grown at 840 ºC and 1300 Pa (9.75 Torr) with oxygen partial pressure of 435 Pa (3.26 Torr). Epitaxial stabilization due to low lattice mismatch substrates enabled the growth of the films in the perovskite structure instead of the stable hexagonal form. Interestingly, it was the hexagonal phase that exhibited multiferroicity.

More recently, Kim et al used organometallics $Y(thd)_3$ and $Mn(thd)_3$ in a liquid precursor injection MOCVD reactor to deposit $YMnO_3$ films on $Pt/Ti/SiO_2/Si$ substrates at 10 Torr and 450-600 ºC [33]. A flash evaporator maintained below 300 ºC was used to vaporize the precursor solution (0.03 M $Y(thd)_3$ & $Mn(thd)_3$ in tetrahydrofuran). Films annealed at 830 ºC in inert ambient were observed to crystallize in hexagonal $YMnO_3$ phase. Ferroelectric loop measurements revealed a remnant polarization of 2 $\mu C/cm^2$ and coercive field of 10 kV/cm. Magnetization behavior was not reported for these films.

Dubourdieu et al synthesized thin films of hexagonal $YMnO_3$ by liquid delivery MOCVD using $Y(thd)_3$ and $Mn(thd)_3$ organometallic precursors [34]. The precursors mixed in monoglyme solvent were injected into an evaporator held at 250 ºC. Films were grown on (111) $ZrO_2(Y_2O_3)$ and $Pt(111)/TiO_2/SiO_2/Si$ substrates at 800-900 ºC and total pressure of 660 Pa (5 Torr) with oxygen partial pressure of 0.33 kPa (2.5

Torr). In-situ annealing of the samples in 100 kPa (750 Torr) O_2 was done after deposition. Though, mainly, *c*-axis oriented films were obtained on both the substrates, films deposited on platinized silicon had larger amount of secondary orientations and also had some perovskite phase present. From the neutron diffraction experiments at different temperatures, T_N was estimated to be 66 K [35].

$HoMnO_3$

Bosak et al deposited single-phase epitaxial $HoMnO_3$ films on $LaAlO_3$ (001) and $SrTiO_3$ (001) substrates using $Ho(thd)_3$ and $Mn(thd)_3$ [30]. The MOCVD used a single-source band-flash evaporation method was used for precursor delivery [32]. The films were grown at 840 ºC and 1300 Pa (9.75 Torr) with oxygen partial pressure of 435 Pa (3.26 Torr). Epitaxial stabilization due to low lattice mismatch substrates enabled the growth of the films in the perovskite structure instead of the stable hexagonal form.

Dubourdieu et al synthesized thin films of hexagonal $HoMnO_3$ by liquid delivery MOCVD using $Ho(thd)_3$ and $Mn(thd)_3$ organometallic precursors [34]. The precursors mixed in monoglyme solvent were injected into an evaporator held at 250 ºC. Films were grown on (111) $ZrO_2(Y_2O_3)$ and Pt(111)/TiO_2/SiO_2/Si substrates at 800-900 ºC and total pressure of 660 Pa (5 Torr) with oxygen partial pressure of 0.33 kPa (2.5 Torr). In-situ annealing of the samples in 100 kPa (750 Torr) O_2 was done after deposition. The films had *c*-axis oriented perpendicular to the substrate. For films thicker than 100 nm secondary orientations were also observed. In the neutron diffraction analysis, T_N was not clearly observed though a magnetic transition at 50 K

corresponding to reorientation temperature on bulk $HoMnO_3$ was observed [35].

$DyMnO_3$

Bosak et al deposited single-phase epitaxial $DyMnO_3$ films on $LaAlO_3$ (001) and $SrTiO_3$ (001) substrates using $Dy(thd)_3$ and $Mn(thd)_3$ [30]. The MOCVD used a single-source band-flash evaporation method was used for precursor delivery [32]. The films were grown at 840 ºC and 1300 Pa (9.75 Torr) with oxygen partial pressure of 435 Pa (3.26 Torr). The films had perovskite structure instead of desired hexagonal structure. In a later report, Bosak et al used (111) $ZrO_2(Y_2O_3)$ substrate to induce epitaxial stabilization to obtain the hexagonal structure [30]. The films were synthesized by liquid injection MOCVD at 900 ºC and 670 Pa using the same precursors as before.

Dubourdieu et al synthesized thin films of hexagonal $DyMnO_3$ by liquid delivery MOCVD using $Dy(thd)_3$ and $Mn(thd)_3$ organometallic precursors [34]. The precursors mixed in monoglyme solvent were injected into an evaporator held at 250 ºC. Films were grown on (111) $ZrO_2(Y_2O_3)$ and Pt(111)/TiO_2/SiO_2/Si substrates at 800-900 ºC and total pressure of 660 Pa (5 Torr) with oxygen partial pressure of 0.33 kPa (2.5 Torr). In-situ annealing of the samples in 100 kPa (750 Torr) O_2 was done after deposition. Though the stable phase for $DyMnO_3$ is the perovskite structure, the metastable hexagonal phase was obtained because of epitaxial stabilization.

$TbMnO_3$

Dubourdieu et al synthesized thin films of hexagonal $TbMnO_3$ by liquid delivery MOCVD using $Tb(thd)_3$ annd $Mn(thd)_3$ organometallic precursors [34]. The precursors

mixed in monoglyme solvent were injected into an evaporator held at 250 ºC. Films were grown on (111) $ZrO_2(Y_2O_3)$ substrates at 800-900 ºC and total pressure of 660 Pa (5 Torr) with oxygen partial pressure of 0.33 kPa (2.5 Torr). In-situ annealing of the samples in 100 kPa (750 Torr) O_2 was done after deposition. Epitaxial stabilization enabled the deposition of the hexagonal phase of $TbMnO_3$.

$ErMnO_3$

Thin $ErMnO_3$ films (450-500 nm) were deposited on (111) $ZrO_2(Y_2O_3)$ substrates by liquid injection MOCVD using $Er(thd)_3$ and $Mn(thd)_3$ as precursors. $T_N \sim 68$ K was estimated from the neutron diffraction experiments for 500 nm thick films [35].

$Pr_{(1-x)}Ca_xMnO_3$

Nakamura et al used a liquid injection MOCVD to deposit 300 nm $Pr_{(1-x)}Ca_xMnO_3$ films on $Pt/SiO_2/Si$ substrates at 480 ºC and 5 Torr [36]. $Pr(thd)_3$, $Ca(thd)_3$ and $Mn(thd)_3$ dissolved in tetrahydrofuran were used as the precursors. Each dissolved precursor was carried by N_2 into a vaporizer and then the reactor where O_2 was mixed in. After deposition the films were annealed at 600 ºC for 5 h. The films showed reversible resistance switching upon application of electrical pulses [36].

2.1.2. $BiFeO_3$ Thin Films

CVD for BFO films-For the DLICVD method, in 2005, Y. Tasaki et al. [37] reported this method for preparing the BFO thin films. A vaporizer and hot-wall type quartz tube reactor were used in the system. Different precursors were evaluated. Tasaki et al compared different precursors for liquid delivery MOCVD of $BiFeO_3$ films [38]. Bismuth aryls, $Bi(o\text{-}Tol)_3$ and Bi(p-Tol)3, were used as bismuth sources,

while iron β-diketonates $Fe(TMOD)_3$, ($Fe(DPM)_3$, $Fe(IBPM)_3$, $Fe(DIBM)_3$, iron cyclopentadienyls ($Fe(Cp)_2$ and $Fe(MeCp)_2$) were used as the iron sources. Toluene was used to dissolved orgaometallic precursors in order to prepare the solution for liquid delivery into the MOCVD apparatus. $Bi(p\text{-}Tol)_3$ was reported to be a more suitable bismuth precursor since the bismuth element ratio within in the films was found to be more controllable between these two compounds. For comparative studies on the iron precursors, iron element ratio within the films was found to be rather low in case of cyclopentadienyls compared to β-diketonates. For deposition of stoichiometric $BiFeO_3$ films, a mixture of $Bi(p\text{-}Tol)_3$ and $Fe(DIBM)_3$ was chosen as precursors. X-ray diffraction (XRD) analyses showed that the films deposited at 500 ºC and 525 ºC were $BiFeO_3$ while films deposited 550 ºC had excessive Bi_2O_3 phase present. The films deposited at 525 ºC were reported to be ferroelectric thought the observed remnant polarization (less than 2 $\mu C/cm^2$) was very low.

Ueno et al deposited epitaxial $BiFeO_3$ films using $Bi((CH_3)_2(2\text{-}(CH_3)_2NCH_2C_6H_4))$ and $Fe(C_2H_5C_5H_4)_2$ as precursors in a bubbler-type delivery MOCVD setup [39]. The films were deposited on $SrRuO_3/SrTiO_3$ substrates at 620 ºC. For 480 nm thick $BiFeO_3$ films, polarization hysteresis loops with remnant polarization 51 $\mu C/cm^2$ and coercive field 166 kV/cm were obtained at 80 K.

Yang et al used liquid delivery MOCVD to grow epitaxial $BiFeO_3$ films on $SrRuO_3/SrTiO_3$ and $SrRuO_3/SrTiO_3/Si$ substrates at 650 ºC [40]. Tetrahydrofuran was used to dissolve to make the $Fe(thd)_3$ and $Bi(thd)_3$ organometallic scource. The Bi/(Bi+Fe) ratio of 0.7 in the precursor solution was found to be optimal to deposit

stoichiometric $BiFeO_3$ films. Polarization and coercive field values were observed to be smaller for films on $SrRuO_3/SrTiO_3/Si$ compared to those films on $SrRuO_3/SrTiO_3$.

Thery et al compared two different bismuth precursors—$Bi(thd)_3$ and $Bi(mmp)_3$—for depositing $BiFeO_3$ films while $Fe(thd)_3$ was fixed as the Fe source [34]. Various commonly used solvents were compared for preparing the precursor solution. $Bi(mmp)_3$ was reported to be more suitable Bi source. The $BiFeO_3$ films were deposited at 550 ºC and 666 Pa (5 Torr) on $SrTiO_3$ substrates in a pulsed liquid delivery MOCVD. XRD and TEM analyses did not reveal any secondary phases. However, XPS indicated presence of Fe in mixed valence states which apparently led to the magnetization value (70 emu cm^{-3}) which is much higher than the bulk value for $BiFeO_3$.

Similarly, Shintaro Yasui et al. deposited $BiFeO_3$-$BiCoO_3$ solid solution films by the mixture gases of $Bi[(CH_3)_2\text{-}2\text{-}(CH_3)_2NCH_2C_6H_4]$, $Fe(C_2H_5C_5H_4)_2$ and $Co(CH_3C_5H_4)_2$ and oxygen as the single source materials.

Kartavtseva et al reported growth of epitaxial $BiFeO_3$ films on (001) $SrTiO_3$ using single source MOCVD[41]. $Bi(Ph)_3$ and $Fe(thd)_3$ were used as the precursors for growing the films in the temperature range 500-800 ºC and a total pressure 1.2-1.8 kPa. The saturation magnetization for the film was measured to be 9 kA/m (9 emu cm^{-3}).

Modification of BFO-Many papers reported that adding dopants in the BFO films could reduce the leakage currents or enhance ferroelectricity and ferromagnetizm. Many kinds of dopants were investigated like Y_2O_3 and CaO [42], Mn [43], Ti [44], Zn [45],

La [46], $LaMnO_3$ [47], Co [48], Nb [49], Tb [50] and Gd [51]. The composites of $BiFeO_3$ were also prepared and characterized to improve its properties. There were few examples about the novel nanocomposites. Epitaxial bi-layer composite γ-Fe_2O_3-$BiFeO_3$/$Bi_{3.25}La_{0.75}Ti_3O_{12}$ (BFO-FO/BLT) showed improved ME properties with low leakage current and good ferroelectric fatigue endurance [52] in which the BLT layer acting as a barrier for the migration of space charges towards the electrode and the epitaxial intergrowth of the maghemite phase with the BFO matrix was promoted. $x$$CuFe_2O_4$-(1-$x$)$BiFeO_3$ composite reported by M. Kumar et al. exhibited strong ME effect because of low coercivity and high magnetization. [53] They also reported that $x$$Ni_{0.75}Co_{0.25}Fe_2O_4$-(1-$x$)$BiFeO_3$ nanocomposites had large ME output due to its low coercivity, high magnetization and small grain size of constituent phases. [54] In $BiFeO_3$/$La_{2/3}Ca_{1/3}MnO_3$ composites, electrical polarization in BFO films can be enhanced greatly by magnetic field at room temperature as the magnetic and ferroelectric domains were strongly coupled. [55] Other nanocomposites, like $MnFe_2O_4$/Mn-doped $BiFeO_3$ [43], (1-x)$Bi_2Fe_4O_9$-xBaO [56], $BiFeO_3$-$CoFe_2O_4$ were also synthesized using different techniques and showed ME effects.

2.2. Heterostructural multiferroic materials

Although some single-phase magnetoelectric materials were discovered and fabricated, they were not very promising for future applications. So far, none of them could exhibit large ME effect at room temperature. Apart from being rare and having very low Néel and Curie temperatures, the single-phase multiferroic compounds suffered from another major limitation. Since most of these compounds had definite

compositions, the possibility of optimization of magnetoelectric property through ion substitution or doping was very limited [1]. Song et al recently reported room temperature ferromagnetism and ferroelectricity in Co-doped $LiNbO_3$ films fabricated using laser beam epitaxy [57]. In the case of $BiFeO_3$, the use of dopants was mainly driven by the idea that it would improve the ferroelectric properties by reducing the current leakage which was a major problem with $BiFeO_3$ films. Several reports indicated that the dopants could affect the electrical properties of $BiFeO_3$ films via a structural modification such as reduced anisotropy, or by modifying the defect chemistry which controlled the oxygen vacancies [58-61].

Therefore, people were developing to form two-phase composites magnetoelectric materials which combined ferroelectric phase and ferromagnetic phase together in the bulk form or different nanostructures. In this way, the ME coupling effect happened between the interfaces of the two phases. When an outside electric field was applied, this field would induce the strain in the ferroelectrics and then the strain would be passed on to the other phase-the ferromagnetics where it formed the magnetization. Therefore, composites with large interface area would enhance the ME coupling effect. The common patterns for fabricating heterostructures were shown in the figure 1.

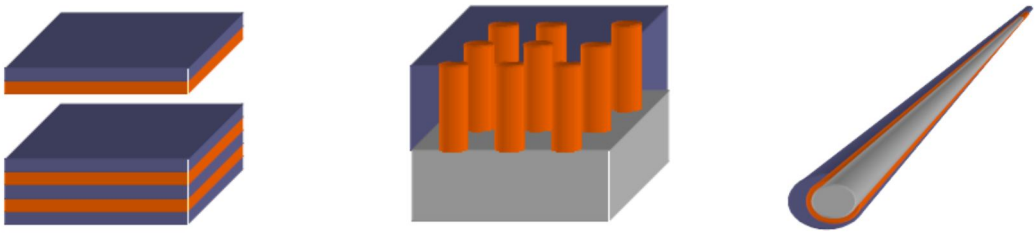

Figure 1. Different heterostructures of magnetostrictive-piezoelectric nanocomposites

2.2.1. Magnetostrictive-Piezoelectric Composites

To explore new degrees of freedom for achieving stronger magnetoelectric coupling, the research was directed towards designing magnetoelectric materials. Fortunately, the timing seemed to be good because recent progress in thin film deposition techniques had provided new routes to deposit novel multiferroics in the form of horizontal multilayer, vertical superstructures or other complex structures in a precise controlled manner [9, 34]. One of the most promising approaches was to synthesize composites of magnetostrictive and piezoelectric materials [1]. The realization of the ME effect in this case could be represented as follows

$$ME\ effect = \frac{magnetic}{mechanical} \times \frac{mechanical}{electrical}$$

The concept was demonstrated in the pioneering works of van der Boomgaard and van Suchtelen on $CoFe_2O_4$–$BaTiO_3$ and $Ni(Co,Mn)Fe_2O_4$–$BaTiO_3$ composites [62, 63]. In such composites the mechanical strain between the two materials was employed to induce the magnetoelectric effect. The ME effects in composites were observed to be about hundred times greater than that in single phase magnetoelectrics. However, the ME effect in this case could be non-linear unlike in the case of single-phase

materials. Also, the interfacial mechanical strain should be transferred between the components with minimal losses. The related theory and experimental works had been reviewed in Refs [1, 64, 65]. Based on this idea, one approach to obtain large magnetoelectric effects was to deposit thin films of a ferromagnet on a piezoelectric substrate such as lead magnesium niobate-lead titanate or $BaTiO_3$. If the strain transfer between the ferromagnet and the substrate was strong, an electrically applied strain in the substrate could induce strain in the ferromagnet film leading to the observation of magnetization changes. This indirect magnetoelectric effect could be due to stress-induced anisotropy or stress-induced phase changes. However, the substrate should have a large piezoelectric effect and at the same time should allow epitaxial growth of magnetic films for quantitative analysis [66]. Similarly, in the case of magnetic materials which have charge carrier density dependent magnetic properties, polarization of an adjacent ferroelectric film can control the magnetization near the interface.

2.2.2. $NiFe_2O_4$ Thin Films on Piezoelectric Substrates

As described in the earlier paragraphs, $NiFe_2O_4$ was a promising magnetostrictive phase for fabricating ME composite materials, so scientists made lots of efforts towards this goal. V. M. Petrov reported $NiFe_2O_4$(NFO)-$Pb(Zr_xTi_{1-x})O_3$(PZT)[65] coupling effects by modeling the different heterostructures of this nanocomposites. The NFO nanopillars in PZT were expected to have a stronger ME effect than other structures for it wouldn't be influenced by substrate. The nanowired structure caused more ME effect than the bilayered one due to the additional radial stress. The Y.

Zhang studied the $NiFe_2O_4$-$BaTiO_3$[67] bilayered thin film using pulsed-laser deposition. The nano composites showed coexistence of ferroelectricity and ferromagnetism. Its ME coupling effect was comparable with that of the bulk composites. The $NiFe_2O_4$-$Ba_{0.7}Sr_{0.3}TiO_3$[68] system was also studied by D. Patil etc. by standard double sintering ceramic fabrication method. Large ME voltage coefficient was observed (about 560 $\mu Vcm^{-1}Oe^{-1}$) for 15% NFO-85% BSTO composite.

2.3. Variant CVD Techniques Employed in Thin Film Deposition

There were many deposition methods for multiferroic thin films which primarily fall into two broad categories, chemical or physical processes. For the physical deposition, there were thermal evaporator (Molecular Beam Epitaxy, Electron Beam Evaporator) which required a high vacuum, sputtering which relied on plasma, Pulsed Laser Deposition (PLD). For the chemical deposition process, there were plating, Chemical Solution Deposition (CSD) and Chemical Vapor Deposition (CVD) according to the phase of the precursor. Among CVD methods, there were Metallorganic Chemical Vapor Deposition (MOCVD), Atomic Layer Deposition (ALD) which usually used low pressure of organometallic gas as precursor, and Plasma enhanced Chemical Vapor Deposition (PECVD) which used an ionized vapor as precursor. Compared to other techniques, MOCVD could deposit conformal thin films over large areas with the right stoichiometry, high yield and high throughput at low cost, which made it ideal for fabrication of thin film-based device. (Figure 2) However, unlike CSD, PLD techniques, there had been very few reports on the use of MOCVD for magnetoelectric films. Maybe it was because the research of multiferroic

material, especially for magnetoelectric materials, was a new field which had some latest mechanisms of the materials' behavior found and developed as has mentioned in this paper before. So far, no more than 10 papers reported on rare earth manganites using CVD methods and only 10~20 papers reported on BFO thin films using this method. Other kinds of magnetoelectric materials like rare earth molybdates, $BiMnO_3$, $TbMn_2O_5$, and 3d transition metal boracites, hadn't any literature about using CVD method to deposit them yet. For the ferroelectric constituent-NFO films in the ME nano composites, even fewer reports were published using this technique. As our research interested in BFO and NFO thin films growth, we are going to introduce some different techniques in CVD for these depositions.

According to the pressure in the reactor's chamber in CVD system, there are atmosphere CVD (APCVD) (at atmospheric pressure), low-pressure CVD (LPCVD) (at about 1 Torr to few Torr) and ultrahigh vacuum CVD (UHVCVD) (below ~10^{-8} Torr). According to the physical conditions of the precursor, there are aerosol assisted CVD (AACVD) which the precursor generated by ultrasonic is in liquid/gas aerosol form, direct liquid injection CVD (DLICVD) which the liquid form precursor or precursor's solution is injected in a vaporization chamber and then delivered to the substrate as the normal way in CVD process. These two methods are the modifications of the classic CVD system in consideration of some precursor's unstableness or low vapor pressure. Atomic layer deposition (ALD) is also another kind of CVD, although the process of the deposition and some operation parameters are very different from the classic CVD. It needs precursors to be delivered into the

reactor separately in sequence and in a very short period of time. Between each precursor, the noble gas is purged and clean the chamber to assure that the precursor only absorbs or reacts on the substrate's surface. The chemical reaction is broken into more than one step and is self-limited. In this way, a single layer in atomic scale can be grown on the substrate. When this is done in cycles, thicker films can be obtained. Other CVD techniques, like plasma-enhanced CVD (PECVD), hot wire CVD (HWCVD), rapid thermal CVD (RPCVD) etc., haven't been reported in magnetoelectric films deposition so far.

MOCVD is an efficient, flexible, simple and robust technique for depositing simple as well as complex oxides. It is an industrially favored technique because in contrast with other techniques such as sputtering, molecular beam epitaxy, and pulsed laser deposition, MOCVD can deposit conformal thin films over large areas with the right stoichiometry, high yield and high throughput at low cost. But the choice of precursors is critical. At the minimum, the precursors should have a stable and reproducible high enough vapor pressure, should not decompose during transport to the reactor and should not be hazardous.[69] Gas or liquid precursors with enough vapor pressures are ideal for MOCVD process because of the ease with which they can be delivered to the deposition chamber in a controllable manner. For gases, a mass flow controller is conventionally used to control the dose of precursor from the precursor cylinder. In case of liquids, the use of bubblers is the most dominant delivery method. Carrier gas at a controllable flow rate is fed through the precursor liquid in the bubbler in order to take the precursor molecules to the reactor. The

bubbler is maintained at a exact temperature by a temperature controller so as to keep stable equilibrium for vapor and liquid phase. Such a simple and inexpensive arrangement can reproducibly control the vapor phase concentration of the precursor in the reactor. On the other hand, solid form precursors pose several problems which may limit their suitability for MOCVD process. Solid precursors have lower vapor pressures compared to liquid ones. More importantly, their vapor concentration in carrier gas decrease because of changing surface area after they are consumed. Also, lower vapor pressures require higher heating temperature for the bubbler; however, this could lead to agglomeration and/or degradation of precursors in the vessel. To overcome these difficulties caused by solid form precursors, expensive and complicated non-conventional delivery equipment, like using a separate heating zone within the reaction chamber, solvent-based direct liquid injection and sublimation in a fluidized bed, have been employed.[70-73] Although such solid precursor's delivery techniques provide possible improvements, they bring in additional parameters that build up the complexity of the MOCVD process comparing with the liquid precursor's delivery schemes.

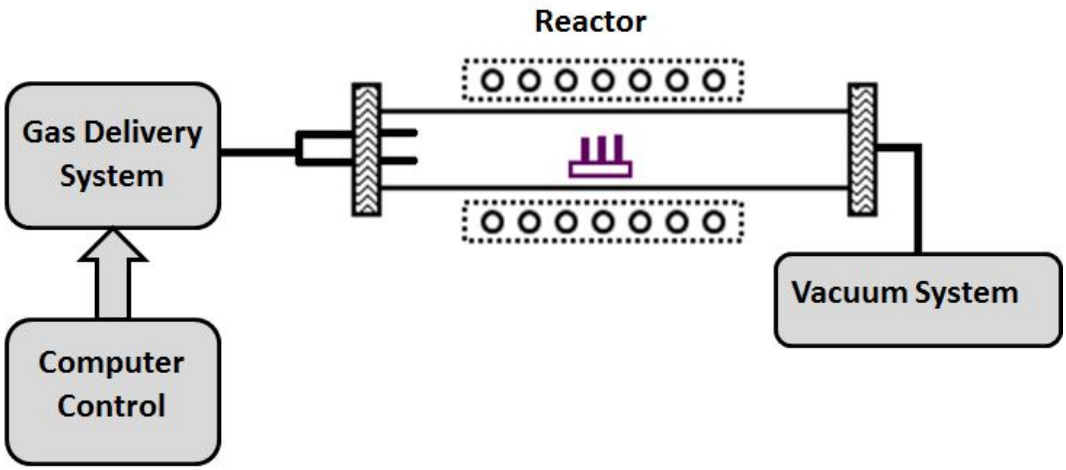

Figure 2. Common CVD setup

2.4. Metalorganic Precursors

In CVD method, the choice of a proper precursor is very critical. For the deposition of bismuth ferrite films, metalorganic compounds are often used as precursors. This type of precursor involves a bonding interaction between one or more carbon atoms of organic functional groups and a metal atom or atoms. The precursors should be stable at room temperature and have sufficient volatility at low temperature so that it can be easily transported to the reactor without condensing in the pipelines. Other important properties are that they should have the ability to react cleanly in the reaction zone and produce at a relatively high growth rate on a high purity scale without side reactions or parasitic reactions.

For gas precursor delivery, a mass flow controller is conventionally employed to measure the dosage of precursor. For liquid precursors, a bubbler is the most common delivery technique. In such a setup, carrier gas at a certain flow rate is fed through the dip tube within the liquid in the bubbler so as to take the precursor molecules to the

reactor [74]. A specific temperature is set to keep the stable vapor generated from the vessel. Solid precursors show challenges which may limit their usage for MOCVD process. Solid precursors, in general, have lower vapor pressures compared to liquid ones. And the vapor mixture of precursor and carrier gas changes as they are consumed due to different surface area. Agglomeration and/or degradation of the solid precursor in the vessel can happen because of high heating temperatures. For many metal depositions, only solid precursors are available. Therefore, scientists found a few major precursor delivery methods to overcome the disadvantage of solid precursor. These methods differ in whether the phase of the precursor is solid or liquid when taken to the reactor. One approach was using an appropriate solvent to dissolve the solid and afterwards the mixture injected into a heated unit where it gets flash vaporized and the molecules are then flowed into the reactor chamber with or without carrier gas. When multiple precursors are needed, precursors may be injected independently from different solutions [38] or they can be injected in the form of a solution by carefully mixing them in the same solvent alternatively [75]. The use of solvent increases the possibility of organic contamination within the films. Particularly in the case of multiple precursors combination, solubility and viscosity tests are needed before usage of suitable solvent[34]. The choice of solvent becomes more relaxed in a band flash kind of setup[32, 75].

Alternatively, various means for using solid precursors directly have been studied instead of a solvent-based approach. In one kind of setup, separate heating zone where a crucible holding the precursor may be kept is provided and then the vapors carried

by noble gas can be flown into the reaction zone. This method cannot have a control of the amount of precursor molecules flowing onto the substrate. In another approach, the precursors are mixed in appropriate quantities in the powder form and made into a disk by compaction. Then microportions of this disk can be sliced and fed into the reactor.

The commonly used precursors can be categorized into several families, (I) β-diketonates, (II) carbonyls, (III) alkoxides, (IV) metallocene, (V) alkyl and (VI) aryl compounds. For depositing BFO and NFO thin films, three precursors should be used based on the three metal elements needed to be introduced.

Bismuth Precusors

For bismuth precursors, several kinds of chemical compounds have been reported. In aryl family, $Bi(C_6H_5)_3$ was most commonly used to grow bismuth oxide [76] and other films like magnetoelectric BFO thin films [41], superconducting Bi-Sr-Ca-Cu-O (BSCCO) films [77], ferroelectric bismuth titanate films [78], ferroelectric $Bi_4Ti_3O_{12}$ single crystal thin films [79], ferroelectric $SrBi_2Ta_2O_9$ (SBT) thin films [80]. The reason why this precursor was commonly used was because of its thermal stability and clean sublimation from 160~280 °C compared to other precursors. It is commercially available and inexpensive. Its melting point is 77~78 °C and it starts to decompose at around 310 °C. [81] Therefore, it's both good for liquid-injection delivery and gas phase delivery for CVD system. $Bi(o\text{-}C_7H_7)_3$ was another aryl family's precursor and could be used for growing bismuth oxide, $BiFeO_3$ thin films [37], $(Bi, Nd)_4Ti_3O_{12}$ (BNT) thin films [82] and $Bi_4Ti_3O_{12}$ thin films [83], [84]. This precursor has a melting

point of 130 °C and decomposes at around 210 °C. Its thermal stability is higher than that of $Bi(C_6H_5)_3$, however, its temperature range for controlling the precursor is narrower. It's often used for liquid-injection delivery as this solid state precursor can be dissolved in a proper solvent.

$Bi(C_{11}H_{19}O_2)_3$ ($Bi(tmhd)_3$) is a β-diketonate family compound. It has been used for growing bismuth oxide films [85], $BiFeO_3$ films [34], BNT films [57], BLT films [81] and SBT films [86]. Its melting point is 114-116 °C and can sublime at 150 °C. Its decomposition temperature is 295 °C. Though it is a novel precursor and is suitable from the viewpoint of MOCVD kinetics, it can easily sublimate and degrade under storage. Besides, it's more difficult to handle this precursor due to the hydrolysis. [87] So people usually use a Direct Liquid Injector (DLI) system for MOCVD method.

$Bi(CH_3)_3$ is a alkyl family compound. It has good volatility and is in liquid form, but it is highly reactive and potentially explosive. It's not suitable for the practical use. It was used for growing SBT films [88], $Bi_4Ti_3O_{12}$ films [36]. There is no report about deposition of BFO films using this precursor.

$Bi(OC(CH_3)_2CH_2OCH_3)_3$ ($Bi(mmp)_3$) was a alkoxide family compound and used for the depositions of BFO films [34], bismuth oxide films [89], $Bi_4Ti_3O_{12}$ films [74]. This is a novel precursor. However, all the reported MOCVD methods about this precursor required the liquid-injection way to deliver this precursor.

Other precursors people used to grow BFO films are $Bi[(CH_3)_2\text{-}2\text{-}(CH_3)_2NCH_2C_6H_4]$ [90], $Bi(o\text{-}Tol)_3$ [37] and $Bi(p\text{-}Tol)_3$ [37]. $Bi(o\text{-}Tol)_3$ and $Bi(p\text{-}Tol)_3$ are in solid form and need liquid-delivery system.

$Bi[(CH_3)_2\text{-}2\text{-}(CH_3)_2NCH_2C_6H_4]$ [91] is a newly developed precursor which is light yellow liquid with excellent volatility and non-explosive. Though it is not commercially available, it's promising to be a suitable precursor for deposition of BFO films.

As the properties of these precursors were shown, we used $Bi(C_6H_5)_3$ as precursor in my experiments because a stable precursor was need to store in the bubbler and there was no liquid-injection process required. $Bi(C_6H_5)_3$ was white crystal powder and air and moisture stable precursor. It had a clean sublimation from 160~280 °C with residue less than 15% (Figure 3). The precursor was kept at 80~165 °C in a bubbler to generate enough vapor pressure from its liquid form and delivered by the carrier gas Ar. The growth rate was low at lower temperature range. When the bubbler's temperature was higher than about 130 °C, the growth rate increased remarkably and we obtained much thicker films. The bubbler for growing BFO was kept at 160 °C (~0.817 Torr). The Figure 6 showed the Antoine equation plot of the $Bi(C_6H_5)_3$ from the Kojima report.[92]

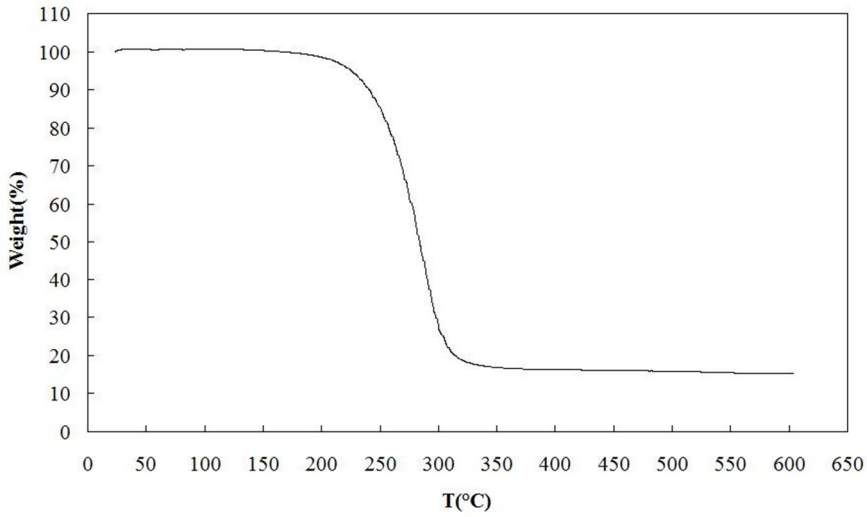

Figure 3. TGA result for triphenylbismuth. The solid powder was heated and decomposed with purging Ar using temperature programming in CAHN TG-131 equipment.

Nickel Precursors

The most commonly used nickel precursors were: (a) carbonyl family, $Ni(CO)_4$; (b) β-diketonates family, $Ni(C_5H_7O_2)_2$[93-96], $Ni(tmhd)_2$, $Ni(acac)_2$, $Ni(acac)_2en$; (c) metallocene, nickelocene ($Ni(C_5H_5)_2$),[97-99] bis-methylcyclopentadienyl nickel ($Ni(CH_3C_5H_4)_2$), $Ni(EtCp)_2$[99].

The precursor I used in the experiments was nickelocene (purity 99%, Strem Chemicals) which had the same ligand as iron precursor. Nickelocene is green crystalline powder with a high vapor pressure of ~0.179 Torr at 60 °C. This vapor pressure was calculated based on the Antoine equation fit from the experimental data.[100] This precursor could degrade and decompose in air. The decomposition temperature by itself was 186 °C. (figure 4). During the TGA anaylsis, it had a clean

evaporation with around 4% residue (figure 4).

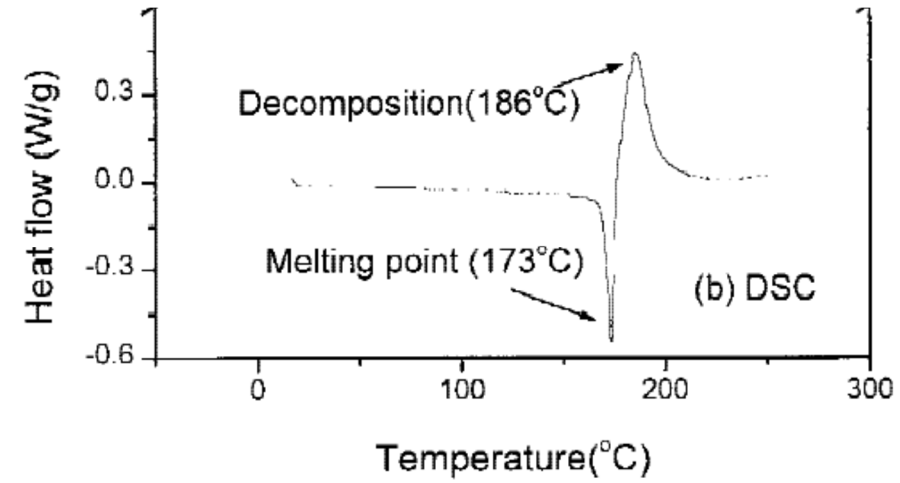

(a)

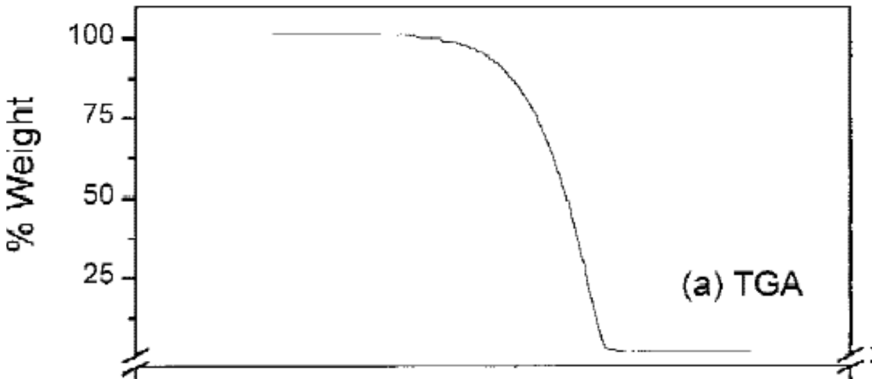

(b)

Figure 4. DSC (a) and TGA (b) plots for nickelocene precursor[101]

Iron Precursors

There have been a number of iron precursors reported since 1970's. They belong to mainly four families: carbonyls, β-diketonates, metallocenes and alkoxides.

$Fe(CO)_5$ is a liquid precursor for the growth of iron oxide thin films. [102], [103], [104],

[105] However, its vapor pressure is too high (~28 Torr at 25 °C). [106] It is pyrophoric and toxic. It reaches its boiling point at 103 °C while decomposes at ~180 °C. [107] This limits its use in the deposition of crystalline iron oxide films which requires a high reactor's temperature. Iron(III) acetylacetonate [$Fe(acac)_3$] [70], [108], [109], [109], [110], [111], [112], [113], ferric dipivaloyl methanate [$Fe(DPM)_3$] [114], [115], iron(III) t-butylacetoacetate [$Fe(tbob)_3$] [116] and tris(trifluoroacetylacetonato) iron (III) [117] are all β-diketonates family's precursors. $Fe(DPM)_3$ (or $Fe(tmhd)_3$, $Fe(thd)_3$) has also been used for atomic layer deposition of iron oxide films. [118] The β-diketonates undergo degradation easily in the delivery lines as well as under storage in the precursor vessel. [76], [119] All these β-diketonates iron precursors used for CVD are in solid form at room temperature. The solid alkoxide precursor $[Fe(O^tBu)_3]_2$ [120], dihydride complexes $H_2Fe[P(OCH_3)_3]_4$ and $H_2Fe[P(CH_3)_3]_4$ [121] have been reported recently. $H_2Fe[P(OCH_3)_3]_4$ and $H_2Fe[P(CH_3)_3]_4$ are not available commercially and $H_2Fe[P(OCH_3)_3]_4$ produced films which were amorphous and had phosphorus contamination. In metalloenes family, only ferrocene has been reported for MOCVD applications. [122] Though it had several advantages over the other precursors, it required a fluidized bed evaporator for its delivery to the reactor.

In our recent study, we reported n-butylferrocene (purity 99%, Strem Chemicals), a liquid precursor which was used for the first time in the low pressure MOCVD of Fe_2O_3 thin films. [123] It is a ferrocene derivative and exhibits good properties similar to those of ferrocene. Its liquid form at the room temperature allows the use of the conventional simple and flexible bubbler-type delivery scheme. Furthermore, it is

thermally stable and air, moisture stable. It has a relatively high vapor pressure and nonpyrophoric. The vapor pressure was calculated to be 0.036 Torr at 62.5 °C based on the Antoine equation fit from the experimental data (Figure 6).[124] The TGA characterization showed it had clean evaporation without any decomposition (residue~2%) (figure 5). The films were crystalline and had a proper growth rate (from 4 nm/min in the kinetics-controlled regime to 50 nm/min in the mass transfer-controlled regime).

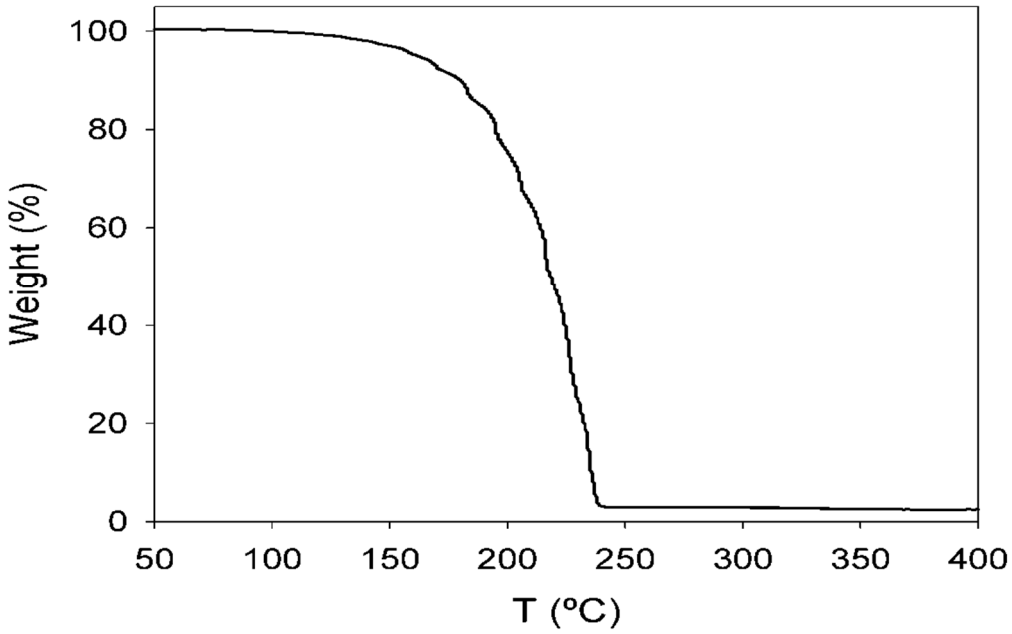

Figure 5. TGA result for n-butylferrocene

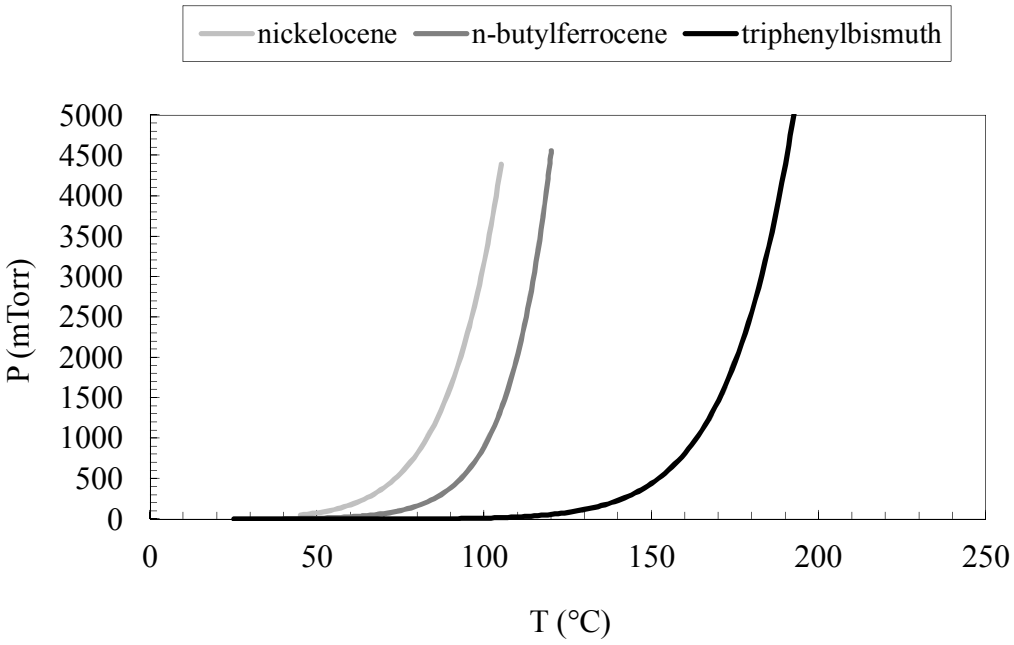

Figure 6. Vapor pressures for three precursor used for depositions of nickel oxide, iron oxide and bismuth oxide thin films.

3. EXPERIMENTAL DETAILS

3.1. Co-Deposition and Cyclic-Deposition Designs for MOCVD Process

This MOCVD (Figure 7) was designed for growing binary metal oxide thin films or two different metal oxide thin films alternatively via co-deposition and cyclic-deposition modes. In the Figure 7, those pneumatic valves were controlled by LabVIEW computer program.

The hot wall horizontal reactor consists of a quartz tube 38 mm in diameter and 48 cm in length. A furnace (Model 1043 Marshall, ThermCraft, Inc.) which holds this quartz tube inside can heat it up to 1000 °C. Dual-tube gas feedthrough which allowed both precursors and oxidizers introduced into the reactor was fixed at one end and a metal part with multiple ports (2-3/4" ConFlat flange 4-way standard 304L stainless steel cross) for the sample loading and vacuum system (mechanical pump, Fisher Scientific Maxima C Plus Model M8C) at the other end. The metal part and the quartz tube joined together with a quick-connect fitting and Viton O-rings. To prevent gas leakage, these o-rings needed to be smeared by silicon based high vacuum grease (Dow Corning DC 976 High Vacuum Grease, Kurt J Lesker Co.) and be changed regularly due to the deformation and degradation caused by high reactor temperature. The consideration of a liquid nitrogen cold trap between V1 and V2 was to clean the excess precursor and byproduct particles in case of blockage inside the pump. V1 manual valve controls the ventilation of the system and V2 adjusts the total pressure (G1) of the reactor. The G1 consists of a thermocouple pressure gauge (Varian Model 536, Varian Vacuum Technologies) and an absolute pressure piezo-transducer (HPS Series 902, MKS Instruments) to allow pressure reading from either 1-2000 mTorr or

1-1000 Torr.

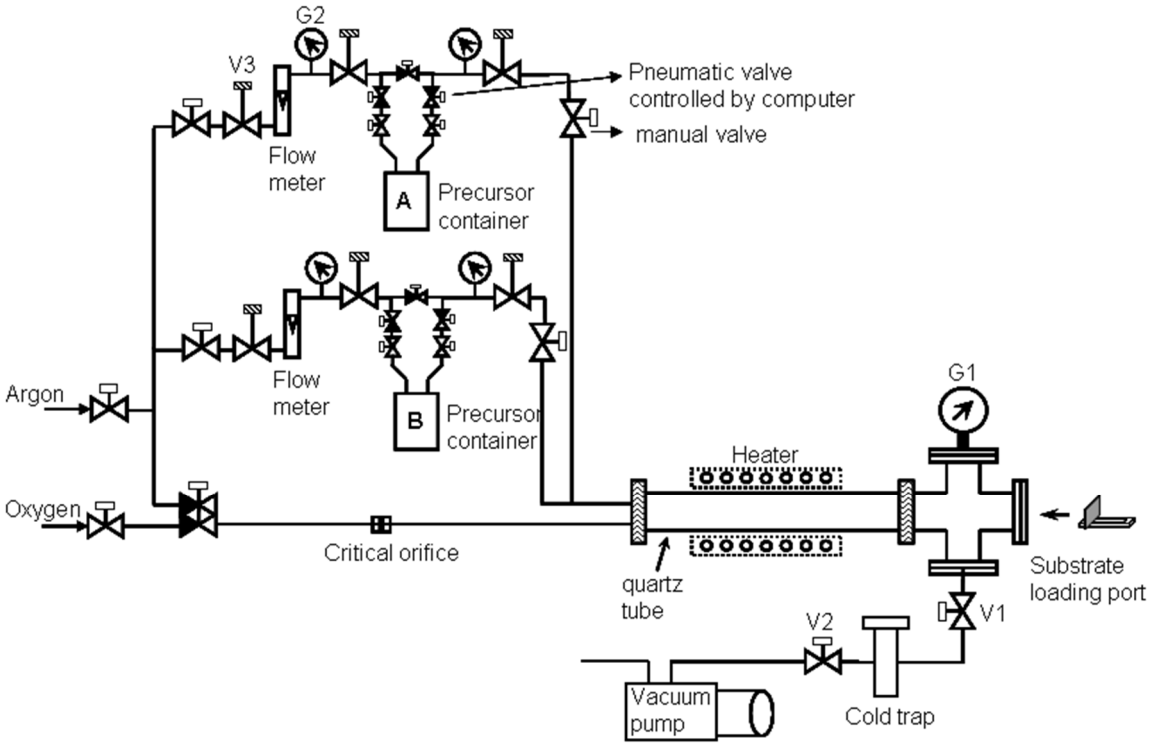

Figure 7. MOCVD equipment configuration. A and B (four canisters totally, using only two of them) represent for different precursors.

3.2. Post Deposition Annealing Furnace

The post deposition annealing processes were performed under 700~1000 °C to investigate the crystallization of metal oxide thin films. The Lindberg/Blue Three Zone Tube Furnace consists of an 80 mm horizontal quartz tube and was heated by three temperature controllers along the tube separately. The three heating parts can heat from room temperature up to 1100 °C, keeping the whole tube heated uniformly. There are one inlet and one outlet set at both ends of the tube for gas purging, allowing the nitrogen and oxygen environments inside the tube (Figure 8.).

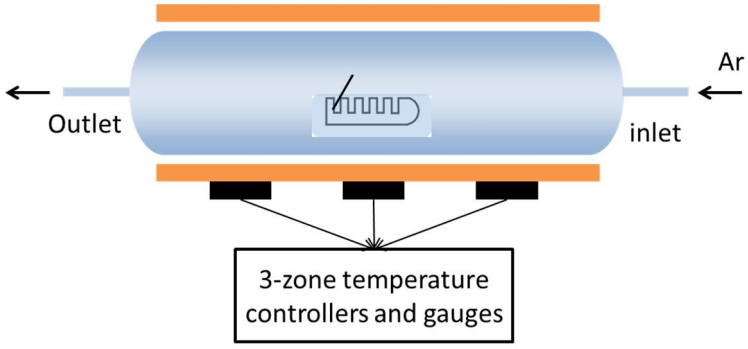

Figure 8. Schematic of the three zone furnace for thermal processing of the as-deposited samples.

Prior to the post deposition annealing process, the furnace is purged with Ar (99.999%) for 10 min at the desired temperature. The samples were located in the middle of the tube from 0.5 to1 hr.

3.3. Characterization Techniques

3.3.1. Spectroscopic Ellipsometry

Ellipsometry is a widely used non-destructive technique for thin film and bulk material characterization. It performs a quick measurement for determining the film thickness and optical constants in the range of 1-1000 nm with sub-nanometer resolution. The change in polarization as light reflects or transmits from a certain material structure was detected and represented as an amplitude ratio (Ψ) and phase difference (Δ). The polarized light is shown in Figure 9. These two values are related to the ratio of Fresnel reflection coefficient R_p and R_s for p- and s- polarized light respectively [125].

$$\rho = R_p / R_s = \tan(\psi)e^{i\Delta}$$

Here ρ refers to complex ellipsometric parameter. From the models built by Jones matrix, Fourier transform and other math calculations, error analysis runs when experimental data points collected. The measurement noise is then converted to standard deviation on Δ and ψ. These values are used to weight the contributions of each data point to the mean-squared error (MSE) during the fitting process.

In this work, a J. A. Woollam Model M-44 ellipsometer installed with a Xenon arc lamp (USHIO UXL-75XE), was utilized to obtain the thickness of thin film samples. The schematics of the equipment are shown in Figure 10 [126].

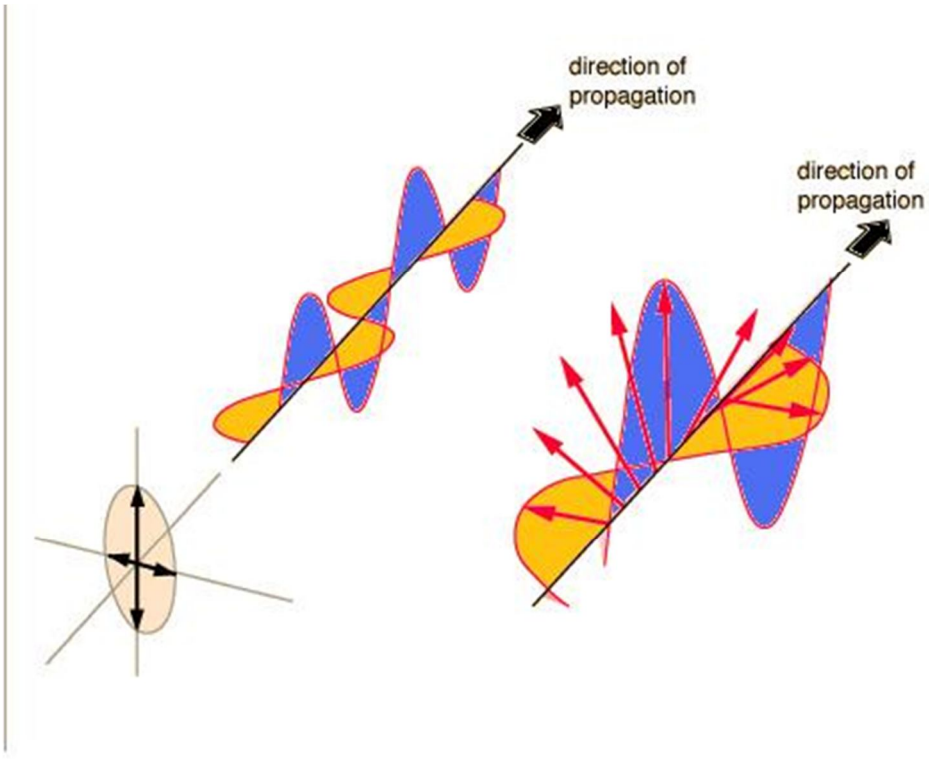

Figure 9. Elliptical polarized light source. The light is composed of two plane waves of equal amplitude. One phase shifted from the other one by some certain degree, not 90°.

(a)

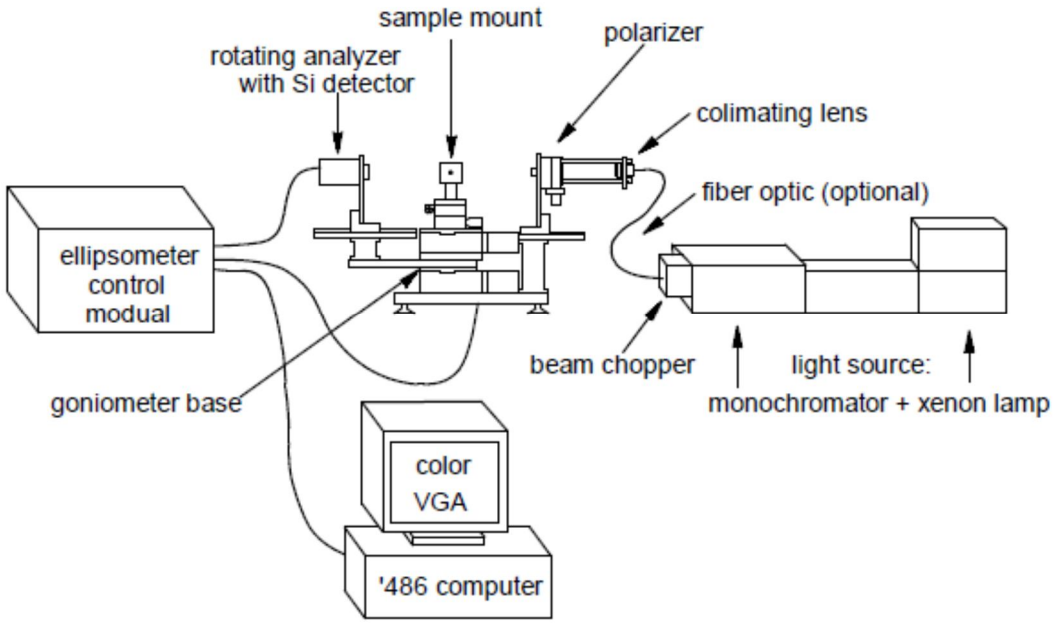

(b)

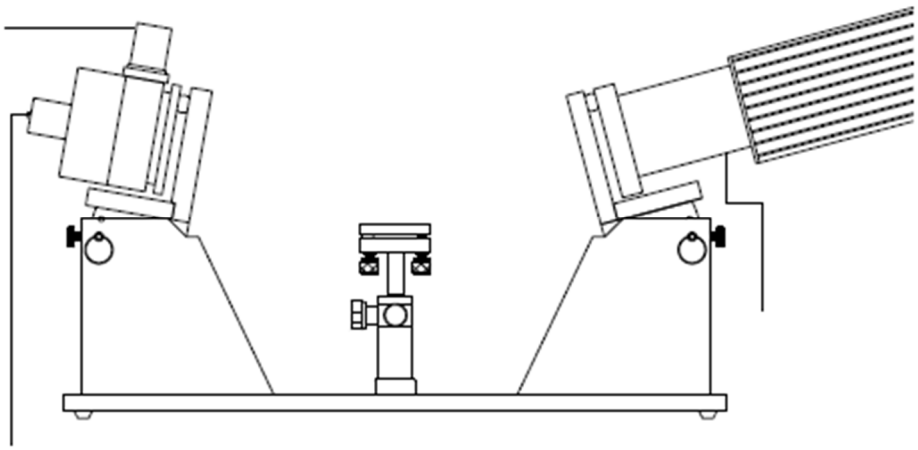

Figure 10. (a) general schematic of a J.A. Woollam Co., Inc. *VASE*® system, variable angle of incidence spectroscopic ellipsometer; (b) ex-situ fixed angle base, *M-44*® rotating analyzer ellipsometer. In the detector unit, the white light beam is dispersed onto an array of silicon detectors, such that measurements are performed at 44 wavelengths simultaneously. (Figure from Handbook of J.A. Woollam Co., Inc. *VASE*® system)

The thin film sample in this work could be measured in the range of 0-1000 nm. Multi-layered sample was also measured accurately through proper model fitting (Figure 11). The uniformity by film thickness could be obtained by measuring different spots on the same sample surface.

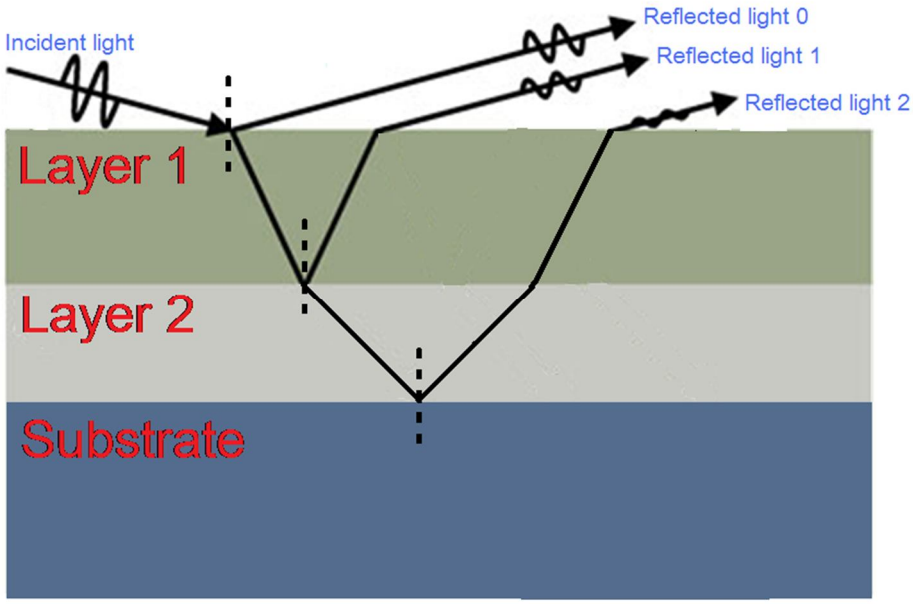

Figure 11. Reflected light and interference during sample measurement using ellipsometer.

3.3.2. X-Ray Photoelectron Spectroscopy (XPS)

X-Ray Photoelectron Spectroscopy is also a commonly applicable surface analysis technique which includes chemical bonding information and chemical composition quantification.

The principle of XPS equipment is based on photoelectric effect. When high-energy photons (from X-ray source) are absorbed by the atoms of the bulk

material, free electron will be emitted and its kinetic energy (KE) will follow the photoelectric law

$$KE = h\nu - BE$$

Where BE is the binding energy of the released electrons. During the data collection, KE can be known from the channeltron detection system, $h\nu$ can be known from the X-ray source. Therefore, the XPS spectra is described as electron intensity depended on BE.

In this study, a Kratos AXIS-165 Surface Analysis System with monochromatic Al Kα X-ray source was used for investigating chemical bonding states of all the elements of the sample and their atomic ratios. The schematic of this XPS spectrometer is shown in Figure 12. The sample holder equipped with charge neutralization system was placed in the ultra-high-vacuum (less than $1x10^{-8}$ Torr) chamber and can be either tilted or moved by the X, Y, Z metal axes (Figure 13). The chamber was installed with a 165 mm mean radius hemispherical analyzer, with an eight channeltron detection system for excellent energy resolution and sensitivity at small analysis areas.

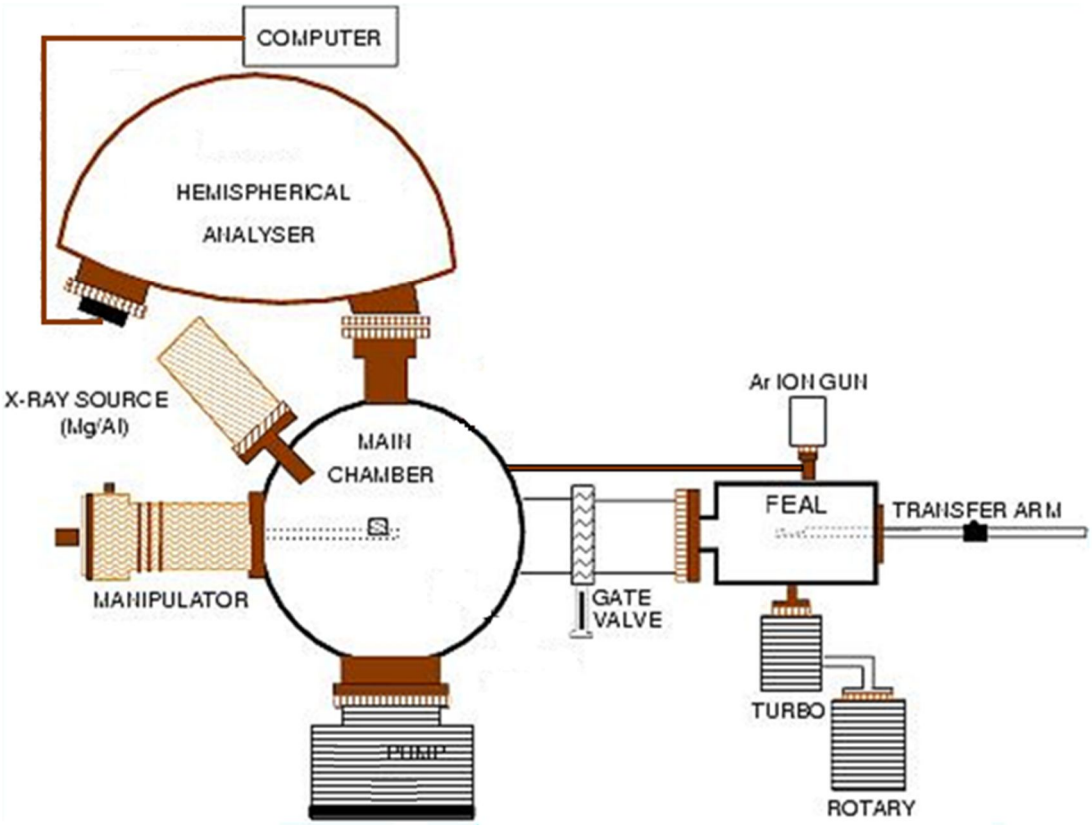

Figure 12. A common X-ray photoelectron spectrometer equipment setup.

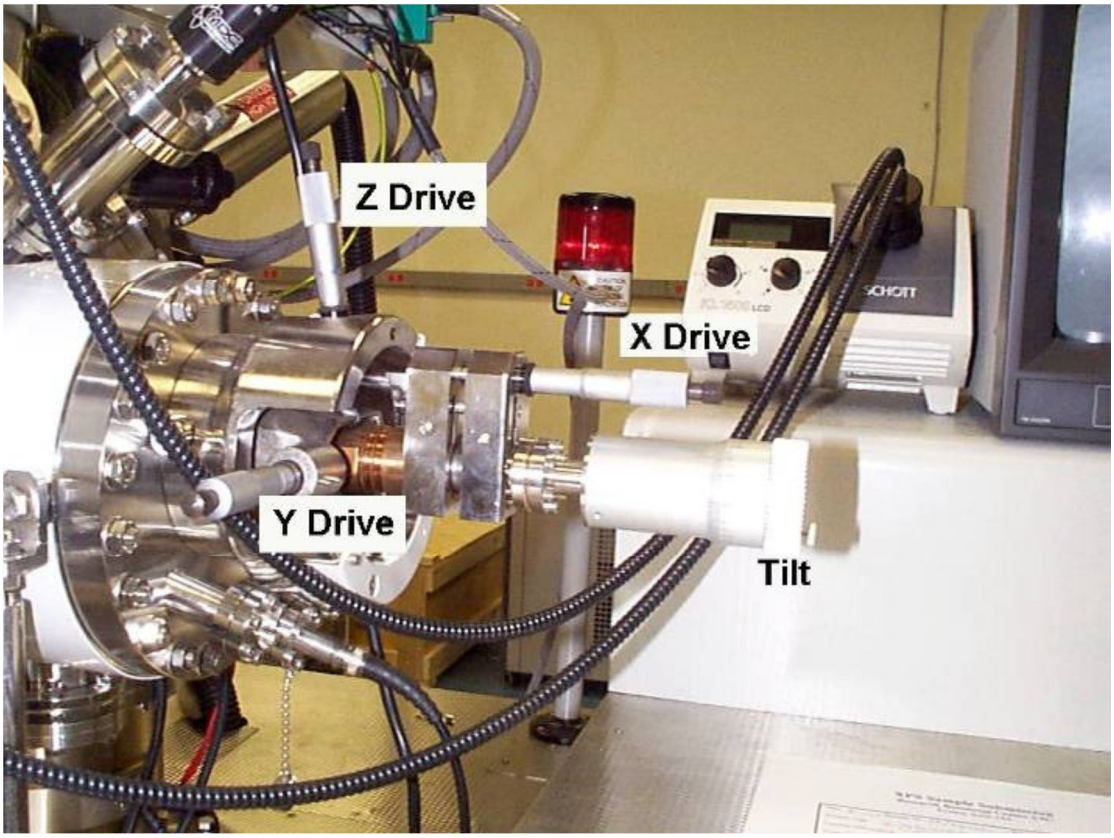

Figure 13. Sample loading system for Kratos AXIS-165. Figure from Research

Resources Center at University of Illinois at Chicago.

3.3.3. Glancing-Angle X-Ray Diffraction (GAXRD)

GAXRD is another non-destructive technology for the surface analysis using X-ray source. For the ordinary XRD, the X-ray diffractogram of nano scale thin film cannot be detectable due to weak diffracted light intensity. After decreasing the angle of incidence, diffracting volume can be increased and stronger signal from top part of materials will be received. The small incidence angle used in this study was 0.7° (Figure 14). The monochromatic X-ray beam with wavelength λ was projected onto the sample material at the angle θ (Bragg angle), and diffraction occurs only when the distance d traveled by the rays reflected from successive planes according to this Bragg's Law.

$$n\,\lambda = 2d\sin(\theta)$$

d is the space between the planes of the lattice in the crystalline sample films. By scanning the diffraction signals from varying the Bragg angle, the resultant diffractogram is formed (Figure 15). The intensity and its angle of each diffracted peak for a certain phase of the material are unique. Those characteristics from different phases or materials can be recognized using the software with the standard data database.

The crystalline phases of thin films including various structural properties can be obtained via GAXRD. Besides the phase information, the lattice constant can also be obtained by fitting the spectra of each crystalline phase.

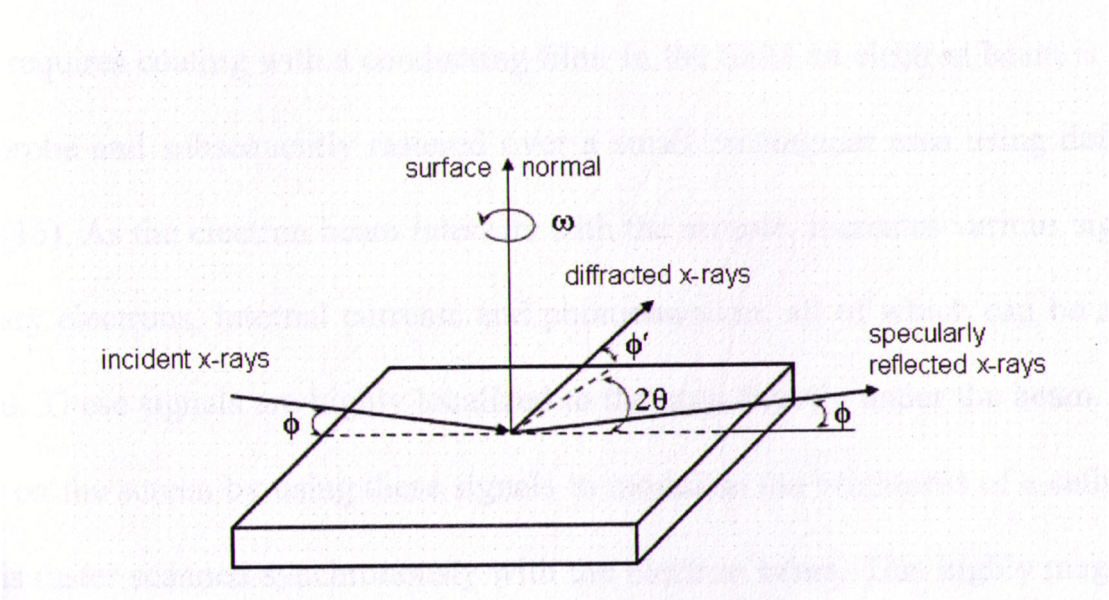

Figure 14. Graphic example of the GAXRD operating principal. Φ is angle of incidence, Φ' is reflected angle of the beam, θ is Bragg angle, ω is angle of rotation around surface normal.

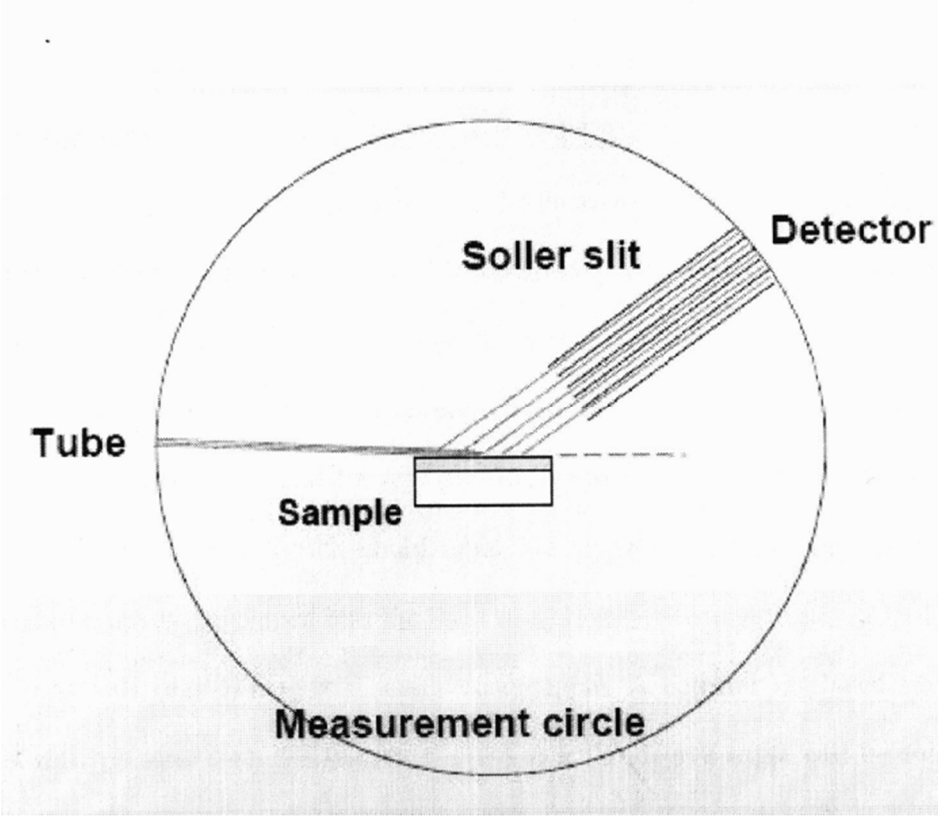

Figure 15. A common schematic of the X-ray diffraction system. Using rotating detector, the scanning of the diffractogram is performed.

3.3.4. Optical Interferometric Profiling

The optical profiler is a quick and non-destructive method to analyze the surface topographic features of thin films. The samples should be smooth and light reflecting to form the interferogram. An interferometer splits the light to two different optical paths and then recombines them at the detector. This recombination can form fringes and phase data can be collected according to this imaging through the CCD camera (Figure 16). To remove phase ambiguities between adjacent pixels, phase data need to be calculated. The relative surface height can be obtained from the phase data using the following equation:

$$h(x, y) = (\lambda / (4\pi)) \Phi(x, y)$$

where λ is the wavelength of the source beam, and $\Phi(x, y)$ is the phase data.

In this work, phase-shifting interferometry (PSI) mode was used through Wyko NT3300. A white light beam is filtered and passed through an interferometer objective to the sample surface. A piezoelectric transducer moves the reference surface for a small known amount to induce a phase shift between the sample's reflection signal and the reference beams. The intensity of this interference pattern is recorded at many different relative phase shifts, and then converted to wavefront data from integration. The samples were measured by different spots on the surface and at least 3 times per spot. The final results were the average values of those raw data. The film smoothness and topographic image were obtained here.

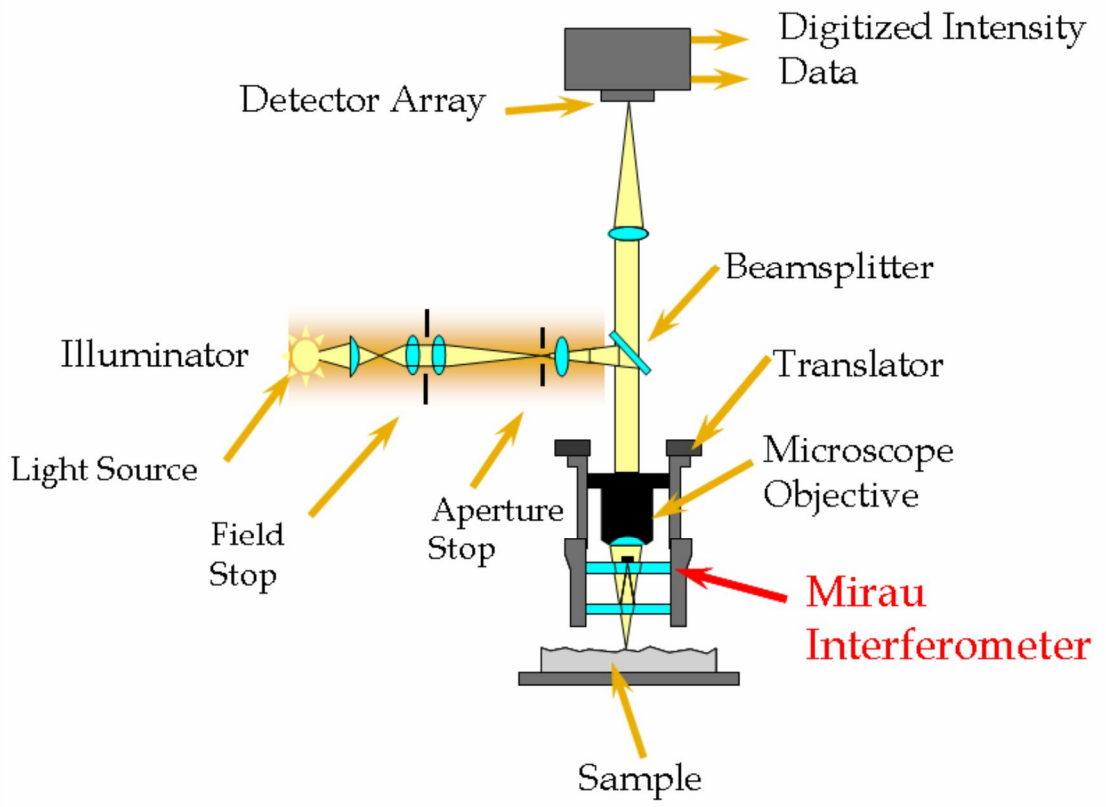

Figure 16. Common schematic of the Wyko optical profiler. (figure from http://cmi.epfl.ch/metrology/Wyko_NT1100.php)

3.3.5. Rutherford Backscattering Spectrometry (RBS)

RBS is a commonly used non-destructive nuclear technique for elemental composition analysis of nano thin films to bulk materials. The backscattering effect of the collision by alpha particles and the nuclei of an atom were first discovered by Lord Ernest Rutherford between 1909 and 1914. Alpha particles were directed at a metal foil and backscattered from the targeted atomic nuclei through a certain position. This proved that the existence of the nuclei and its positive charges which could repel the alpha particles if they came close enough.

A high energy He++ beam (2 to 4 MeV) is used in the RBS instrument. The ions

after hitting the sample will change their energy which depends on the mass of the sample atom and the energy transferred to the sample atom. The measurement of the scattered ions can provide the chemical composition of the targeted sample. As the ion may travel much further than X-ray, it will continue to hit deeper atom if it doesn't meet any near the surface. The deeper it goes into, the more energy it loses. Therefore, the RBS can perform a depth profile of the composition of a sample. This is especially useful for multi-layered nano thin film analysis. The drawback of such method is that it is not sensible to light target atoms, for instance, carbon. Due to this backscattering effect related to the mass of the measured elements, heavy metals in the films can be measured and compared with each other.

3.3.6. Thermogravimetric Analysis

This technique was used here to investigate the thermal properties of the metal precursors. As the chosen of metal precursor was critical, a compound with stable and clean evaporation advantages was preferred in this work. The furnace of the thermogravimetric analysis (TGA) equipment could heat the sample (around 125 mg) in a small container in a nitrogen flow (Figure 17). The temperature was programmed and the weight loss of the sample could be measured through comparison with the standard sample outside the furnace. A balance was installed for balancing the standard sample and the measurement for the weight difference. The computer recorded the data for the weight lost according to each temperature point and formed the TGA plot for the chemical compounds. From the dramatic change of the weight loss and little amount of the residue, clean evaporation property of the sample could

be known.

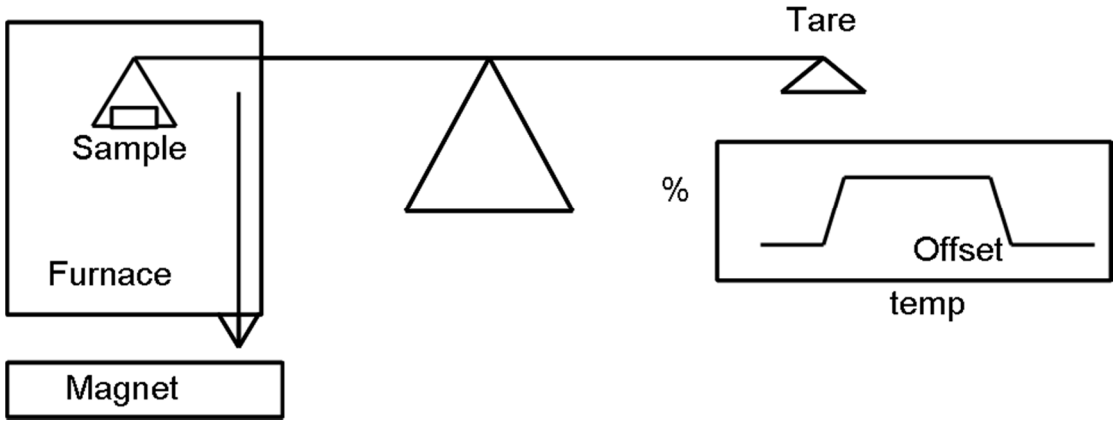

Figure 17. Common schematic of the common TGA instrument

4. RESULTS AND DISCUSSION

4.2.Low Pressure Metalorganic Chemical Vapor Deposited Single Metal Oxide Thin Films

4.2.1. Introduction

There were three kinds of single metal oxide thin films investigated during the research towards fabricating the binary metal oxides. The purpose to deposit the iron oxide, bismuth oxide and nickel oxide was first to establish their growth modes and tuning the process parameters. The optimal conditions for the depositions of $BiFeO_3$ and $NiFe_2O_4$ could be approached through these efforts.

Iron oxides have found several applications ever since the Iron Age. For several thousand years, these oxides have been used as pigments because of their varied colors and non-toxicity.[127] In modern technological context, they find applications as catalysts for various industrial syntheses, gas sensors,[128, 129] and photomasks.[130, 131] Upon incorporation of other metals to form iron-based oxides, interesting material properties have been obtained and these have led to new applications. Iron-based perovskite materials have been developed as promising materials for solid oxide fuel cell cathodes[132] and photocatalysis.[107] Thin epitaxial ferrite films of $CoFe_2O_4$, $NiFe_2O_4$ and $(Mn,Zn)Fe_2O_4$ deposited using pulsed laser deposition and sputtering have been recently studied because of their potential use in exchange-coupled biasing based devices.[133] More recently, iron-based perovskite $BiFeO_3$ has generated a lot of interest due to its room temperature multiferroic properties that could lead to the development of novel devices.[15, 134] In order to deposit such complex oxide

structures for fabrication of devices at a commercially viable scale, metalorganic chemical vapor deposition (MOCVD) is one of the most suitable techniques. But the applicability of this deposition technique is largely dependent on the availability of suitable liquid precursors. Precursors belonging to mainly four classes have been reported in the open literature for the chemical vapor deposition of different metal element containing oxide films: (i) carbonyls, (ii) β-diketonates, (iii) metallocenes and (iv) alkoxides.

For iron precursor families, iron pentacarbonyl ($Fe(CO)_5$) is a liquid precursor that has been used with different carrier gases to deposit iron and iron oxide films.[102-105, 135] But its vapor pressure is too high (~28 Torr at 25 °C)[106] to easily control its delivery to the reaction chamber in the deposition of thin films for electronic applications. Furthermore, apart from being toxic and pyrophoric, it has a low decomposition temperature (~180 °C)[107] which could be a limitation for its use in the deposition of crystalline iron oxide films requiring high deposition temperatures. All the other iron precursors used for CVD are in the form of crystalline powder at room temperature. β-diketonate-based iron precursors have been the most widely reported sources for depositing iron oxide films: iron (III) acetylacetonate ($Fe(acac)_3$)[70, 108-113] ferric dipivaloyl methanate ($Fe(DPM)_3$),[114, 115] iron(III) t-butylacetoacetate ($Fe(tbob)_3$)[116] and tris(trifluoroacetylacetonato) iron (III).[117] $Fe(DPM)_3$ is also known as iron(III) tris(2,2,6,6-tetramethyl-3,5-heptanedionate) ($Fe(tmhd)_3$ or $Fe(thd)_3$) and its use for atomic layer deposition of iron oxide films has been reported recently.[118] Besides being solid at room temperature, the β-diketonates

suffer from potentially serious disadvantages; they undergo degradation easily in the delivery lines as well as under storage in the precursor vessel.[76, 119] Recently, solid iron tert-butoxide ($[Fe(O^tBu)_3]_2$), which belongs to the alkoxide family, has been used as a single source precursor.[120] More recently, Fe(II) dihydride complexes $H_2Fe[P(OCH_3)_3]_4$ and $H_2Fe[P(CH_3)_3]_4$ have been reported for MOCVD of iron oxide films.[121] These precursors are not available commercially and, furthermore, $H_2Fe[P(OCH_3)_3]_4$ produced films that were amorphous and had phosphorus contamination. Among metallocenes, only $Fe(C_5H_5)_2$ has been reported for MOCVD applications.[122] Though it had several advantages over the other precursors mentioned earlier, being a solid precursor it required a use of fluidized bed evaporator for its delivery to the reactor.

As the earlier introduction of organometallic precursors mentioned, n-butylferrocene was used in the iron oxide deposition for the first time. Because of its thermal stablility and liquid form at room temperature, n-butylferrocene was once chosen as a potential precursor before our first study for the MOCVD of Fe_2O_3 thin films at low pressure. N-butylferrocene ($(C_4H_9C_5H_4)Fe(C_5H_5)$) is a ferrocene derivative and it exhibits good properties similar to those of ferrocene with the added advantage of being liquid at room temperature. This allows the use of the conventional simple and flexible bubbler type delivery scheme which can be used to deposit ferrites or other mixed iron oxides. Furthermore, n-butylferrocene is air- and moisture-stable, non-pyrophoric and has a sufficiently high vapor pressure. In this work, we also investigate the appropriate precursor temperature under which it can

continuously provide enough vapor and less waste during the CVD process. The reactor temperature is also tuned for the optimal growth of the film. Different kinetics in CVD process were elaborated based on the findings in the Arrhenius plot. The results of the morphology and composition of the films evidenced the uniform polycrystalline Fe_2O_3 film that we obtained.

The nickel oxide is usually in the form of nickel (II) oxide or nickel (III) oxide when is oxidized by oxygen. The mineralogical form of NiO, bunsenite is very rare on the surface of the earth. Usually, the Ni^{2+} has a green color while the Ni^{3+} is black. The pure NiO exhibits antiferromagnetism at room temperature and other metal ions such as Ni^{2+} or Li^{+} can be doped inside to increase its conductivity. Recent research also observed that the ferromagnetism exists within the Fe-doped NiO thin film and Li codoping can enhance this property.[136, 137] Therefore, transition metal doped NiO film was investigated to approach the goal of ferromagnetism tuning.[138] This metal oxidel can be in the applications of gas sensor, p-n junction for photonic device, hole transport layer for solar cells, battery electrode and electrocatalyst.[139-143] Various fabrication techniques have been used for growing nickel oxide thin film for different applications. Reactive magnetron sputtering[144, 145] for gas-sensing, pulsed laser ablation/deposition for electrode in Li-ion batteries[146], electro-deposition process, molecular beam epitaxy, chemical vapor deposition[94], atomic layer deposition, chemical bath deposition[147] for highly porous electrochromic films after annealing treatment, sol-gel method and spray pyrolysis technique[148] for automotive smart window due to its electrochromic properties. The precursor used in depositions of

nickel oxide films was nickelocene which had the same ligand as n-butylferrocene. The growth rates and process conditions were reported in Kang's and Yeh's studies.[97, 98, 101] The similar structures of the nickel and iron precursors are good for temperature window overlapping, no other chemical reactions besides their own oxidizations.

The bismuth oxide which can combine with other metal ions or oxides has very high oxide ion conductivity or multiferroic properties.[12, 149] It has attracted scientists' attention as being a suitable material for solid oxide fuel cells (SOFC). At room temperature, the bismuth oxide stays as monoclinic α-Bi_2O_3 while above 727 °C it changes to cubic fluorite-type δ-Bi_2O_3 phase which is the one with high ion conductivity (1 Scm^{-1}). Fabrication methods for Bi_2O_3 thin films includes chemical bath deposition[150], electrodeposition[151], CVD[85, 152], radiofrequency magnetron sputtering[153]. In this study, we used aryl family precursor, triphenylbismuth to grow bismuth oxide films in the CVD process. As the aromatic rings need higher temperature to detach from the metal ion, the rate-limiting steps of Bi_2O_3 growth are quite different from ones of the other two metal oxides, Fe_2O_3 and NiO. The bubbler temperature was also kept at around 130 °C to maintain its liquid form. Although there is no temperature window for Bi_2O_3 film growth, other process parameters were controlled under a suitable way to let the bismuth oxide deposit with iron oxide successfully.

4.2.2. Experimental

This MOCVD (Figure 18) was designed for growing single, binary metal oxide thin films or two different metal oxide thin films alternatively via co-deposition and

cyclic-deposition modes. In the figure 18, those pneumatic valves were controlled by LabVIEW computer program.

The hot wall horizontal reactor consists of a quartz tube 38 mm in diameter and 48 mm in length. A furnace (Model 1043 Marshall, ThermCraft, Inc.) which holds this quartz tube inside can heat it up to 1000 °C. Dual-tube gas feedthrough which allowed both precursors and oxidizers introduced into the reactor was fixed at one end and a metal part with multiple ports (2-3/4" ConFlat flange 4-way standard 304L stainless steel cross) for the sample loading and vacuum system (mechanical pump, Fisher Scientific Maxima C Plus Model M8C) at the other end. The metal part and the quartz tube joined together with a quick-connect fitting and Viton O-rings. To prevent gas leakage, these o-rings needed to be smeared by silicon based high vacuum grease (Dow Corning DC 976 High Vacuum Grease, Kurt J Lesker Co.) and be changed regularly due to the deformation and degradation caused by high reactor temperature. The consideration of a liquid nitrogen cold trap between V1 and V2 was to clean the excess precursor and byproduct particles in case of blockage inside the pump. V1 manual valve controls the ventilation of the system and V2 adjusts the total pressure (G1) of the reactor. The G1 consists of a thermocouple pressure gauge (Varian Model 536, Varian Vacuum Technologies) and an absolute pressure piezo-transducer (HPS Series 902, MKS Instruments) to allow pressure reading from either 1-2000 mTorr or 1-1000 Torr.

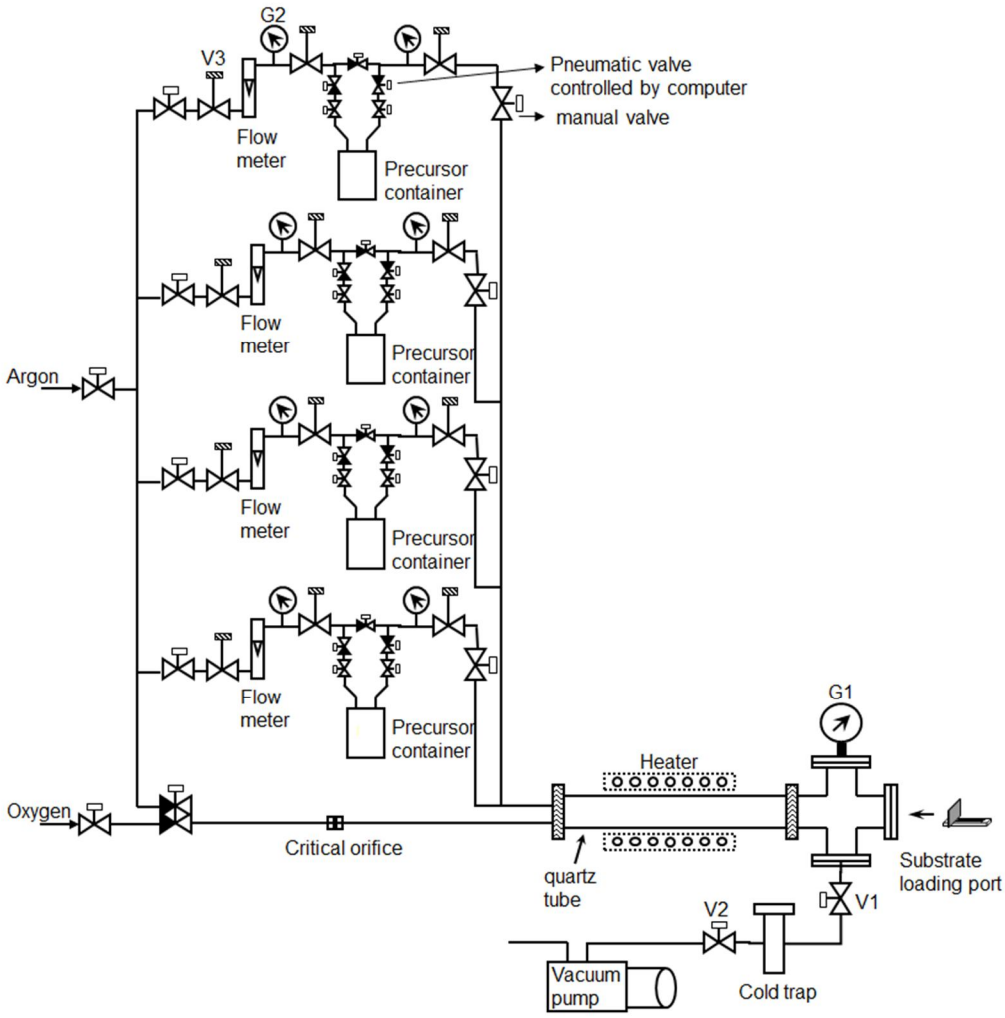

Figure 18. Custom-made MOCVD equipment configuration. Four canisters were able to hold for different organometallic precursors (nickelocene, n-butylferrocene and triphenylbismuth).

Thin films were deposited on p-type (100) Si substrates. The 1.5 cm × 2 cm substrates were placed on a quartz boat perpendicular to the gas flow direction. The film thicknesses were measured by spectroscopic ellipsometry (J. A. Woollam Co., Inc., model M-44).

X-ray photoelectron spectroscopy (XPS) was used to obtain the film element

composition and chemical state. This was done by Kratos AXIS-165 surface analysis system with a monochromatic Al Kα X-ray source. Quantitative study was done using relative sensitivity factors with the spectral peak areas obtained after Shirley background subtraction. The sputtering process cleaned the surface carbon contamination by using ~300 nA beam current argon ion gun for 10 minutes.

The film stoichiometry was measured by Rutherford backscattering spectroscopy (RBS) with a Tandetron accelerator employing 2 MeV He^{2+} particles. The backscattering spectra were collected via a silicon surface barrier detector at scattering angle of 150°.

The phase and crystallinity of the films were investigated using glancing-angle X-ray diffraction (GAXRD) in the θ-2θ scan mode. The GAXRD beam was at an incident angle of 0.7º using Philips X'pert equipped with a monochromatic Cu Kα source. MDI Jade 8.0 X-ray diffraction (XRD) pattern was used for processing data.

The structure and morphology of the deposited films was analyzed using a Siemens Diffraktometer D5000 in the powder diffraction mode with Cu K_α (λ = 1.5418 Å) X-rays. The measurements were performed at the setting of 40kV and 30 mA in the detector range $40° < 2\theta < 60°$. The scan step was 0.02° with a 1 s dwell. The peaks were identified using the International Centre for Diffraction Data (ICDD) database of diffraction pattern Powder Diffraction Files (PDF).

Film composition and morphology were studied in a Hitachi S-3000N scanning electron microscope (SEM) employed with an Oxford Inca Energy Dispersive X-ray spectroscopy (EDX) system. The analysis was done at 20 kV accelerating voltage.

WYKO NT3300 optical profiling system was used for imaging the topographic feature of thin film and calculating the surface roughness in the phase shifting interferometry measurement.

4.2.3. Results and Discussion

4.2.3.1. Rate Limiting Steps for Iron Oxide, Bismuth Oxide and Nickel Oxide Thin Films

In CVD system, there are some other processing parameters which are also essential for the fabrication of high quality metal oxide films. The Arrhenius plot for thin film deposition has two sections so called the rate-limiting steps. One is surface-reaction kinetics; the other is mass-transport process. High quality thin films can be obtained under the surface-reaction conditions. Temperature and pressure, these two parameters are the variables which determine the rate-limiting steps.

Pressure used for the bismuth oxide, nickel oxide and iron oxide films was usually controlled at around 5~20 Torr. That means the methods used so far are mainly based on low-pressure MOCVD. Because by lowering the pressure, the gas-phase transfers of reactants to the substrate's surface and diffusion out by the by-products both increase. The mass-transfer variables are much less critical than at high pressure. In our study, we found 15~17 Torr was a proper pressure range for later BFO and NFO films deposition. When reducing the pressure less than 1 Torr, the residence time of the reactant was short and the growth rate was low. During the recent experiments on NiO_x/FeO_x, the total pressure was kept around 16 Torr so far.

The reactor's temperature was usually kept at from 350~650 °C. However, as the

different precursor and delivery method were used, the chemical reaction's free-energy change (ΔG_r) was also changed. The maximum temperature of BFO films deposition is usually no more than 750 °C. Higher temperature helps to increase the K value of the chemical reaction, however, it also cause the mass-transfer effect remarkable. To grow crystalline stoichiometric BFO thin films, we used to keep the reactor's temperature at 550 °C. The temperature range for Bi_2O_3 deposition was in the range of kinetic control from our working temperature range, which was similar as the literature reported[76]. We could not investigate higher temperature range as this was limited by the heating range of our furnace. For NiO_x/FeO_x thin films deposition, the temperature kept from 400~500 °C as it was found that below 400 °C, the growth rates were in the surface reaction control regime and were very sensitive to the reactor's temperature (Figure 18). However, for higher temperature range, in the mass-transfer controlled process, the films cannot be deposited uniformly on the substrate due to the more significant influence of the gas flow profile.

Other parameters, like the flow rates of precursors and oxidizer, should also be considered carefully. Flow rates of precursors in our experiments were controlled by heating their bubble type vessels or sublimator. Carrier gas's flow rate didn't change during those experiments. Sufficient vapor should be generated by heating the vessel; however, if the temperature is too high, excess vapor will condense inside the reactor chamber, affect the base pressure of the CVD system and cause a waste. The proper temperatures for BFO/NFO precursor containers were listed in the later paragraphs with relatively high grow rates. The flow rate of oxygen was controlled by the orifice

and the pressure of gas cylinder. We calculated the amount of the oxygen and kept it at least 200 hundred times of the precursors' to ensure the complete oxidations of the precursors.

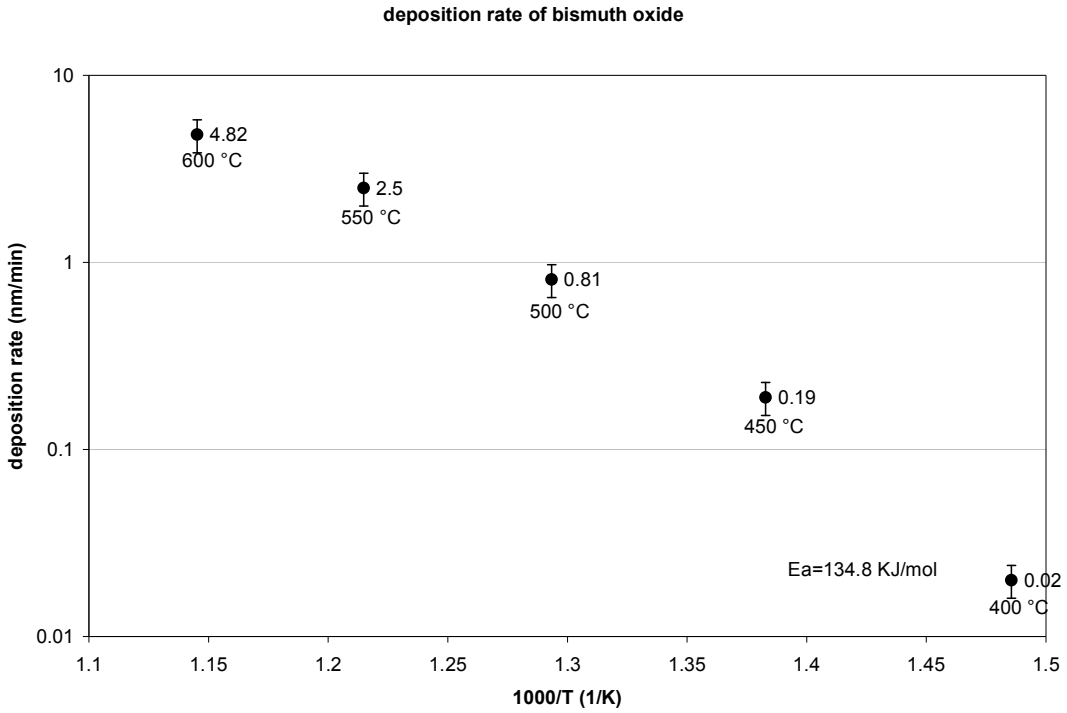

Figure 19. Arrenhnius plot of bismuth oxide thin films using MOCVD.

Condition for deposition of nickel oxide: total pressure=15 Torr, bubbler temperature=157.5 ºC, flow rate(oxgyen)=200 sccm, flow rate(carrier gas)=40 sccm.

From 400 ºC to 600 ºC, Bi_2O_3 deposition was in the range of kinetic control which was the same trend as the literature reported[76]. The activation energy was 134 KJ/mol, which was a little higher than the value given in that report (100±10 KJ/mol).

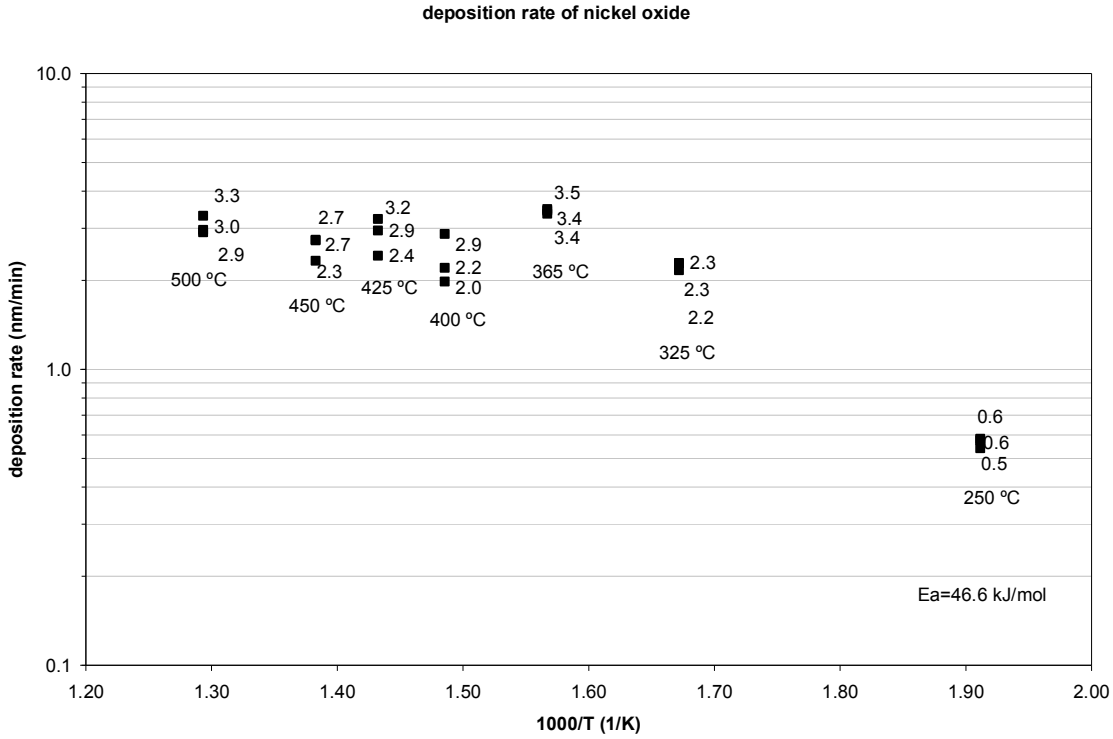

Figure 20. Arrenhnius plot of nickel oxide thin films using MOCVD.

Condition for deposition of nickel oxide: total pressure=16 Torr, sublimator temperature=60 ºC, flow rate(oxgyen)=122 sccm, flow rate(carrier gas)=59 sccm.

The kinetic control region was below 365 ºC. The films fabricated in this region had very good uniformity in thickness. Above 365 ºC, the mass-transfer dominated, causing a flat platform for the growth rate trend. The activation energy was calculated to be 46.6 KJ/mol.

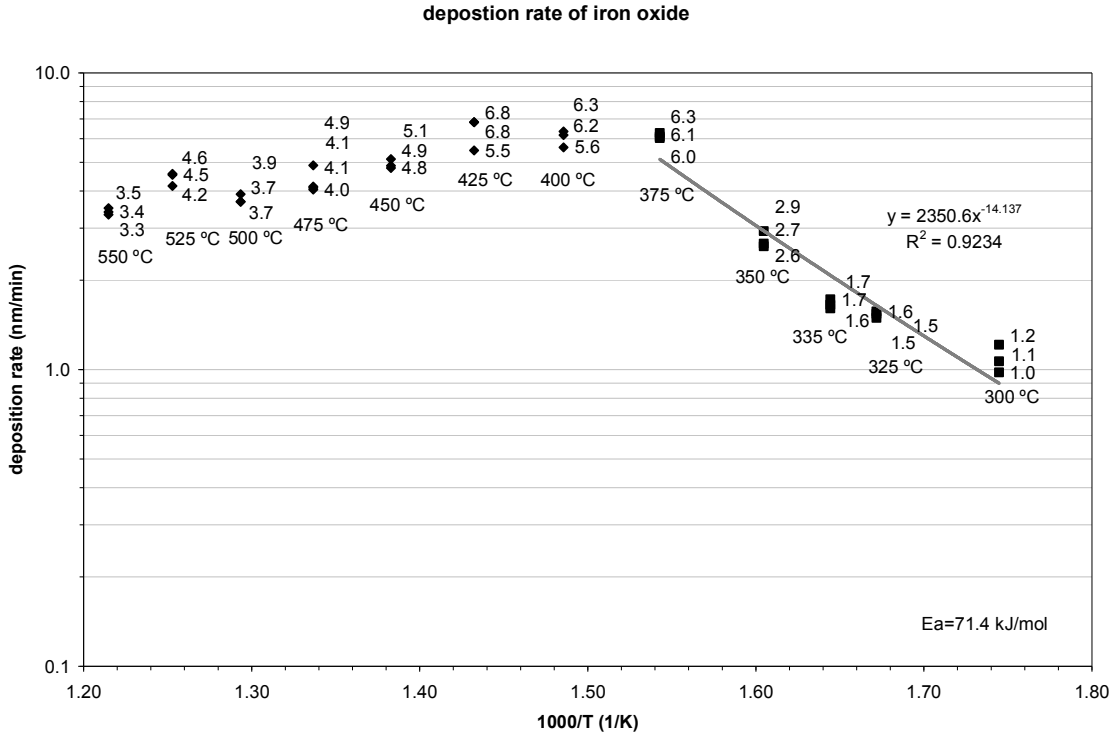

Figure 21. Arrenhnius plot of iron oxide thin films using MOCVD.

Condition for deposition of iron oxide: total pressure=16 Torr, bubbler temperature=62.5 ºC, flow rate(oxgyen)=122 sccm, flow rate(carrier gas)=59 sccm.

The uniformity of the sample was good before 375 ºC in the kinetic control region. Above this temperature, the mass-transfer effect caused lower growth rates for the lower part of samples. This was mainly due to the blockage of the quartz boat (sample holder).

Before 375 ºC, it was kinetic control region. The activation energy was calculated to be 71.4 KJ/mol. From 375 ºC to 450 ºC, mass-transfer effect dominated the reactions. The slowly decreasing growth rate at higher reactor's temperature (above 450 ºC) was because of more gas phase reaction and the decomposition of precursor before reaching the substrate surface, which was a common phenomenon in hot-wall

CVD process.

4.2.3.2. Characterizations

Iron oxide:

Composition of the films

The composition of the as-deposited films was analyzed using EDX (Figure 22). The films deposited at 450 °C were found to have about 8% carbon impurity. This would suggest that such a deposition temperature was likely not high enough to result in the decomposition of the precursor and removal of the resulting volatile organics, for the reaction chamber conditions used. The films deposited at higher temperatures had no detectable carbon contamination and the stoichiometry, within the limit of the accuracy (~ 5%) of the technique, was close to that of stoichiometric Fe_2O_3. This indicates that at these deposition conditions the organic ligands in the precursor molecules cleave cleanly during the deposition process.

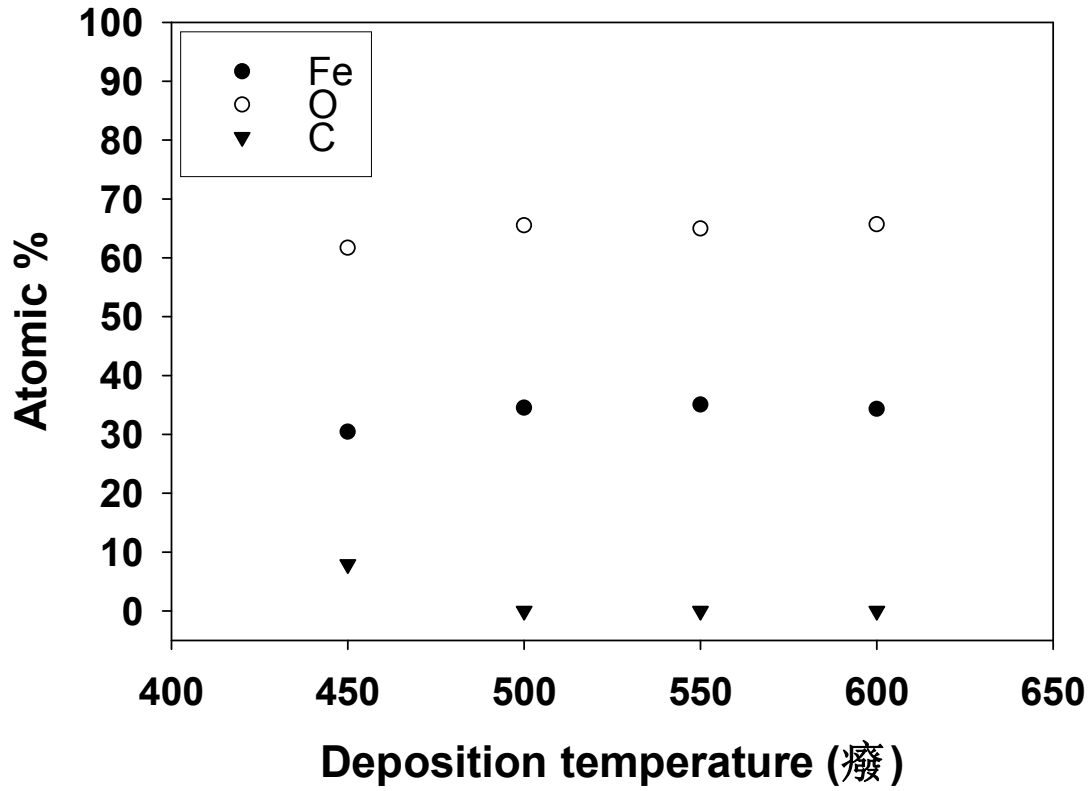

Figure 22. Composition of the iron oxide films deposited for 180 min as determined using EDX.

34 nm iron oxide film was also investigated using RBS. The result showed the atomic ratio of Fe and O was around 2/3, indicating the pure phase of Fe_2O_3 (Figure 23).

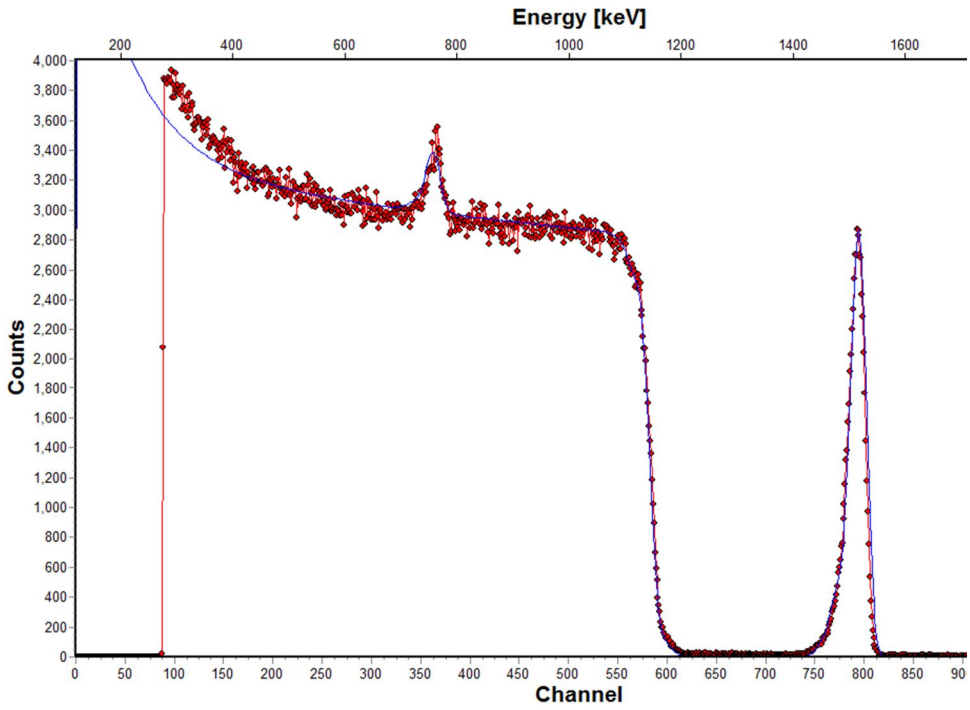

Figure 23. RBS result for iron oxide film composition. Atomic ratio of Fe : O was 39.4% :60.4%.

In order to probe the oxidation states of the elements present in the thin films, X-ray photoelectron spectroscopy (XPS) was also used. XPS is a surface sensitive technique for the analyses of the composition and chemical bonding states near the surface. Figure 24 shows the typical Fe 2p core spectrum for the deposited films. The Fe $2p_{3/2}$ and Fe $2p_{1/2}$ peaks are located at about 711 and 725 eV, respectively. There is a shake-up satellite at 719 eV that is indicative of the Fe^{3+} oxidation state. There is also a small step (indicated by arrow) in the $Fe2p_{3/2}$ peak which, in the literature, has

been reported to be characteristic for α-Fe_2O_3.[154, 155] This corroborates our XRD data in which only peaks corresponding to α-Fe_2O_3 were observed.

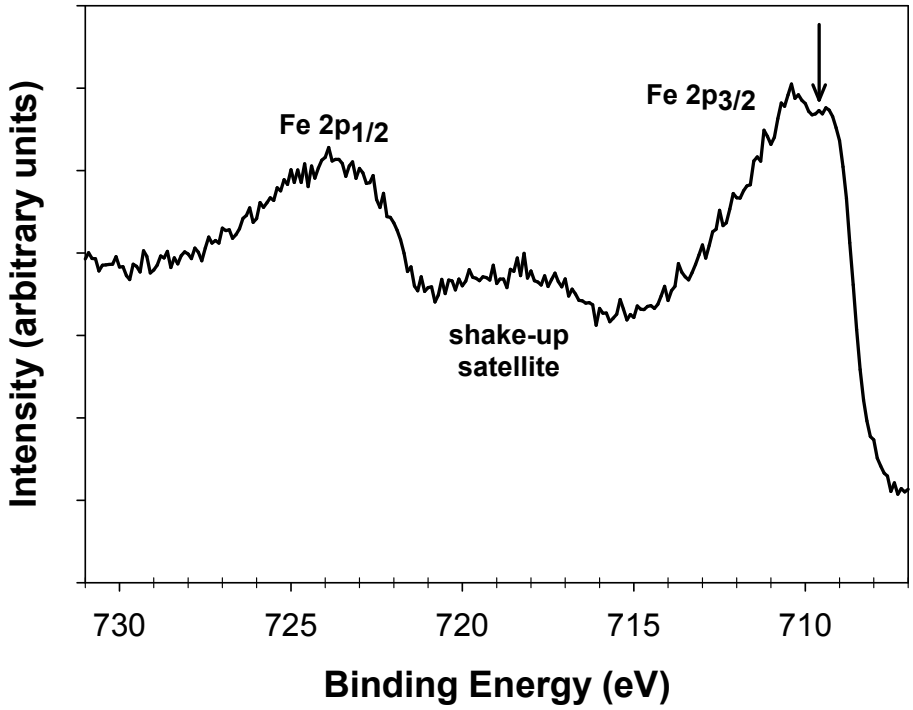

Figure 24. Normal incidence Fe 2p core XP spectrum of the iron oxide film deposited at 500 °C and 800 mTorr. The arrow indicates the small step present on the $Fe2p_{3/2}$ peak, which is indicative of α-Fe_2O_3.

Structure and morphology of the films

For studies on the phases of iron oxide present in the deposited films, films were grown for 180 min at temperatures 450-600 °C. In order to exclude interference from peaks of the substrate, the X-ray diffraction (XRD) scan was done in the region of 40° ≤ 2θ ≤ 60°. From the small intensities of the peaks in the diffraction spectrum shown in Figure 25 4(a), it could be inferred that the film deposited at 450 °C had very low crystallinity. The peaks at 40.85°, 49.48°, 54.09° and 57.59° corresponding to Fe_2O_3

[PDF# 33-0664] reflection planes (113), (024), (116) and (018) were observed. No other additional peaks from other phases were observed indicating that the films are single-phase α-Fe_2O_3. This is to be expected because the oxidizing atmosphere used for the deposition would preferentially lead to formation of α-Fe_2O_3 which is the most stable phase at high oxygen pressure and high temperature.[156] At 500 °C, the deposited films were highly crystalline with strong peaks corresponding to the preferred orientations (113), (024), (116) and (018) (Figure 25 4(b)). At higher deposition temperatures the relative intensity of the (113) reflection diminished considerably indicating changes in the morphology of the deposited films. The films were still crystalline α-Fe_2O_3 but the strongest reflection intensity changed from the preferred orientation (024) to that of (116) (Figure 25 4(c) and 4(d)). This indicates a change in the preferential growth plane due to the different crystal energy.[157]

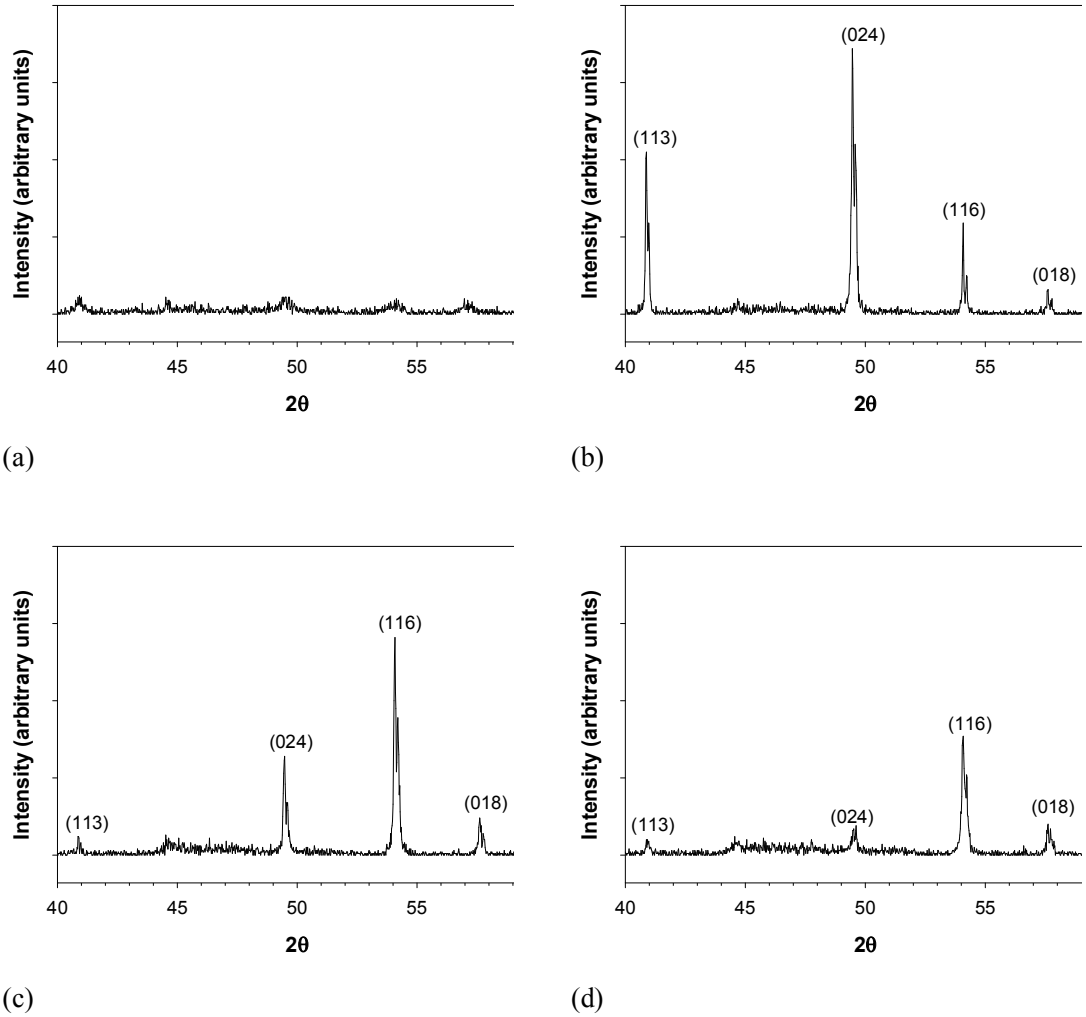

Figure 25. X-ray diffraction data for thin iron oxide films deposited on Si (100) substrates at (a) 450, (b) 500, (c) 550 and (d) 600 °C for 180 min.

Small-sized crystallites could be observed in the SEM image for the film grown at 450 °C (Figure 26(a)). This is in agreement with the XRD data where low degree of crystallinity was observed for these films. The crystallites developed into large (2-3 μm long) thin overlapping plate-like structures at 500 °C (Figure 26(b)). At 550 °C, the thickness of the plates increased (Figure 26(c)). For the films grown at 600 °C, the shape of the crystallites had changed from overlapping plate-like structure to closely packed crystallites with random shapes (Figure 26(d)). This corroborates the earlier results from the XRD patterns in which films grown at 600 °C showed mainly a strong (116) orientation in comparison with films deposited at lower temperatures. The finding that the shape and orientation of crystallites deposited at 600 °C is so different from those of the other films again supports the assertion (corroborated by XRD data) that there is a change in the preferential growth plane at higher deposition temperature.

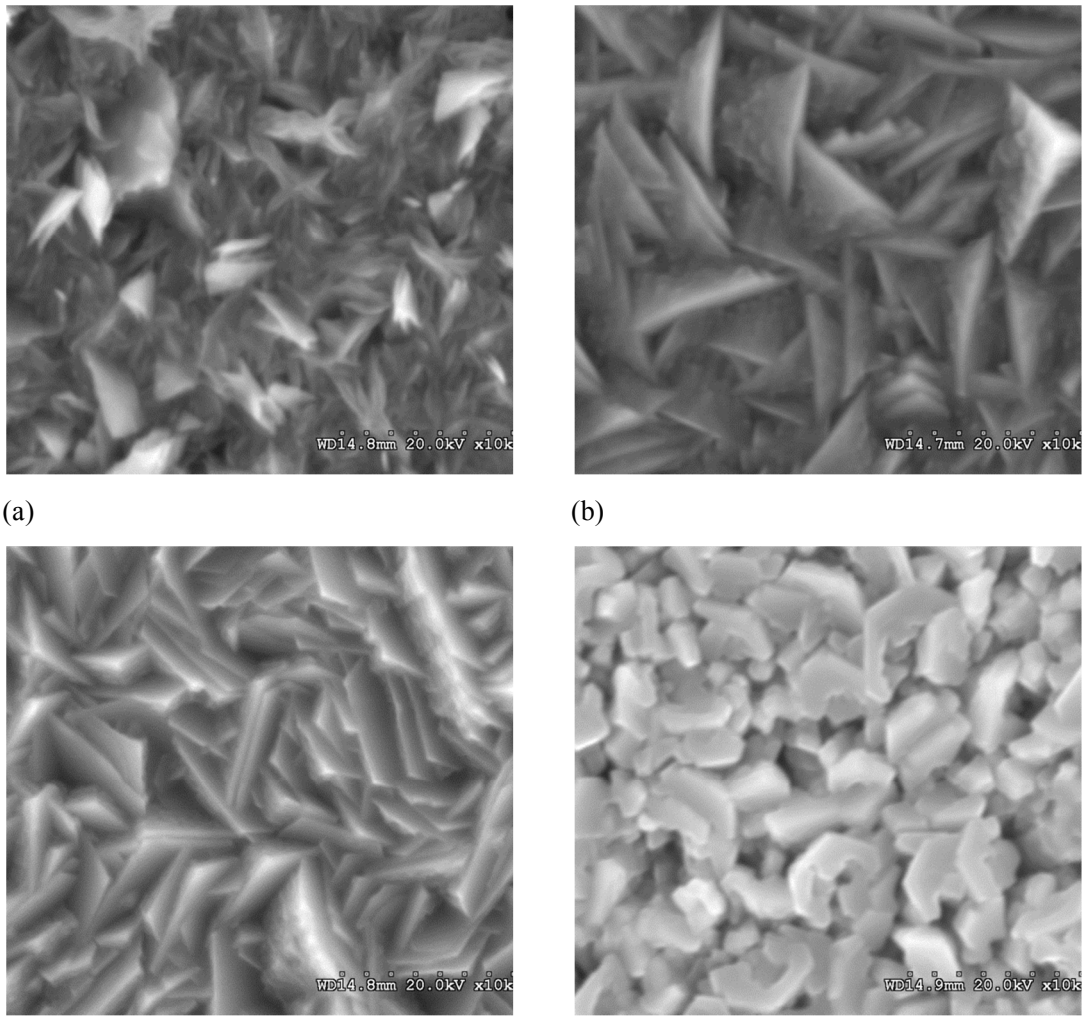

(a) (b)

(c) (d)

Figure 26. SEM images for thin iron oxide films deposited on Si (100) substrates at (a) 450, (b) 500, (c) 550 and (d) 600 °C for 180 min.

Bismuth oxide:

The XPS result showed that bismuth element was at +3 status because the core scan of Bi $4f_{5/2}$=164.5 eV and Bi$4f_{7/2}$=159.2 eV. Therefore the bismuth oxide contained the pure phase of Bi_2O_3. There were no other oxidation states for Bi. Therefore as Bi^0 was not shown here, there should only be Bi^{3+} inside the film.

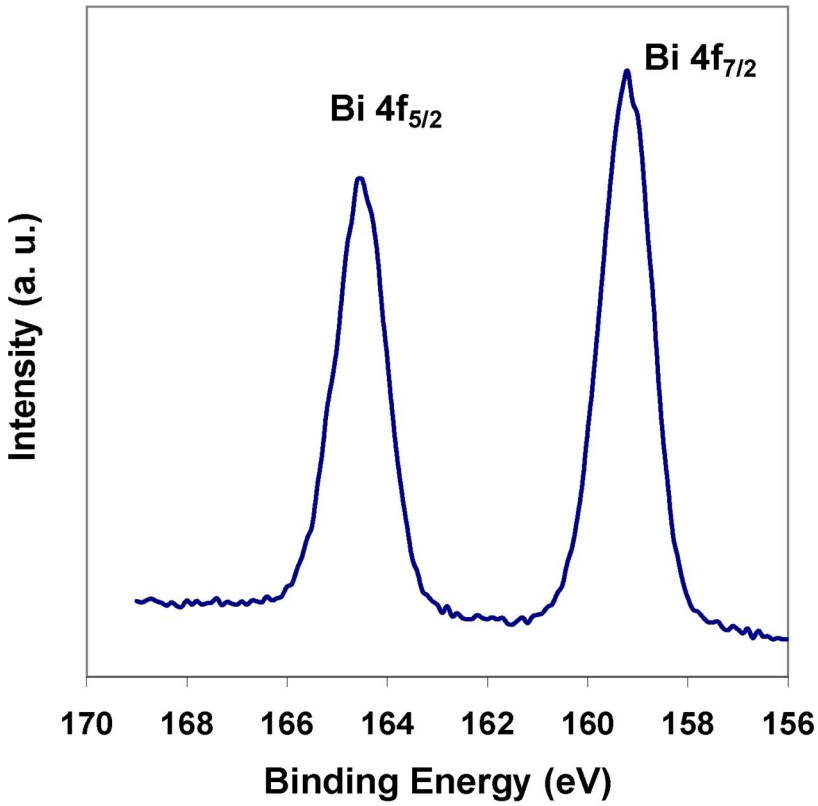

Figure 27. XPS core scan of Bi 4f.

Nickel oxide:

45 nm nickel oxide film was analyzed by RBS method. RBS result showed that the nickel oxide mainly contains NiO, and small amount of Ni_2O_3. This could also be confirmed by XPS O 1s scan (Figure 29). The Ni^{3+} state due to the Ni_2O_3 constituent could be proved by the strong peak at 532 eV. The other major constituent NiO had a peak at 529.3 eV for O 1s low binding energy component peak. For the small core line peak around 530-531 eV, there was minor amount of adsorbed OH^- species or O^- with coordinations integrated in the subsurface of the films, which was a common phenomenon of transition metal oxides.[158]

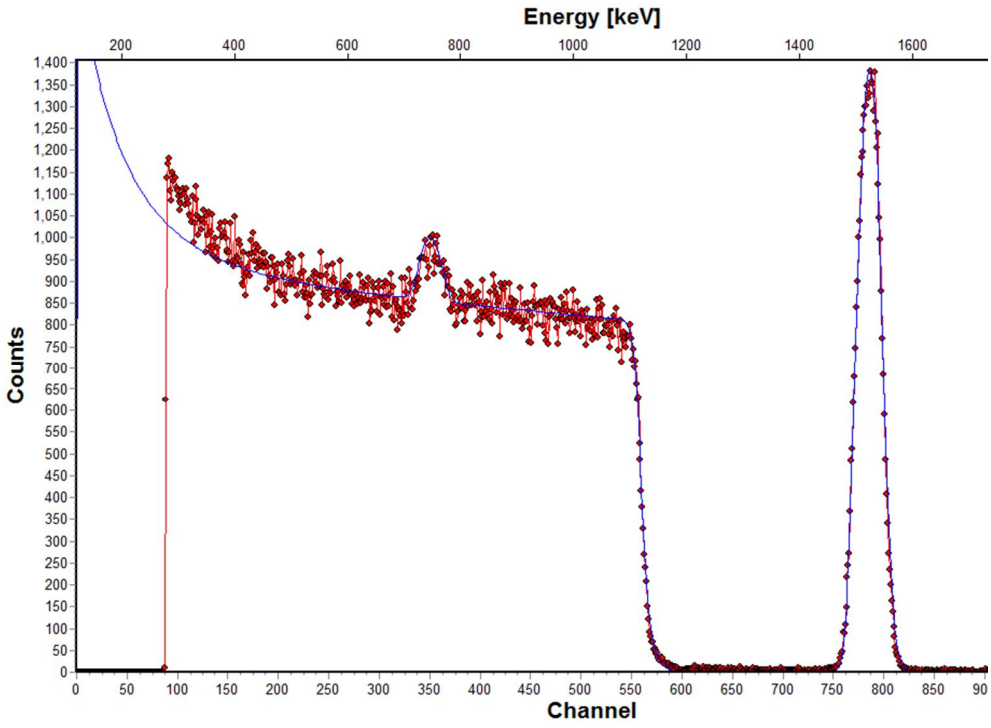

Figure 28. RBS result for the composition of whole nickel oxide thin film. Atomic ratio of Ni : O=45.3%: 54.6%.

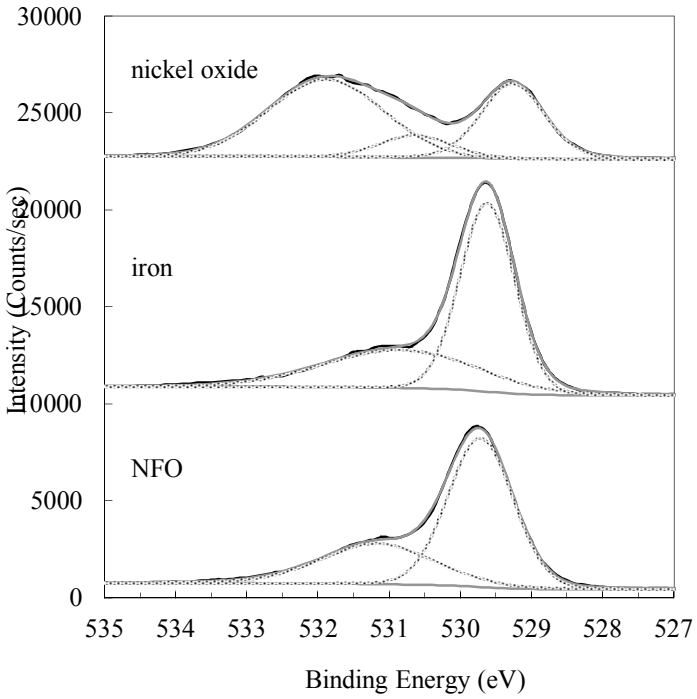

Figure 29. XPS spectra of the O 1s core scans for nickel oxide, iron oxide and NFO thin films.

4.2.4. Conclusions

Thin crystalline films of α-Fe_2O_3 on silicon substrates were successfully deposited using, for the first time, n-butylferrocene and oxygen. TGA characterization showed it to be a good MOCVD precursor; it is thermally stable and liquid at room temperature, air- and moisture-stable and undergoes clean evaporation without any decomposition. Temperature dependence on the growth rate of iron oxide films was studied. In the temperature range investigated, two growth rate regimes were observed: growth rates increased rapidly with deposition temperature at temperatures lower than 500 °C, while they were practically temperature independent at MOCVD temperatures greater than 500 °C. The activation energy in the kinetically-controlled regime was calculated to be 105 kJ/mol. The deposited Fe_2O_3 films were found to be phase-pure. The films exhibited low degree of crystallinity at low deposition temperatures (<500 °C) as indicated by XRD analyses. The films were crystalline at deposition temperatures higher than 500 °C and the preferential growth plane apparently changed at even higher temperatures. XRD, EDX and XPS analyses further indicated that the deposited films were α-Fe_2O_3. This precursor could be a viable iron MOCVD source that could be efficiently used to deposit iron-based ternary or higher oxides.

Bismuth oxide was found to have the kinetic controlled growth trend from 400 to 600 °C. The precursor was stable and not easily decomposed as the metallocene precursors. XPS result proved that the films were in the pure phase of Bi_2O_3. It was a good source of fabricating BFO thin films.

The nickel oxide thin films' growth trend was investigated and the mass transfer controlled step was found in the range of 365 °C to 500 °C. The reaction at higher temperature hadn't been looked into due to the limitation of the furnace. The RBS and XPS results proved that the nickel oxide thin film was a combination of NiO and Ni_2O_3. The precursor was using metallocene which had the same ligand as the novel iron precursor. This consideration helped prevent other side reactions to occur inside the reactor.

The reaction conditions and analysis results of these three metal oxides helped us to establish an optimized environment for fabricating BFO and NFO thin films. It played a basic but important role in later complex work.

4.3.Low Pressure Metalorganic Chemical Vapor Deposition of $BiFeO_3$ Thin Films

4.3.1. Introduction

Single-phase multiferroic materials, particularly $BiFeO_3$, have been the focus of a renewed interest in recent years. Bismuth ferrite ($BiFeO_3$) is multiferroic, having a high ferroelectric Curie temperature and developing spiral-antiferromagnetic order below 643 K. $BiFeO_3$ (BFO) is the only known single phase material which has multiferroic behavior at room temperature. Therefore, it has potential applications in non-volatile ferroelectric random access memory, spintronic devices, microwave technology, microactuators and sensors.[159] BFO thin films attracted special attention with regards to the future potential integration of BFO into the semiconductor technology and its large polarization which is an order of magnitude higher than its bulk form.[40] Recently, enhanced magnetization behavior has been reported for $BiFeO_3$ thin films, though the reasons for such enhancements are still not fully understood and are still debated.[15, 160]

Among the various preparation techniques, pulsed laser deposition (PLD) and chemical solution deposition (CSD) have been the main reported methods used for fabricating BFO films. There have been very few reports on using metal organic chemical vapor deposition (MOCVD) for depositing BFO films.[34, 38, 40, 87, 161] MOCVD technique is one of the suitable techniques for depositing such complex metal oxide structures for future commercially fabrication of microelectronic devices. These films can grow continously over large areas with good control of composition,

conformal step coverages and high uniformities. The applicability of this CVD technique is highly based on the availability of appropriate precursors which should have a stable and reproducible high vapor pressure, should not decompose during delivery to the reactor chamber, and is hazardous free.[162] Gas/liquid precursors are preferred over solid precursors because of the easier and reproducible control of their flow rates, and their higher volatilities in general.[69] The unavailability of suitable liquid precursors has been the major reason for so few reports on MOCVD of $BiFeO_3$. The commercially available iron precursors that have been used for the MOCVD of $BiFeO_3$ are iron(III) tris(2,2,6,6-tetramethyl-3,5-heptanedionate) [$Fe(tmhd)_3$ or $Fe(thd)_3$][34, 40, 87] and tris(diisobutyrylmethanato)iron [$Fe(DIBM)_3$][38]. Both these precursors are solids and have low decomposition temperatures. Therefore, these require non-conventional precursor delivery set-ups such as liquid injection[34, 38, 40] and solid feeder systems[87] thereby increasing the complexity of the deposition and film quality variability by introducing more parameters. Recently, we reported the first use of n-butylferrocene as a MOCVD liquid precursor for depositing iron oxide films.[163] n-Butylferrocene was shown to be an air- and moisture-stable liquid precursor with good thermal stability and sufficiently high vapor pressure for use in MOCVD. In the present study we report the electrical and magnetic properties of the MOCVD BFO thin films deposited using this liquid iron precursor.

Earlier reports on MOCVD of $BiFeO_3$ focused on the ferroelectric properties for non-volatile ferroelectric random access memory applications. Ueno et al deposited $BiFeO_3$ films on $SrRuO_3/SrTiO_3$ using $Bi((CH_3)_2(2\text{-}(CH_3)_2NCH_2C_6H_4))$ and

$Fe(C_2H_5C_5H_4)_2$ as precursors which, however, are not available commercially.[161] They did not observe ferroelectric behavior at room temperature due to large leakage currents and no data on magnetization was reported. Yang et al reported switched polarization values of 110-120 $\mu C/cm^2$ and 85-90 $\mu C/cm^2$ for $BiFeO_3$ films deposited on STO and STO/Si substrates, respectively, using $Fe(thd)_3$ and $Bi(thd)_3$ as precursors for their direct liquid injection MOCVD studies.[40] However, Tasaki et al reported a very small remnant polarization value (~2 $\mu C/cm^2$) measured at an unspecified temperature for their liquid injection MOCVD $BiFeO_3$ films deposited using $Fe(DIBM)_3$ and $Bi(p\text{-}Tol)_3$.[38] Again, no magnetization data were reported in either of these studies. More recently, Kartavtseva reported a saturation magnetization value of ~9 emu/cm^3 at 10 K for $BiFeO_3$ films deposited using $Fe(thd)_3$ and $Bi(C_6H_5)_3$.[41] Thery et al used $Bi(mmp)_3$ & $Fe(thd)_3$ for liquid injection MOCVD of $BiFeO_3$ films and reported a high saturation magnetization (~70 emu/cm^3) attributed to the presence of impurity phases. No direct data on ferroelectric properties was, however, reported in either of these reports.[34] In view of these varied and fragmentary results, we investigate the room temperature ferroelectromagnetic properties of MOCVD $BiFeO_3$ films deposited using a new combination of precursors.

4.3.2. Experimental

BFO nanofilms were prepared by MOCVD on platinized silicon substrates ($Pt(111)/TiO_2/SiO_2/Si$). They were fabricated in the horizontal hot wall low-pressure MOCVD reactor (Figure 30). The base pressure of the system was 30 mTorr. The

bismuth and iron precursor bubblers were kept at 160 °C and 62.5 °C, respectively. The delivery line section from those containers to the reactor was maintained 10-15 °C higher than the precursor's temperature to prevent condensation of the vapor phase. Argon (99.999% purity) with a flow rate of 40 sccm and oxygen (99.999% purity) with a flow rate of 200 sccm was used as carrier gas and oxidizer, respectively. The depositions were done at 550 °C under a total pressure of 15 Torr. All the valves were manually controlled and operated as the co-deposition mode that was to flow both precursors together into the reactor.

The film thicknesses were measured using spectroscopic ellipsometry (J. A. Woollam Co., Inc., Model M-44).

The phase and crystallinity of the film were characterized by glancing angle x-ray diffraction (GAXRD) in the θ-2θ scan mode. The GAXRD diffractogram were obtained at an incident angle of 0.5º using Philips X'pert equipped with a monochromatic Cu Kα source. The results were analyzed using MDI Jade 8.0 XRD Pattern Processing software.[5] X-ray photoelectron spectroscopy (XPS) was used to obtain the film stoichiometry and oxidation states of Fe and Bi. The XPS analysis was done using Kratos AXIS-165 Surface Analysis System with a monochromatic Al Kα X-ray source. Quantitative analysis was done using appropriate relative sensitivity factors with the spectral peak areas obtained after Shirley background subtraction.

The film topography and ferroelectric properties were studied with a Park Systems (XE-100E) scanning probe microscope in the dynamic contact mode electrostatic force microscopy (DC-EFM).[44] In these experiments performed at room

temperature, EFM images of the films were acquired by first polarizing the sample with a tip voltage of 10 V dc and then imaging the poled region by switching off the dc and applying an ac voltage with amplitude 0.25-0.5 V at 18 kHz. A Ti-Pt DC-EFM tip with a spring constant of 3.5 N/m was used for these studies. The topographic and EFM images of the films were obtained simultaneously. We measured the magnetization of the BFO thin film using a Quantum Design MPMS superconducting quantum interference device (SQUID) magnetometer. The room temperature magnetization curve was corrected for the background contribution from the diamagnetic substrate by fitting the high field magnetization. The temperature dependent magnetization was measured in an applied field of 1 kOe; these data were not corrected for the temperature independent diamagnetic background from the substrate. The dielectric constant at 18 GHz was measured with the sample placed in a wave guide and measurements of scattering parameters with a vector network analyzer.

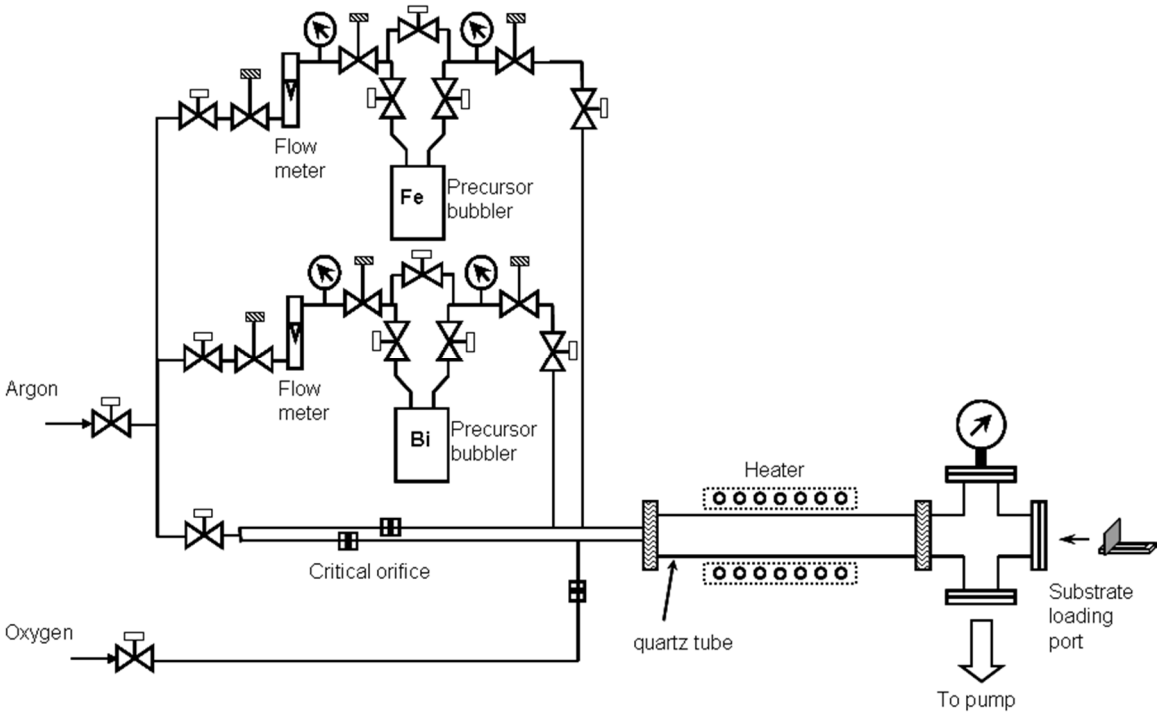

Figure 30. MOCVD equipment configuration for BFO thin film deposition (four canisters totally, using only two of them).

4.3.3. Results and Discussion

The GAXRD diffractogram for the deposited film is shown in Figure 31. The diffraction peaks (012), (104), (024) and (214) corresponding to rhombohedral (R3c spacegroup) $BiFeO_3$ (PDF pattern 04-009-2327) phase were observed indicating that the deposited film was polycrystalline $BiFeO_3$.[48] Furthermore, no secondary phases such as iron or bismuth oxides were observed. Figure 32 shows the XPS scans of the Fe 2p and Bi 4f core regions. In the Fe 2p core scan, the $2p_{3/2}$ peak is positioned at 710.5 eV, with an additional distinctive shake-up satellite peak observed at 719 eV. These features indicate that the oxidation state of Fe in the deposited BFO films is Fe^{3+}.[164] In the Bi 4f spectrum, the $4f_{7/2}$ peak is located at 159 eV, indicating that Bi is in the 3+ oxidation state.[164] Moreover, quantitative analysis showed the Bi:Fe ratio to be unity, within the experimental uncertainty of the technique.

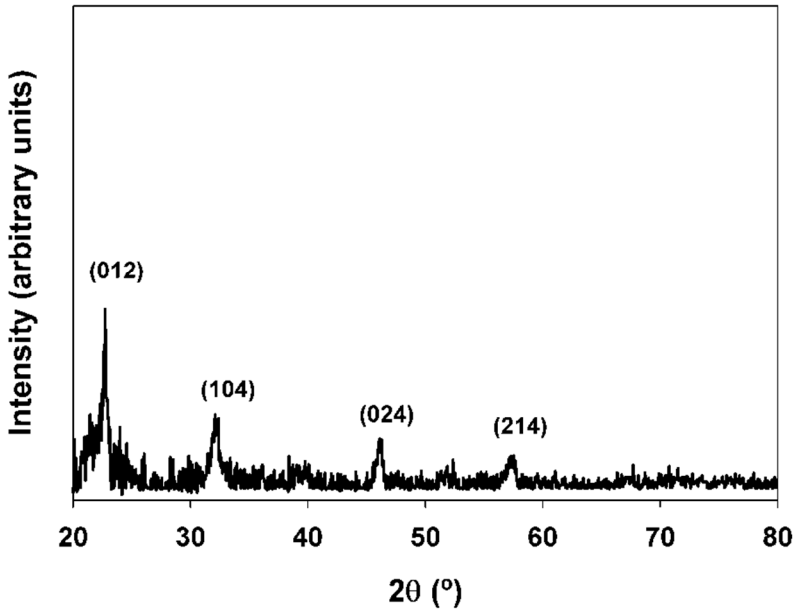

Figure 31. GAXRD diffraction patterns of $BiFeO_3$ 170 nm-thick nanofilm deposited at 550 °C and 15 torr system pressure.

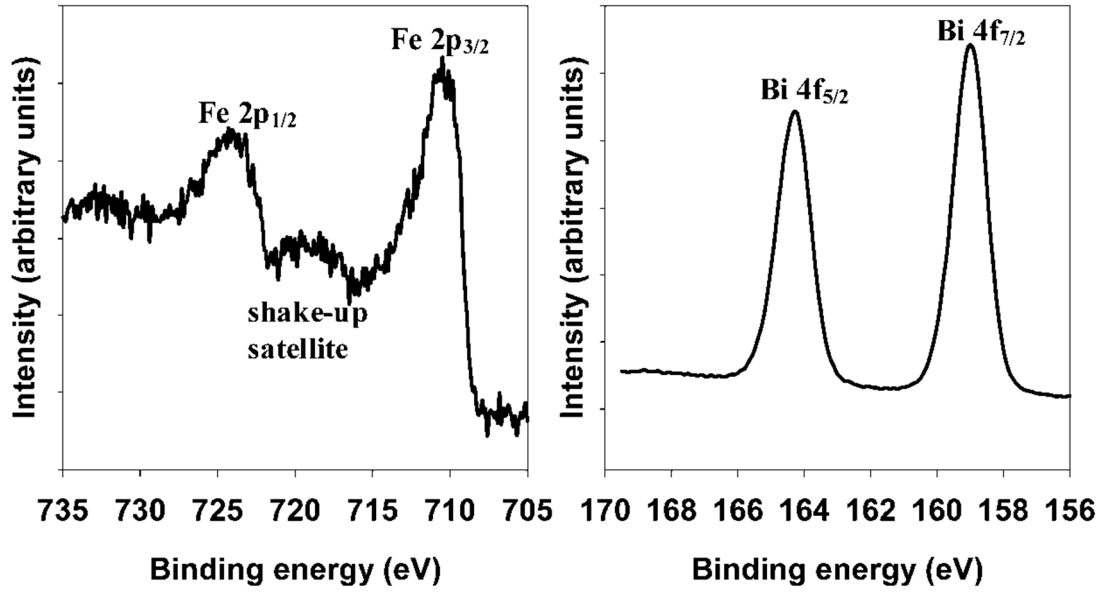

Figure 32. X-ray photoelectron spectra of the (a) Fe 2p line and (b) Bi 4f line of the $BiFeO_3$ nanofilm.

The AFM topographical image is shown in Figure 33 (a) and is indicative of this area of the film free of voids or defects. In order to probe the ferroelectric characteristics of this sample, we poled a portion of the film with 10V dc applied to the tip as it was scanned over 5×5 μm^2 area of the film (scan speed = 5ms/pxl over 1024×1024 pxl^2). We then obtained DC-EFM images of a 10x10 μm^2 area of the film that included the poled region. The images were obtained at different intervals of time elapsed after the initial poling. Figure 33 (b) shows representative EFM images for a 170 nm-thick film. The poled region appears as bright area with the unpoled region having a darker contrast than the poled region. As time elapsed, the charge density of the single-poled region remains invariable. Figure 33 (c) shows profiles of the EFM intensity as a function of time for t = 1 min to t = 143 min after poling. It is observed that the film retains its polarization over this period. The EFM measurements clearly indicate the ferroelectric nature of the films, although additional data such as P(E) would be helpful to obtain further information on the ferroelectric order.

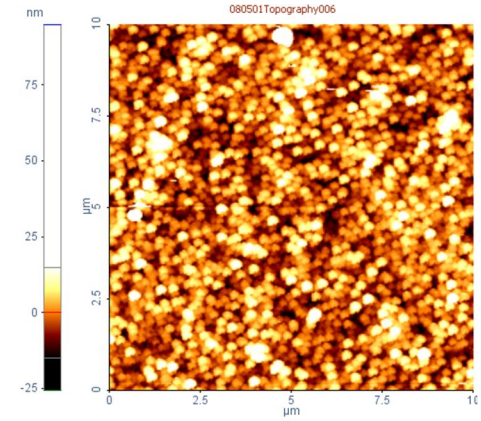

(a)

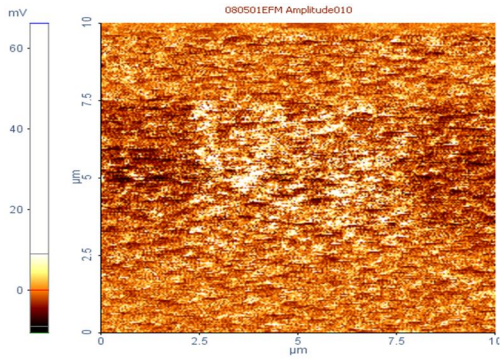

(b)

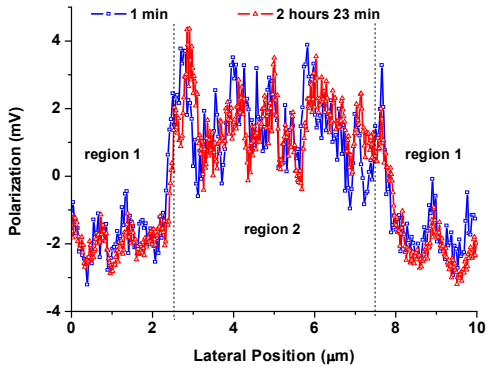

(c)

Figure 33. (a) Topographic images of the 170 nm-thick $BiFeO_3$ film grown at 550 ˚C, (b) EFM image of the films 1 min poling, and (c).EFM intensity vs. time profiles after poling. Regions 1 and 2 are unpoled and poled regions, respectively.

These BFO films prepared by MOCVD also exhibited weak ferromagnetism. The room temperature magnetic hysteresis loop, shown in Figure 34(a), yields a saturation magnetization of approximately 8 emu/cm^3. This is in agreement with the magnetization expected in bulk $BiFeO_3$ (~7 emu/cm^3) as suggested by density functional theory calculations,[8, 34] and is also consistent with the values observed previously for phase pure BFO thin films grown by PLD and CSD.[160, 165] Higher values have earlier been reported in literature, however, the enhancement of magnetization in those reports has been attributed to the presence of either Fe^{2+} ions or γ-Fe_2O_3 precipitates in the films.[34, 158, 160] Thus, the saturation magnetization value obtained in the present study is a further indication of the high quality of the films as evidenced by the XRD and XPS results discussed earlier. We also plot the temperature dependent magnetization in Figure 34(b). The small peak near 50 K likely arises from magnetic ordering of oxygen adsorbed on the surface of the film,[16] but we also observe a significant magnetic anomaly near 140 K that could be related to a spin-reorientation transition at this temperature as suggested by Raman measurements on single crystal BFO.[46] This decrease in magnetization associated with a magnetic transition in $BiFeO_3$ is consistent with our argument that the room temperature magnetization observed is an intrinsic property of these samples.

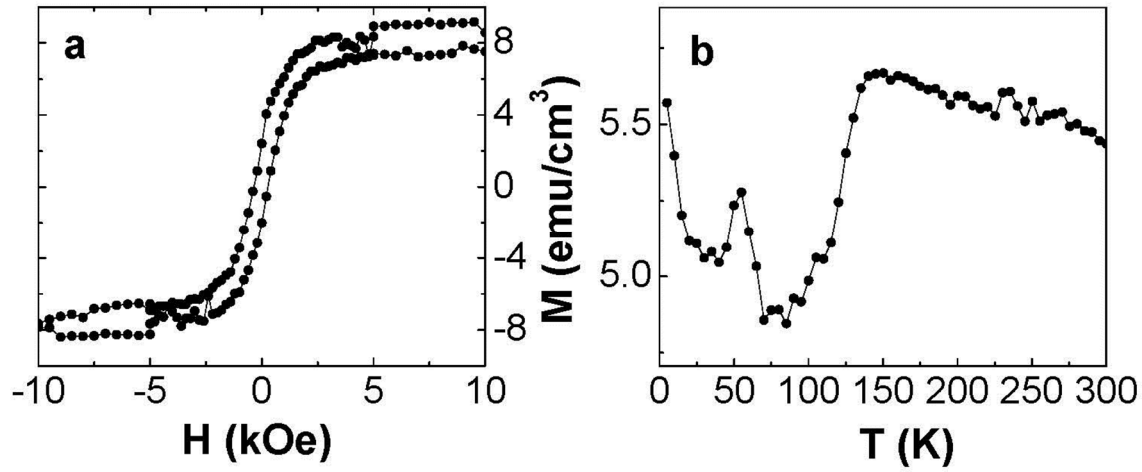

Figure 34. (a) $BiFeO_3$ magnetization as a function of applied magnetic field measured at 300 K; (b) $BiFeO_3$ magnetization as a function of temperature measured at 1 kOe.

Evidence for magneto-dielectric coupling in the samples was obtained through the measurements of H dependence of real (ε′) and imaginary (ε″) parts of the effective dielectric constant for the film and the substrate at 18 GHz. The choice of microwave frequencies for the measurement was to demonstrate the *magnetic field* control of a ferroelectric device such as a resonator. A vector network analyzer (Agilent E8361A) and commercial materials property measurement software (Agilent 85071) were used to obtain data on the real and imaginary parts of the dielectric constant. The technique involves inserting a sample of dimension approximately equal to the cross section of an 18-26.5 GHz waveguide and measurements of reflection and transmission coefficients. The permittivity of the sample was estimated from the microwave reflection and transmission data.[166]

Figure 35 shows such data for the 170 nm film. With increasing H, an increase in ε′ and a decrease in ε″ are observed. The magnetic field tunability of the permittivity $\delta\varepsilon'/\varepsilon'$ is on the order of 9% for H = 4 kOe which must be compared with 10% tunability for $TbMnO_3$ for H = 90 kOe at very low temperatures.[167] The BFO films may have potential use in tunable high-frequency devices.

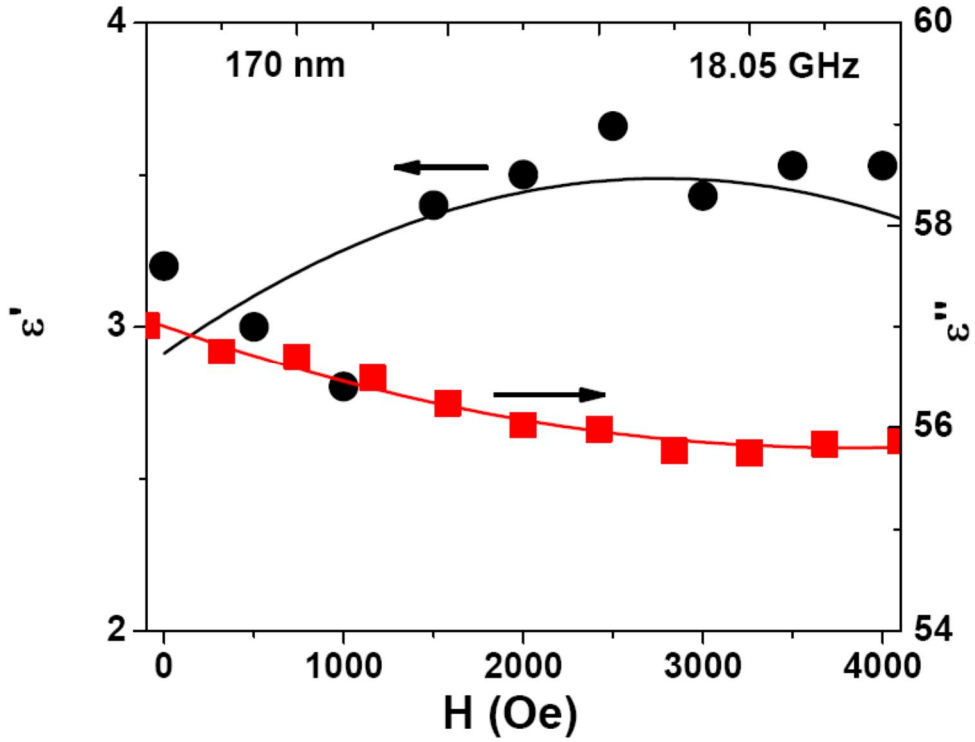

Figure 35. Magnetic field dependence of real and imaginary parts of the relative dielectric constant at 18.05 GHz for the 170 nm-thick film on the substrate.

Effects of different substrates-Various substrates have been used for the fabrication of BFO films. From Table1, the lattice parameters of each kind of substrate were shown. The lattice mismatch between BFO and its epitaxial under layer can cause strain in plane and elongated out of plane. For instance, less than 30 nm thick $BiFeO_3$ with good crystallinity on $SrRuO_3/SrTiO_3$ (100) is fully epitaxial strained.[168] This strain can cause the formation of monoclinically distorted structure which leads to a larger polarization. The orientations of the substrate also influence a lot on the properties of the BFO films. The BFO films prefer to grow on $SrTiO_3$ (111) rather than $SrTiO_3$ (100) substrates and have higher polarization value.[60]

Table 1. Some lattice constants of different substrates for BFO film deposition

Substrate	Lattice constant (Å)
$BiFeO_3$ (100)	3.96
Si (100)	3.14
SiO_2 (100)	4.91
$SrTiO_3$ (100)	3.91
$SrRuO_3$ (100)	3.93
$La_{0.7}Sr_{0.3}MnO_3$ (LSMO)	3.88
$LaNiO_3$ (100)	3.84
$(LaAlO_3)_{0.3}$-$(Sr_2AlTaO_6)_{0.7}$ (LSAT) (100)	3.87
$DyScO_3$ (110)	3.94

When grown on Si substrate, it is necessary to use a buffer layer which can be $Pt/TiO_2/SiO_2$ or $SrTiO_3$ as a template layer. [169] LSMO is a good choice for a ferromagnetic substrate. It has *a*-axis lattice constant closely matching typical perovskite ferroelectric materials. It can be made into ferroelectric-ferromagnetic composite. [170] Among those substrates, $SrTiO_3$, $(La,Sr)MnO_3$, $LaNiO_3$ and Pt work as the conducting bottom electrodes to measure the ferroelectric property of BFO films.

4.3.4. Conclusions

$BiFeO_3$ thin films were grown on platinized silicon substrates at 550 °C by MOCVD using a liquid iron precursor n-butylferrocene. Electrostatic force microscopy evidenced the ferroelectric properties at room temperature in the $BiFeO_3$ films and also indicated that the films had good charge retention properties. From

SQUID measurements at 300 K a saturation magnetization value of ~8 emu/cm^3 was obtained. Coupling between the magnetic and dielectric subsystems has been demonstrated through magnetic field dependence of dielectric permittivity. Thus the existence of both a weak ferromagnetism and ferroelectricity at room temperature was demonstrated for deposited $BiFeO_3$ films. n-butylferrocene and triphenylbismuth form a promising combination of MOCVD precursors for depositing crystalline $BiFeO_3$ films.

4.4.Cyclic-Deposited $NiFe_2O_4$ Thin Films using Low Pressure Metalorganic Chemical Vapor Deposition

4.4.1. Introduction

The focus of this study was to fabricate and characterize high quality nano scale thin films of nickel ferrite (NFO) using metalorganic chemical vapor deposition (MOCVD). NFO is not only a superior material for future integration of high-frequency microwave device, but also a promising magnetic phase for magnetoelectric (ME) heterostructures due to its low anisotropy, high permeability with high resistivity, low eddy current losses and smaller coercive field.[18-21] The NFO thin film can produce the magnetostrictive phase in heterostructural multiferroics, exhibiting better ME coupling effect than single phase ME material. Multiferroic magnetoelectric materials[124] have attracted increasing research interest in recent years. Although some single-phase materials exhibit ME effect, these pure phase materials, for instance $BiFeO_3$, may suffer from problems such as current leakage, weak ME coupling and low ordering temperatures.[10-12] Furthermore, since most of these compounds have definite composition, the possibility of optimization of

the magnetoelectric property via ion substitution or doping is limited. Consequently, heterostructures such as bilayered/multilayered thin films, nanopillars and nanowires are more promising for future controlled switching at the nanoscale. The ME coupling effect was theoretically calculated to be higher in a multilayered structure.[171] Ferromagnetic nanopillar arrays embedded in ferroelectric materials exhibited enhanced ME coupling coefficient which circumvented the problem of the clamping effect for the nano-layered composites.[172] The NFO has been a ferromagnetic phase to be fabricated with other piezoelectric materials to form ME nanocomposites, such as $NiFe_2O_4$(NFO)-$Pb(Zr_xTi_{1-x})O_3$ (PZT) [173], $NiFe_2O_4$-$BaTiO_3$ [174], $NiFe_2O_4$-$Ba_{0.7}Sr_{0.3}TiO_3$[175] and NFO-BFO [176].

Various fabrication approaches can be used for growing NFO, such as pulsed laser deposition, sputtering, e-beam reactive evaporation and chemical solution deposition. Very few studies reported the MOCVD process of NFO films. Fitzgerald and Ito reported NFO films using chlorides as precursors[177, 178], which may not be desired for CVD processes due to the corrosive effect of the resulting byproducts; acetylacetonato complexes were once used as precursors, but they needed high reaction temperature.[179] Studies based on direct liquid injection CVD process[180-182] could lead to stoichiometric NFO films with a small amount of carbon contamination (<2%) and formation of undesirable nano particles (10-150 nm) due to incomplete precursor decomposition and gas-phase nucleation.[182] The present study introduces a flexible MOCVD setup to perform fabrications of NFO nano films. The ferromagnetic NFO thin films were deposited via either a cyclic- or co- /deposition method at a low pressure. Due to CVD's advantages of conformal coverage over a large area, good

stoichiometric control and high throughput, such a fabrication process can be a suitable technique to deposit NFO nano films with desired properties.

4.4.2. Experimental

Nickelocene (purity 99%) and n-butylferrocene (purity 99%) were purchased from Strem Chemicals. Nickelocene is green crystalline powder with a vapor pressure of 0.179 Torr at 60 °C.[100] N-butylferrocene is a novel precursor which was first introduced in our earlier work on iron oxide and bismuth ferrite depositions.[123, 183] It is a liquid precursor with brownish orange color at room temperature and is stable in the presence of both air and moisture. The vapor pressure is calculated to be 0.036 Torr at 62.5 °C from experimental data.[124]

Thin NFO films were fabricated in a horizontal hot wall low-pressure MOCVD reactor (Figure 36). The reactor was a 48 cm in long, 38 mm in diameter quartz tube positioned inside a furnace (model 1043 Marshall, ThermCraft, Inc.). Dual-tube gas feed through allowed both precursors and oxidizers to be introduced into the reactor with precise dosage control (Figure 36). The base pressure of the system was less than 30 mTorr. Argon (99.999% purity, Airgas) was kept at a flow rate of 60 standard cubic centimeter per minute (sccm) and was used as the carrier gas for precursor delivery. The sublimator of powder nickelocene and the bubbler of liquid n-butylferrocene were kept at 60 °C and 62.5 °C, respectively. The gas lines from those canisters to the reactor were maintained at least 20 °C higher than the precursors' temperatures to prevent condensation. Oxygen was used as the oxidizer at a flow rate of 150 sccm.

With the calculation of the flows through sublimator and bubbler saturated with precursors (assuming the carrier gas completely mixed with precursors' vapor) as ideal gases, the molarity of precursor generated within a certain time could be calculated and the estimated molar ratios used were O_2: $Ni(C_5H_5)_2$ =240:1 and O_2: $Fe(C_5H_4C_4H_9)(C_5H_5)$ =1200:1.

All depositions were done at a total pressure of 17 Torr from 200 °C to 550 °C. Pneumatic valves were controlled automatically by a LabVIEW 8.2 program and were capable to deliver four precursors together or individually (Figure 36 and Figure 37). The bypass design for the four precursor lines were used to stabilize system pressure and flush the delivery lines. This way, nickel ferrite thin films could be fabricated by either co-deposition or cyclic-deposition mode. Thin films were deposited on p-type (100) Si substrates subjected to an RCA clean prior to deposition. Those 1.5 cm × 2 cm substrates were placed on a quartz boat perpendicular to the gas flow direction. The post-annealing process was performed in a Lindberg/Blue Three Zone Tube Furnace at 700 °C for 1 hour; after analysis, the same samples were further annealed at 1000 °C for another hour to study the film morphology and magnetic property. Argon was flowing through the furnace during the annealing processes.

The film thicknesses were measured with spectroscopic ellipsometry (J. A. Woollam Co., Inc., model M-44). X-ray photoelectron spectroscopy (XPS) was used to quantify the film element composition and chemical states. This was done in a Kratos AXIS-165 surface analysis system with a monochromatic Al Kα X-ray source. Quantitative studies were done using relative sensitivity factors and the spectral peak

areas obtained after Shirley background subtraction. The sputtering process cleaned the surface carbon contamination by using ~300 nA beam current argon ion gun for 10 minutes. The film stoichiometry was measured by Rutherford backscattering spectroscopy (RBS) with a Tandetron accelerator employing 2 MeV He^{2+} particles. The backscattering spectra were collected via a silicon surface barrier detector at the scattering angle of 150°. The NFO film structure and crystallinity were investigated using glancing-angle X-ray diffraction (GAXRD) in the θ-2θ scan mode. The GAXRD beam was at an incident angle of 0.7º using Philips X'pert equipped with a monochromatic Cu Kα source. The MDI Jade 8.0 X-ray diffraction (XRD) pattern was used for processing data. A WYKO NT3300 optical profiling system was used for imaging the topographic feature of the NFO thin films and calculating the surface roughness in the phase shifting interferometry measurement. NFO film magnetization was measured by quantum design superconducting quantum interference device (SQUID) magnetometer at 300 K (Oakland University).

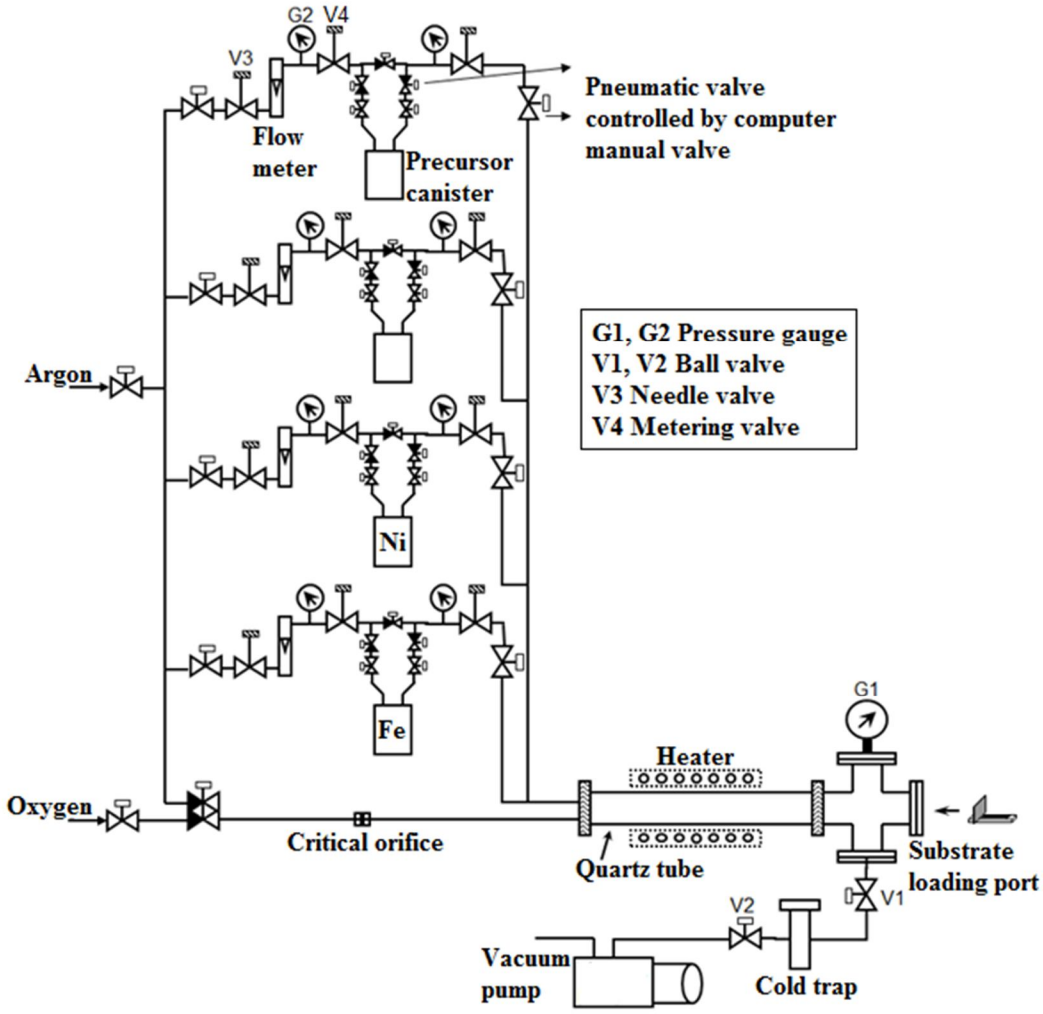

Figure 36. Schematics of the experimental setup used in the deposition of nickel oxide, iron oxide and nickel ferrite thin films. Two of the four canisters contain organometallic precursors.

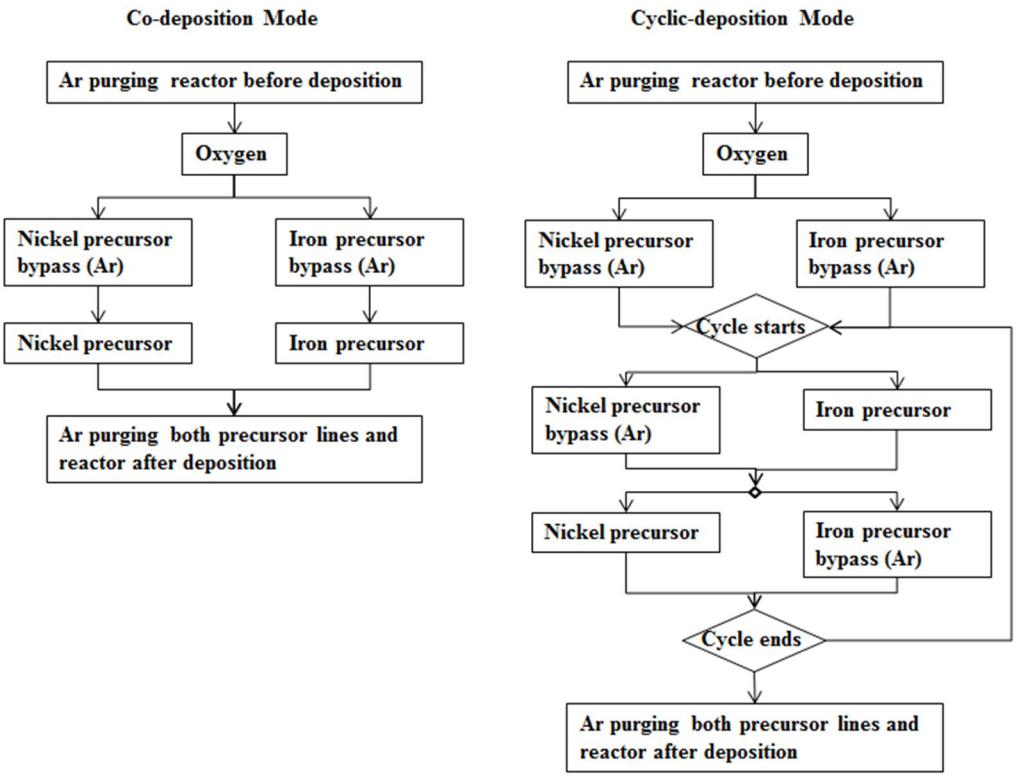

Figure 37. Flow charts of two deposition processes for nickel ferrite thin film fabrication (nickel precursor: nickelocene, iron precursor: n-butylferrocene). Process conditions are identical for both flow charts.

4.4.3. Results and Discussion

Investigation for MOCVD process parameters

Growth rates for nickel oxide, iron oxide films were studied so as to fabricate stoichiometric NFO films under optimized deposition conditions. Figure 38 shows the growth rate of each metal oxide film versus temperature of the precursor canister. Figure 38 (a) manifests nickel oxide growth rate at 400 °C reaction temperature and 12 Torr. Figure 38 (b) corresponds to the iron oxide growth rate at 400 °C and 500 °C, at 12 Torr. As the precursor temperatures increased, the precursor vapor pressure ramped up exponentially (experimental data fitted according to the Antoine equation

[100, 124]) resulting in a higher precursor concentration in the carrier gas flow. Therefore, both deposition rates of nickel oxide and iron oxide thin films apparently increased exponentially.

Figure 39 shows the growth rates of those two metal oxide films versus the reactor temperature. Below 300 °C, the nickel oxide growth kinetics is found to be dominated by surface reaction with growth activation energy (Ea) of 57±5 kJ/mol. [184] At the higher temperature region (300 to 365 °C) the E_a is found to be 10±5 kJ/mol. The total E_a was a little lower than the reported data by Jin-Kyu Kang[98] and Wen-chang Yeh[97]. The observation of the slight increase of the nickel oxide deposition rate from 300 to 365 °C is likely because the reaction rate is fast and the reactants/byproducts' diffusion may become a controlling factor for the deposition process; the data shows almost a flat temperature window indicating that the rate-limiting step is mass transfer[184].

For the iron oxide deposition process, the low temperature region below 375 °C is apparently reaction controlled while the higher temperature region becomes mass transfer controlled. The E_a of iron oxide growth is found to be 80±5 kJ/mol, i.e., slightly higher than the value of 75 kJ/mol in deposition using ferrocene[122] perhaps because more energy was needed for detaching cyclopentadienyl ligand. The decreasing deposition rate above 425 °C is likely due to precursor decomposition and depletion. The precursor is prone to react in the gas phase due to increasing gas phase nucleation and decomposition before it reaches the hot substrate surface.[122] This phenomenon was also indicated by the grayish film morphology and the some visible

small particles found on the film surface after high temperature processing.

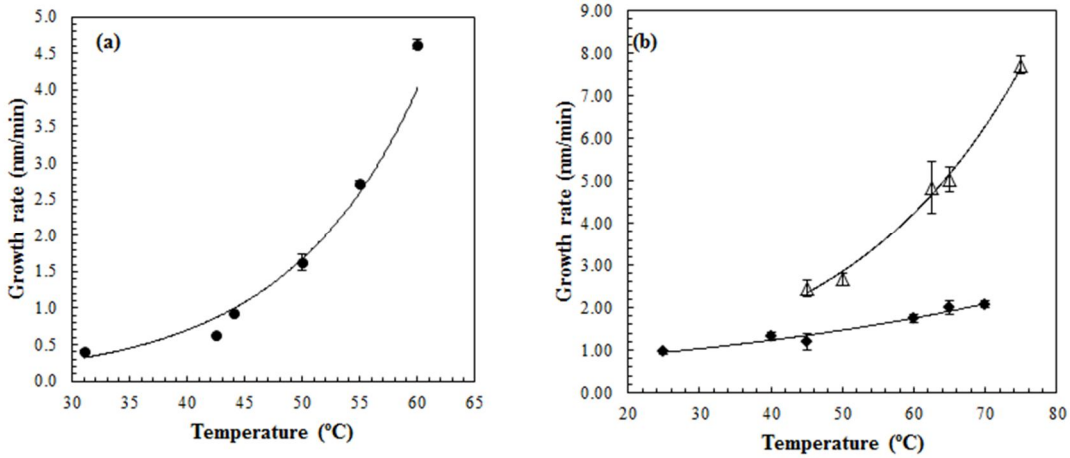

Figure 38. Growth rates of metal oxide films versus precursor container temperature. (a) nickel oxide film growth rate vs $T_{nickelocene}$ ($T_{reactor}$=400 °C); (b) iron oxide film growth rate vs $T_{n\text{-}butylferrocene}$. △: $T_{reactor}$=400 °C and : ◆: $T_{reactor}$=500 °C.

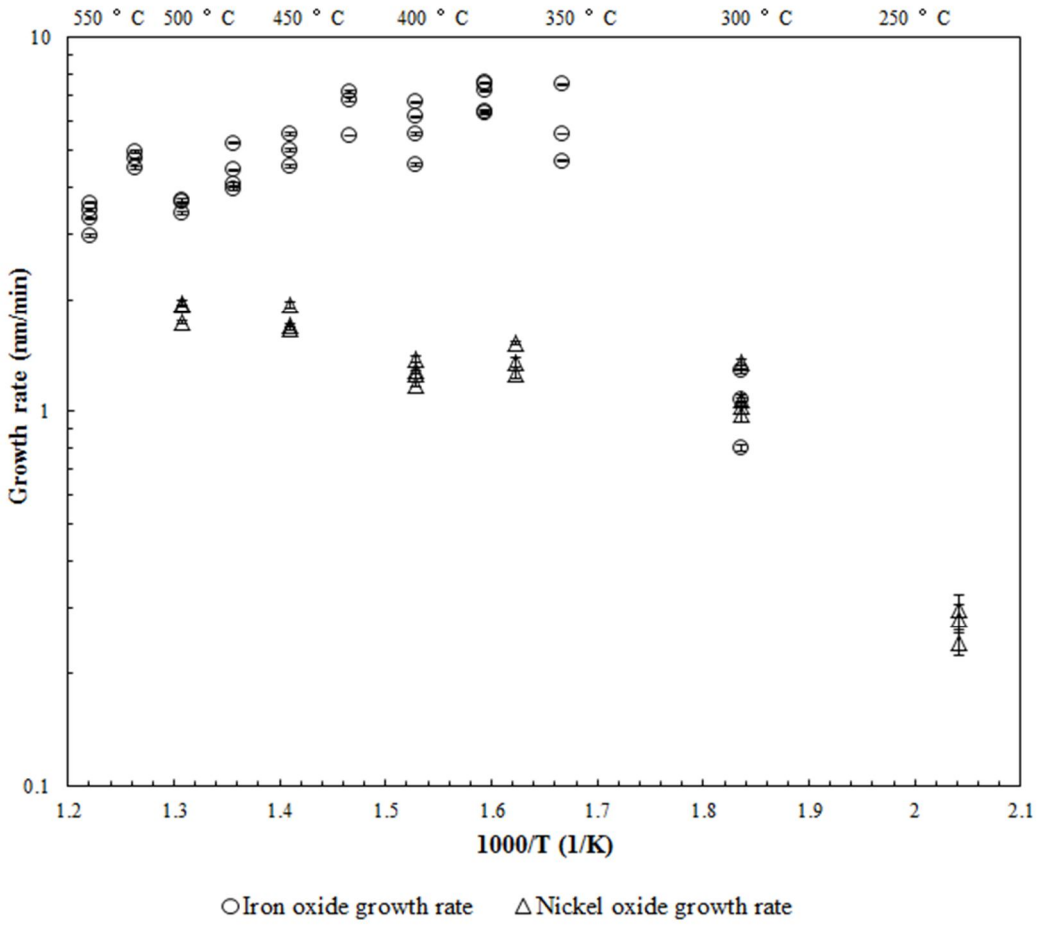

Figure 39. Arrhenius plot for iron oxide and nickel oxide depositions. $T_{n\text{-butylferrocene}}$=62.5 °C, $P_{reactor}$=12 Torr for iron oxide films; $T_{nickelocene}$=60 °C, $P_{reactor}$=12 Torr for nickel oxide films.

For the thermogravimetric analyses of the two organometallic precursors,[101, 123] the n-butylferrocene had a clean evaporation from 150 °C to 240 °C, leaving only 2% residue after the decomposition at 310 °C. The nickelocene had a clean sublimation from 170 °C to 190 °C, leaving around 5% residue after decomposition at 186 °C. The differences between the two oxides' growth modes could be controlled by both the decomposition temperatures and the amount of precursors. Nickelocene was present at a higher concentration than that of n-butylferrocene in the reactor as stated in the

experimental section.

With different CVD apparatuses and depositing conditions, the growth rates of the two metal oxides may vary.[97, 98, 123] The nickel oxide has similar growth rates but different Ea than that reported by Jin-Kyu Kang.[101] On the other hand, iron oxide deposition resulted in lower growth rates compared with those in our earlier work,[123] likely due to differences in the precursor delivery (the n-butylferrocene canister was at 80 °C in our earlier study resulting to almost 4.7 times higher vapor pressure than the one used here). Differences in CVD apparatus, such as temperature detection and control, pressure stabilization and automatic valving, might also have accounted for some of the difference in the iron oxide growth rate (Table 2).

Table 2. Development of the CVD apparatus for iron oxide growth

	Earlier CVD apparatus	newly designed CVD apparatus
Bubbler temperature	80 °C	62.5 °C
Flow rate	Oxygen-40 sccm; Carrier gas-35 sccm	Oxygen-150 sccm; Carrier gas-60 sccm
Reactor temperature control	±5 °C	±1 °C
Pressure control	Flow meter stables in 30 s at the beginning of CVD process; P(reactor)=0.8 torr	Bypass tubing; no pressure fluctuation; P(reactor)=12 torr
Valve type	Manually-operated	Computer controlled

In order to balance the precursor consumption and throughput, the nickelocene sublimator was kept at 60 °C and n-butylferrocene bubbler was kept at 62.5 °C. For better film crystallinity, lower contamination and robust growth rate, the optimal

reactor temperature was found at 500 °C.[123] At these conditions, a much larger average crystal grain size was observed in nickel oxide[98] which is desired to form a polycrystalline nickel ferrite thin film structure. The two metal oxides had different deposition rates at the described process conditions, making the cyclic deposition mode a more viable path for obtaining stoichiometric NFO thin film. The apparatus parameters were investigated, especially for the two precursors' purging ratios (Figure 41). The anticipated atomic ratio of Fe/Ni is 2, i.e., close to stoichiometric NFO, and our findings approached this value when the molar ratio of n-butylferrocene/nickelocene (Fe/Ni) reached 0.5. The data in Figure 40 shows a monotonic, almost linear trend through the regression analysis with R^2=0.96, indicating that the cyclic control was effective in tuning film compositions. The optimal cyclic NFO deposition had a growth rate of 1.6±0.2 nm/min with precursor purging time of 60 s for nickelocene and 155 s for n-butylferrocene in each cycle. The growth rate of co-deposition of NFO film was determined to be 3.0±0.2 nm/min.

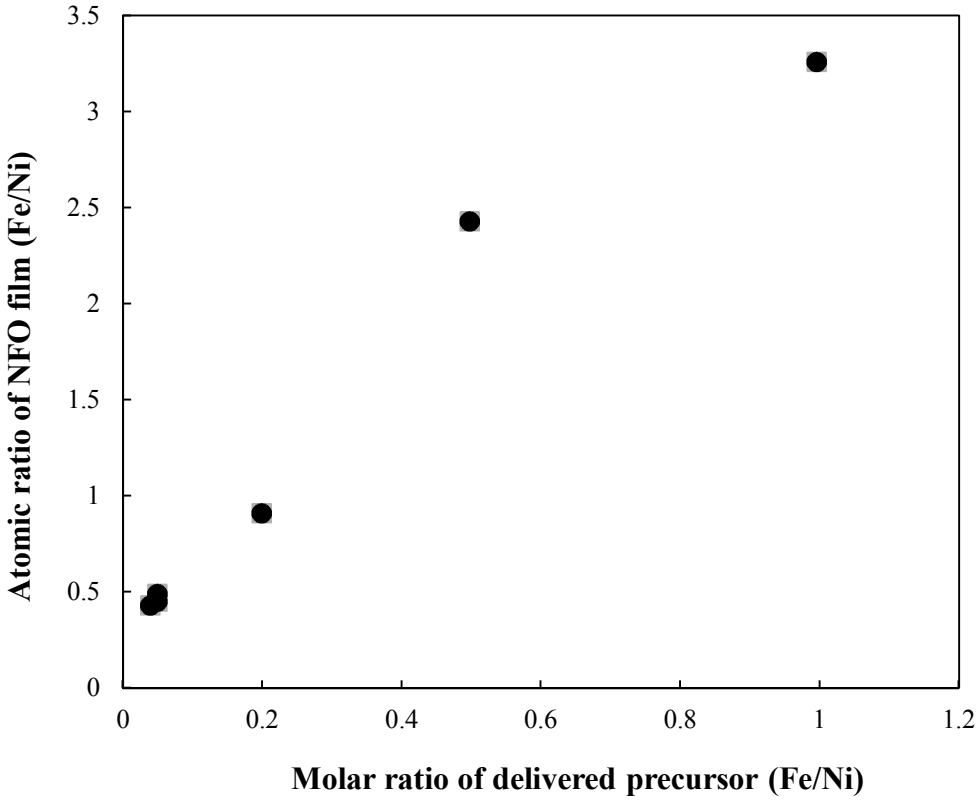

Figure 40. Composition vs precursor molar ratio of the nickel ferrite films deposited through the cyclic mode. NFO films composition were calculated from XPS data using Shirley background correction.

NFO thin film composition

The Figure 41 shows the survey XPS scans of all elements in 500 °C cyclic-deposite NFO thin film, before and after 10 min-long sputtering. The sputtered thin film was found free from carbon contamination (at 284.6 eV), indicating that the MOCVD process results in a complete surface reaction without precursor residue or

by-products. The unsputtered film was estimated to have 12.5±1% Ni, 25.8±1% Fe, 43.3±1% O and 18.4±1% C, i.e. $Ni_{1.1}Fe_{2.2}O_{3.7}$. The lower ratio of oxygen and higher ratio of carbon are likely due to adsorption or incompleted decomposition of the two precursors at the film surface and the likely surface contamination from the air. After sputtering for 10 min, the atomic ratio of Ni/Fe remained 2 and the concentration was calucated to be 13.2% Ni, 27.3% Fe, 59.5% O, i.e. practically $NiFe_2O_4$.

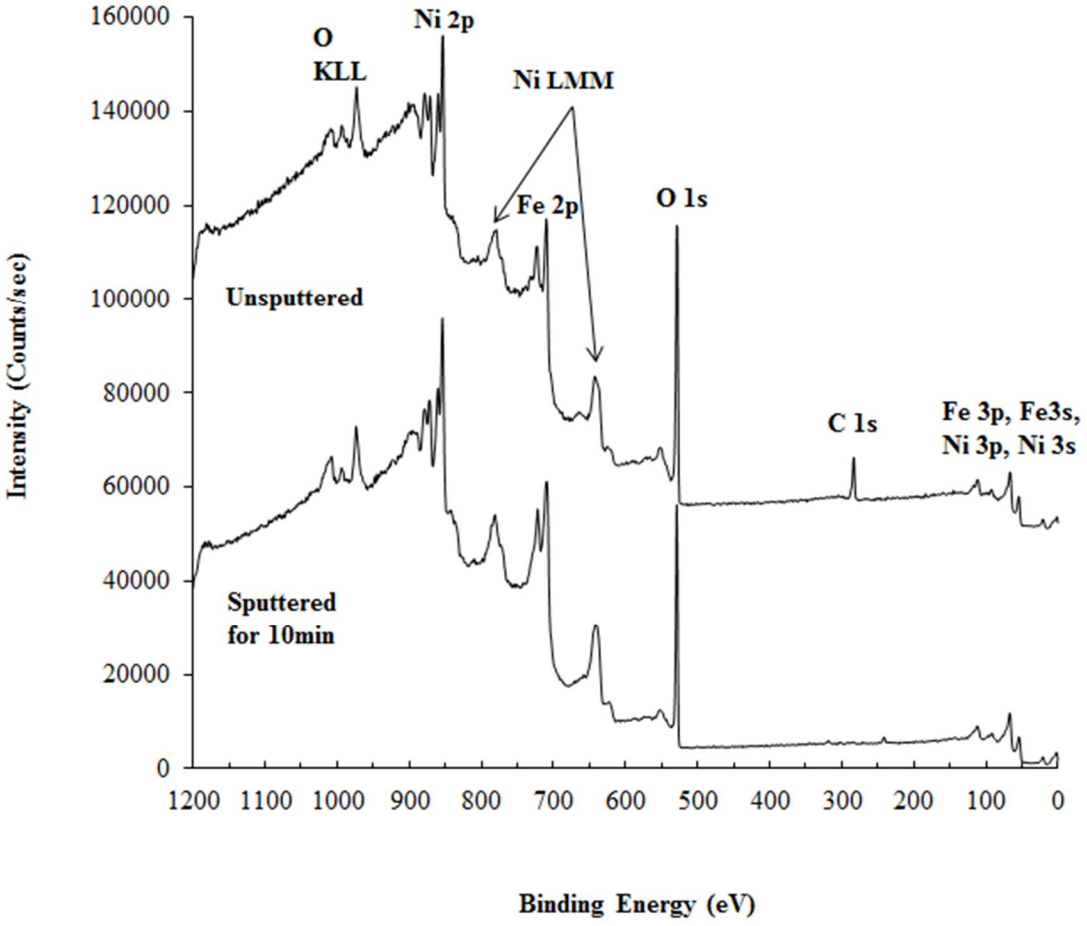

Figure 41. Survey scan of unsputtered and sputtered cyclic deposited NFO thin films. At 284.6 eV, the survey plot has no C 1s peak, indicating that the sputtered film is carbon free.

In the XPS core scans for Ni 2p3/2, Fe 2p and O 1s, the deconvolution of peaks are used to further identify small features of each peak. All the peak positions and full width at half maximum (FWHM) are shown in Table 3. In Figure 42 (a) and (c), the Ni $2p_{3/2}$ XPS core scan of nickel oxide thin film deposited under the same condition as NFO films shows no Ni^0 state at 852-853 eV.[185] The shoulder peak at 855.5 eV indicates the Ni^{3+} due to the Ni_2O_3 constituent in the nickel oxide sample. This is also corroborated by the 532.3 eV peak of the O 1s XPS core scan (Figure 43 (a)). The other major constituent, NiO, has peaks at 853.6 eV for Ni $2p_{3/2}$ main peak and 529.3 eV for O 1s.[186] The core scan of the nickel ferrite sample, both the Ni $2p_{3/2}$ main peak at 854.1 eV and the satellite peak at 861.2 eV are seem to shift to higher binding energies than those of nickel oxide thin film, indicating the formation of new metal oxide compound. The feature of Ni^{3+} appears to be as a shoulder of the main peak, resulting in an asymmetric Ni $2p_{3/2}$ peak.[187, 188]

In Figure 42 (b), the shoulder peak and the shake-up feature of iron oxide XPS core scan are indicative of α-Fe_2O_3.[123, 155] The absence of these features for the NFO XPS core scan (Figure 42 (d)) suggests that all the Fe atoms are in the structure of $NiFe_2O_4$.[155]

In Figure 43 and Table 3, the O 1s oxidation states of those different films are compared using XPS core scans. At $T_{reactor}$=500 °C and excess amount of oxygen (150 sccm), features of both Ni_2O_3 and NiO are found for nickel oxide film (Figure 43 (a)), while a pure Fe_2O_3 phase is seen for the iron oxide film(Figure 43 (b)). The nickel ferrite sample results in one strong main peak at 529.7 eV, suggesting a sole oxidation

state of nickel ferrite lattice oxygen (Figure 43 (c)).)). In all cases, there are two small peaks at ~531 eV and ~532 eV indicating a small amount of adsorbed OH^- species (likely from the air) and O^{2-} incorporation in the subsurface of the films, which is rather common in transition metal oxides.[158]

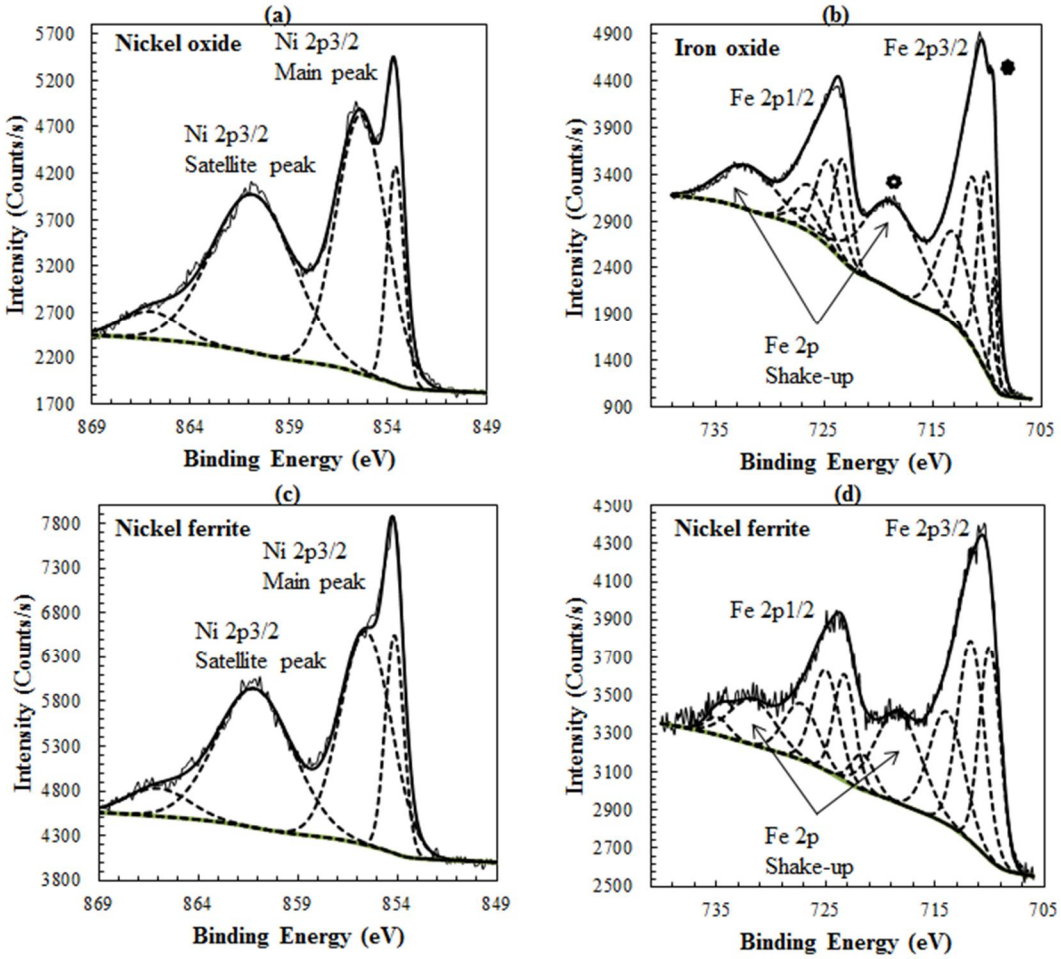

Figure 42. XPS core scans of Ni 2p and Fe 2p for as-deposited (a) nickel oxide thin film; (b) iron oxide thin film; (c) and (d) cyclic-deposited nickel ferrite thin film. In (a), black star ✹ refers to the shoulder peak of Ni^{3+}. In (b), the ✹ and ✿ refer to the shoulder peak and the shake-up features of α-Fe2O3, respectively, which disappear in NFO. Samples prepared conditions: $T_{reactor}$=500 °C, $P_{reactor}$=17 Torr.

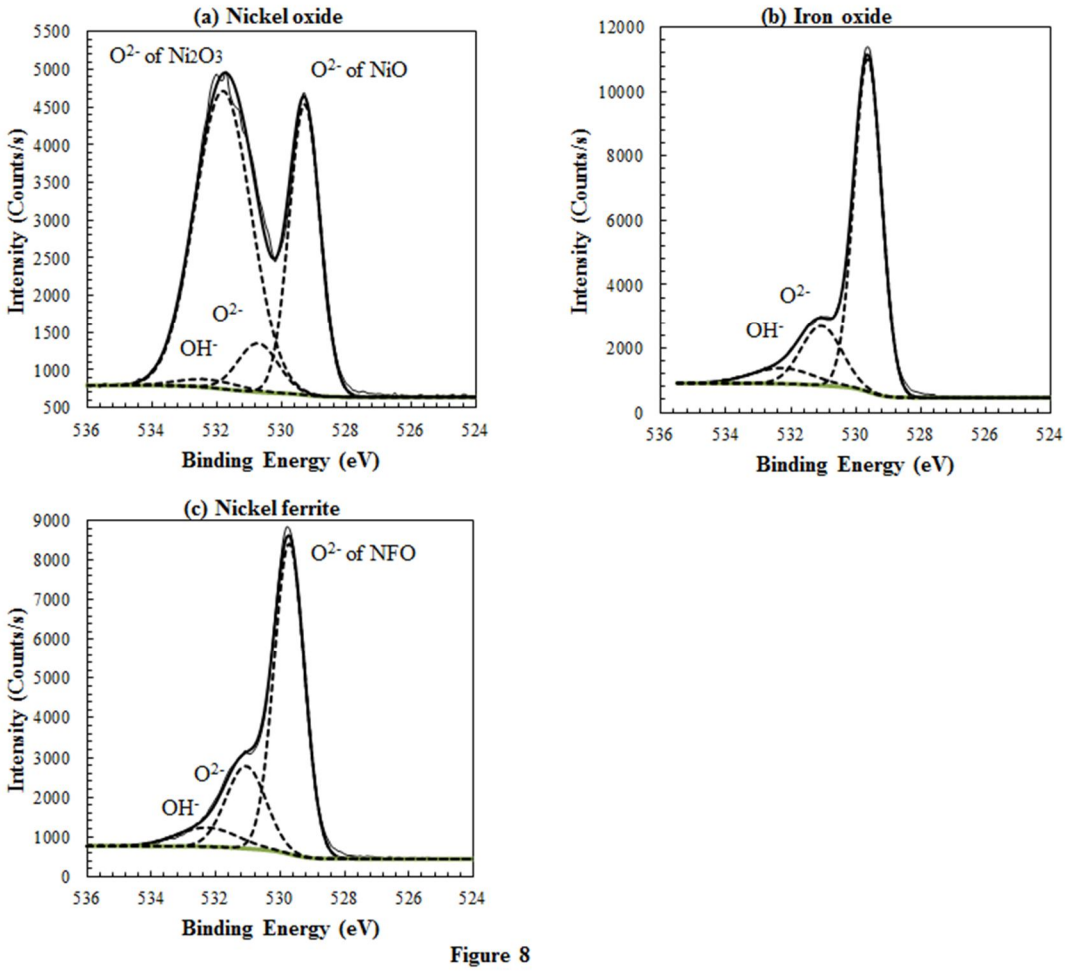

Figure 43. XPS spectra of the O 1s core scans for (a) nickel oxide film, (b) iron oxide film and (c) cyclic deposited nickel ferrite film. Samples prepared conditions: $T_{reactor}$=500 °C, $P_{reactor}$=17 Torr.

Table 3. XPS core scan peak parameters of different oxide films

		Position	Type	FWHM
Ni 2p3/2	Nickel Oxide	853.6	s	1.012
	χ^2=1.07	855.3	s	2.99
		860.8	s	4.929
		866.0	s	3.495
	NFO	854.1	s	1.084
	χ^2=0.72	855.6	s	2.99
		861.2	s	4.497
		866.0	s	3.727
Fe 2p	Iron Oxide	709.4	s	0.655
	χ^2=0.72	710.0	p	1.889
		711.3	p	2.654
		713.1	p	3.586
		718.8	p	6.245
		726.8	s	3.308
	NFO	710.0	p	2.258
	χ^2=0.42	711.7	p	2.868
		713.9	p	3.68
		718.3	p	4.891
		721.6	p	2.51
O 1s	Nickel Oxide	529.3	s	1.121
	χ^2=2.3	530.7	s	1.45
		531.8	s	2.044
		532.3	s	2.23
	Iron Oxide	529.6	s	1.002
	χ^2=3.2	531.1	s	1.452
		532.3	s	2.23
	NFO	529.7	s	1.112
	χ^2=3.6	531.1	s	1.45
		532.3	s	2.23

Due to the penetration limitation of X-ray beam and its surface sensitive, RBS was also performed for each element and was used to probe the entire film stoichiometry. Figure 44, the RBS spectra spectra illustrate for films of co-deposition (Figure 44 (a)) and optimal cyclic-deposition processes (Figure 44 (b)) at $T_{reactor}$=500 °C and $P_{reactor}$=17 Torr. The elemental composition was found to be Ni: Fe:

O= 0.85: 1.9: 4.2 for co-deposited NFO films and Ni: Fe: O=1: 1.9: 4 for cyclic-deposited NFO films. The ratio of Fe/Ni in the co-deposited film was found higher than that in the cyclic-deposited film due to the different growth rate of two metal oxides on the substrate surface. In co-deposition mode, n-butylferrocene and nickelocene together reacted with oxygen in the furnace. At the same temperature and pressure conditions, iron oxide grew at a higher rate than nickel oxide for the same amount of precursor vapor delivered into the reactor (Figure 40), indicating a likely preferential growth for iron oxide occurs during the co-deposition. Considering the elemental analysis of XPS and RBS results, the co-deposited film is estimated to have a slight excess of iron oxide; for the cyclic-deposited one, it may have no more than 5% nickel oxide and the film is almost stoichiometric $NiFe_2O_4$. Therefore, both precursors underwent an oxidation reaction and led to composition toggles in the binary composite film. From the comparison of chemical compositions of the NFO films using two different deposition modes, the cyclic-deposition mode seems to have more precise control of NFO stoichiometry.

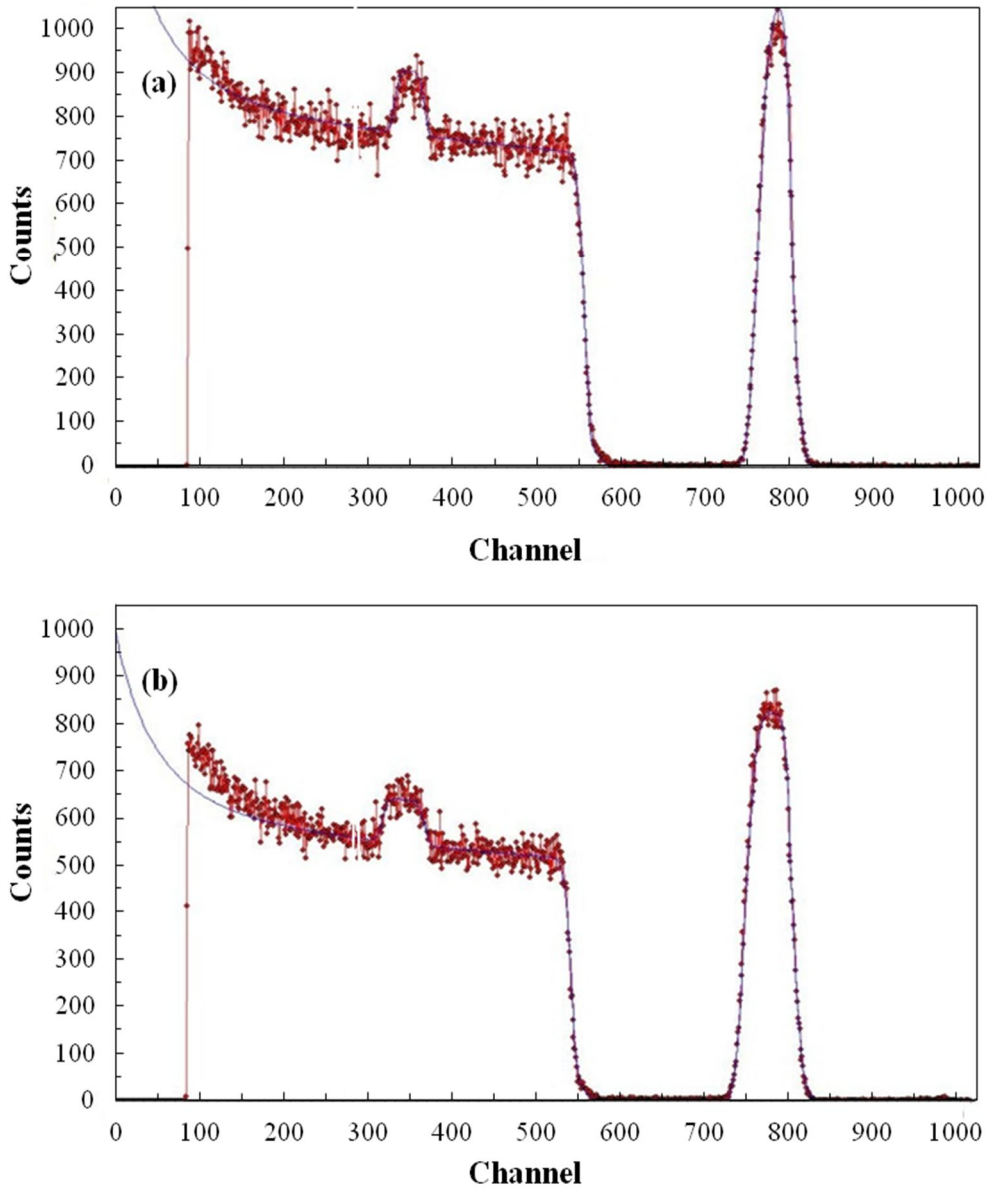

Figure 44. RBS spectra of (a) 40 nm-thick co-deposited nickel ferrite film, and (b) 30 nm-thick cyclic-deposited nickel ferrite film. RBS analysis was done by SIMNRA program (program for the simulation of backscattering spectra for ion beam analysis). Samples prepared conditions: $T_{reactor}$=500 °C, $P_{reactor}$=17 Torr.

.

NFO structure and morphology

Figure 45 shows the GAXRD diffractogram for a NFO thin formed through

cyclic deposition at 500 °C. The reflection planes indexed as (222), (311), (400) and (440) indicate pure trevorite NFO. No diffraction peaks of impurities such as α-Fe_2O_3 or NiO were observed. After one hour annealing at 700 °C, the diffractogram remained the same in terms of the peaks' intensity, while the peaks' width was found to increase likely due to an increase of grain size (about 10 nm difference).[189] The FWHM of the XRD peaks was used to calculate the crystallite size of NFO using Jade 8.0 software based on Scherrer's relation. The annealed NFO's lattice constant was calculated to be 8.27±0.03 Å which slightly differed from the value of its bulk form (8.34 Å). The lattice mismatch and strain from the substrate could affect this value. Different thermal expansion coefficients could also contribute to this result because of the residual stress at the interface after the annealing process. A similar value (8.26 Å) was reported by Srivastava using a sol-gel method to grow NFO nanocrytalline structure.[190]

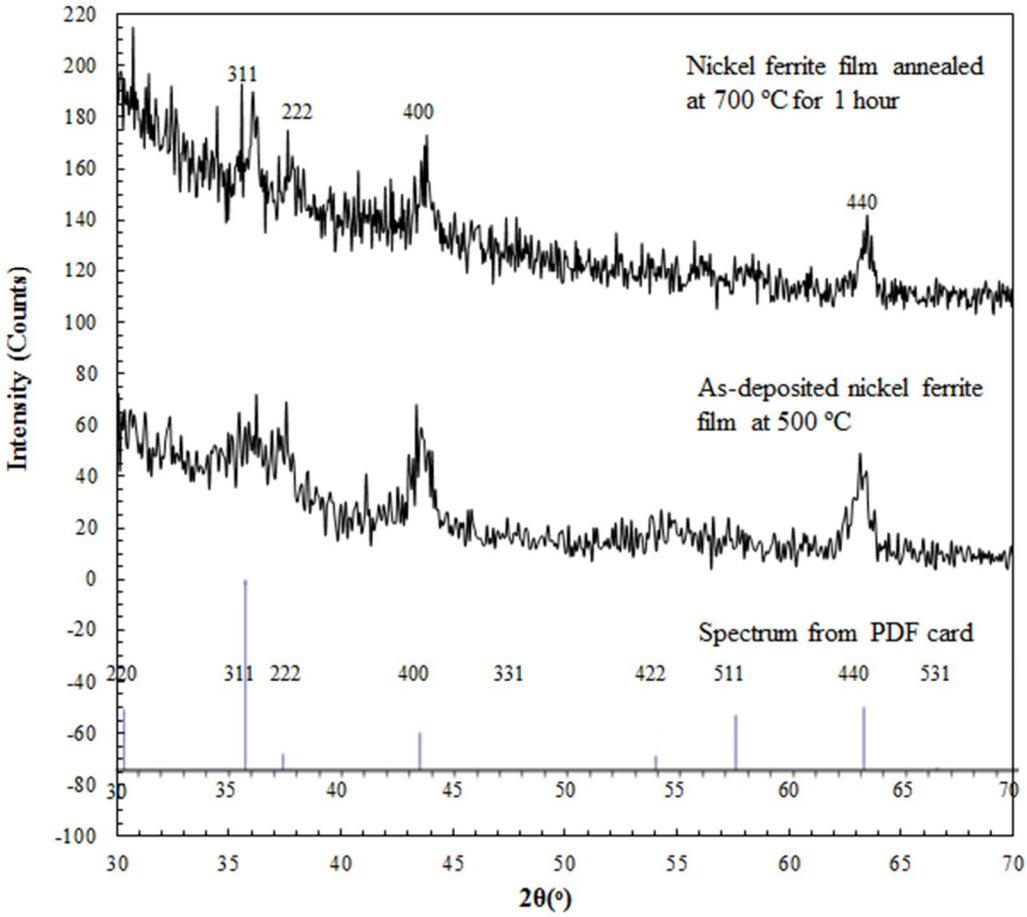

Figure 45. GAXRD diffraction patterns of 80 nm-thick NFO thin films. The as-deposited film was fabricated at $T_{reactor}$=500 °C and $P_{reactor}$=17 Torr on Si (100) and was post-annealed at 700 °C for 1 hour in argon ambient. (PDF card 04-006-2755).

The optical profilometer imaging showed the topographical map of 80 nm-thick cyclic-deposited and annealed NFO thin films (Figure 46). The film roughness is presented in Table 4. After annealing at 700 °C for 1 hour, both the average roughness and RMS roughness were found to increase by 0.2-0.25 nm. After annealing at 1000 °C for 1 hour, both the average roughness and RMS roughness we found increase by an additional 0.2-0.3 nm. The maximum height of the observed surface

topography was seem to increases by 1.6~2.0 nm after each annealing at 700 and 1000 °C. These values indicates that the NFO uniformly deposited on the substrate with a smooth surface.[182, 191] After the annealing (Figure 46 (b) and (c)), the texture of the surface topography showed small need-like features compared with that of the as-deposited one (Figure 46(a)), and this is most likely due to higher grain size induced by extra thermal energy.[192] The roughness increase and the change of film topographic feature can be attributed to the increasing grain size from the GAXRD results.

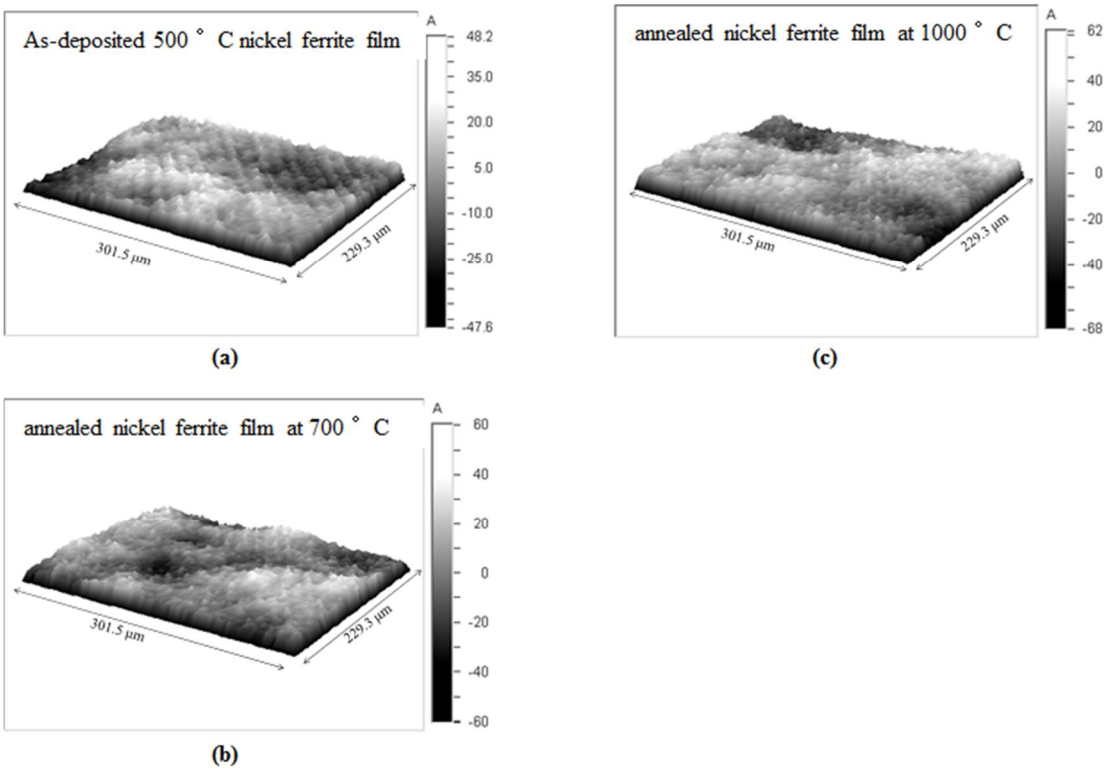

Figure 46. Topographical map of the 80 nm-thick NFO thin film surface. (a) 500 °C cyclic deposited NFO film; (b) NFO film annealed at 700 °C for 1 hour; (c) NFO film annealed at 1000 °C for 1 hour.

Table 4. Nickel ferrite film roughness for as-deposited and different annealing temperature

Temperature	Roughness Average (Å)	RMS Roughness (Å)	Maximum Height (Å)
500 °C (as-deposited)	9.3	11.5	85.8
700 °C	11.4	14.0	105.7
1000 °C	13.7	16.9	122.0

NFO magnetic measurement

The saturation magnetization (M_s) for post-annealed crystalline NFO film with grain size ~30 nm was measured to be 25 emu/g (Table 5) which is similar to the value reported by Shafi et al.[193] Lower values of magnetization were observed for smaller grain sizes of NFO films, while the M_s for bulk nickel ferrite is about 50 emu/g.[17] Other studies reported low magnetization values with grain size under 45 nm; for bigger grain size NFO, M_s seems to increase slowly with increasing grain size (Figure 47).[193-197] This decreasing trend of NFO M_s along with the decreasing crystal size was also reported in another study.[196] The low M_s values of different nano size particles can be caused by spin noncollinearity predominantly at the particle surface or by the random spin canting due to competing antiferromagnetic interactions between ferromagnetic oxides' sublattices.[197] Further studies indicate this phenomenon can be rather a finite-size effect throughout the entire particle.[198]

Table 5. Saturation magnetization values for nickel ferrite thin films. Films were identical as described in Table 4.

Temperature	Grain Size	Saturation Magnetization
500 °C	5-8 nm	<10 emu/g
700 °C	10-20 nm	10 emu/g
1000 °C	30 nm	25 emu/g

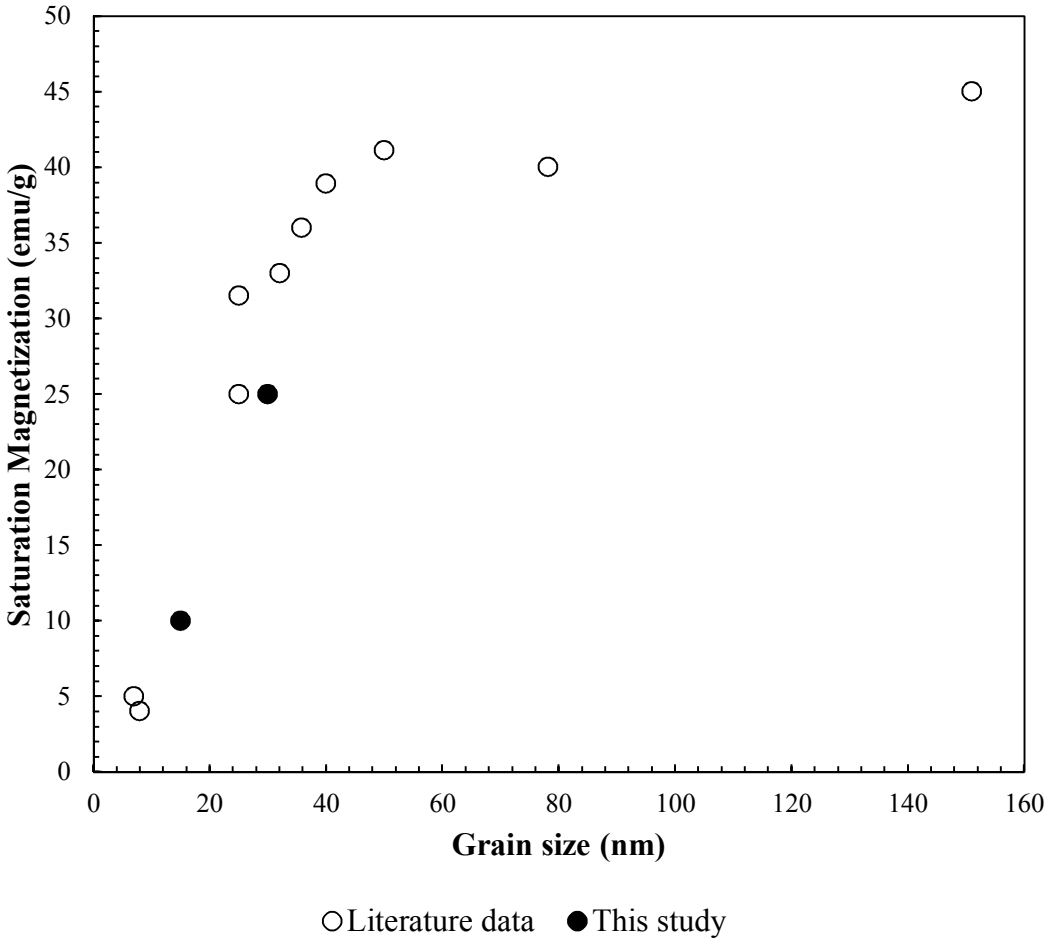

Figure 47. Saturation magnetization of NFO materials vs grain size (data from reports [193]-[197]).

4.4.4. Conclusion

A novel MOCVD process with both co-deposition mode and cyclic deposition mode was utilized to form NFO material nanostructure with controllable stoichiometry, desired crystalline phase and smooth surface morphology. In our custom-designed system, the optimal deposition conditions for iron oxide, nickel oxide and NFO films were found to be 500 °C at 17 Torr. The reactor temperature was controlled in the apparently mass transfer regime for metal oxide deposition. The cyclic deposition resulted in an almost stoichiometric composition of $NiFe_2O_4$ with a small amount of nickel oxide (less than 5%) and no detectable carbon incorporation in the film. The measured magnetization values of the NFO films were in agreement with values reported in the literature, albeit lower than the value of bulk NFO. High quality NFO thin films could be used in future microelectronic devices as promising nanometer scale composite materials with desired magnetoelectricity.

5. CONCLUSIONS

5.1. Metalorganic Chemical Vapor Deposition of Single Phase Multiferroic $BiFeO_3$ Thin Film

Single-phase mutilferroic BFO was fabricated using MOCVD method using novel precursor, n-butylferrocene. This cyclopentadienyl family of precursor is in liquid phase under room temperature and is convenient to be used in a bubbler which is an easily controlled delivery method for CVD system. It is also stable as it cannot react with air or moisture; moreover, its thermogravimetric analysis showed it had a clean evaporation without any decomposition and with little amount of residue.

Using this precursor, pure alpha phase of iron oxide thin films could be synthesis on silicon substrate. The different temperature controlled regimes for the CVD iron oxide growth process were investigated through Arrhenius plot. Growth rate was stable after the 400 °C. The earlier work of XRD, XPS showed above 500 °C the films were pure alpha phase.

The bismuth oxide growth process was using triphenylbismuth as precursor. As this precursor was based on phenyl ligands, the decomposition of precursor during the reaction became harder than the cyclopentadienyl family. From the temperature range 400 °C to 600 °C, the growth rate increased continuously. The bismuth oxide had only the 3+ status for bismuth element, which proved its pure form of Bi_2O_3.

The BFO was synthesis successfully and characterization results showed its pure rhombohedral phase. No other metal or metal oxide was discovered in the XRD and XPS results. With its smooth surface and chemical uniformity, the film had the potential use for the future integrated electronic devices.

5.2. Metalorganic Chemical Vapor Deposition of $NiFe_2O_4$ Thin Film in Cyclic Mode

Using the same novel iron precursor-n-butylferrocene, and nickelocene, $NiFe_2O_4$ was fabricated in the form of nano thin films in cyclic deposition mode of CVD system. The advantages of those precursors were listed here: 1) same chemical ligands, preventing side reactions; 2) cyclopentadienyl family, small ligand size and easily decomposed during the reaction; 3) containing only C, H and metal element, less complicated by-products.

The growth of iron oxide was summarized in the earlier paragraphs and the growth of nickel oxide showed the films containing the Ni^{2+} and Ni^{3+} oxides. The growth rate became stable after 350 °C, leaving a temperature window for the synthesis of NFO from 400 °C to 500 °C. After 500 °C, the mass transfer effect became severe and the quality of the films might be affected.

The cyclic deposited NFO thin films showed trevorite phase of $NiFe_2O_4$. The chemical status of Ni element also stayed at Ni^{2+} status. The surface topology showed smoothness and no observation of any cracks or major defects. The films were also uniform for the chemical composition. These evidences indicated that the cyclic CVD process was ready to fabricate more heterostructural nano composites, including the ones that show good ME coupling effect.

6. FUTURE WORK

The coupling effect in single-phase multiferroics is still too weak to be ready in device applications. The most advanced one, BFO also suffers from current leakage although adding dopants may improve the property to some extent. The more promising approach to synthesizing multiferroic material is the heterostructural composite fabrication which takes the advantage of the mechanical strain between the enlarged interfacial layers of the two different individuals-magnetostrictive and piezoelectric materials. The three dimensional structures of the nano- or micron- scale composites may vary in different ways as described in the early chapters. The most common one is to deposit multilayers of those magnetostrictive and piezoelectric thin films alternatively. Our CVD/ALD system is capable to do this work in a more flexible way. The four independent precursor delivery systems help to provide different metal sources to the reactor and can be oxidized or reduced under the pressure ranging from 500 mTorr to one atmosphere. The computer controlled pneumatic valves assisted in alternative depositions between different nano and micron scale film layers in CVD or ALD modes. Therefore, multilayered- and high aspect ratio structural composites can be later fabricated in the further research.

More specifically, coupling effect for NFO on PZT, PMN-PT or $BaTiO_3$ substrates can be investigated because the theoretical studies indicated the strong ME property for them. The later multilayered thin films can also be fabricated for these ME system.

CITED LITERATURE

1. Fiebig, M., *Revival of the magnetoelectric effect.* Journal of Physics D: Applied Physics, 2005. **38**(8): p. R123-R152.
2. Eerenstein, W., N.D. Mathur, and J.F. Scott, *Multiferroic and magnetoelectric materials.* Nature (London, United Kingdom), 2006. **442**(7104): p. 759-765.
3. Wood, V.E. and A.E. Austin, *Magnetoelectric Interaction Phenomena in Crystals*, A.J. Freeman and H. Schmid, Editors. 1975, Gordon and Breach: London.
4. Curie, P., *Sur la symétrie dans les phénomènes physiques, symétrie d'un champ électrique et d'un champ magnétique.* Journal de Physique Théorique et Appliquée, 1894. **3**(1): p. 393.
5. Dzyaloshinskii, I.E., *The magnetoelectric effect in antiferromagnetic materials.* Zhurnal Eksperimental'noi i Teoreticheskoi Fiziki, 1959. **37**: p. 881-2.
6. Astrov, D.N., *The magnetoelectric effect in antiferromagnetic materials.* Zhurnal Eksperimental'noi i Teoreticheskoi Fiziki, 1960. **38**: p. 984-5.
7. Hill, N.A. and A. Filippetti, *Why are there any magnetic ferroelectrics?* Journal of Magnetism and Magnetic Materials, 2002. **242-245**(Pt. 2): p. 976-979.
8. Ederer, C. and N.A. Spaldin, *Recent progress in first-principles studies of magnetoelectric multiferroics.* Current Opinion in Solid State & Materials Science, 2006. **9**(3): p. 128-139.
9. Ramesh, R. and N.A. Spaldin, *Multiferroics: progress and prospects in thin films.* Nat Mater, 2007. **6**(1): p. 21-29.
10. Lee, C.-C. and J.-M. Wu, *Studies on Leakage Mechanisms and Electrical Properties of Doped BiFeO3 Films.* Electrochemical and Solid-State Letters, 2007. **10**(8): p. G58-G61.
11. Ederer, C. and N. Spaldin, *Weak ferromagnetism and magnetoelectric coupling in bismuth ferrite.* Physical Review B, 2005. **71**(6): p. 1-4.
12. Catalan, G. and J.F. Scott, *Physics and Applications of Bismuth Ferrite.* Advanced Materials, 2009. **21**(24): p. 2463-2485.
13. Zavaliche, F., et al., *Electric Field-Induced Magnetization Switching in Epitaxial Columnar Nanostructures.* Nano Letters, 2005. **5**(9): p. 1793-1796.
14. Kumar, M.M., et al., *Ferroelectricity in a pure $BiFeO_3$ ceramic.* Applied Physics Letters, 2000. **76**(19): p. 2764-2766.
15. Wang, J., et al., *Epitaxial $BiFeO_3$ Multiferroic Thin Film Heterostructures.* Science, 2003. **299**(5613): p. 1719-1722.
16. Fujino, S., et al., *Ferroelectric properties of multiphase Bi-Fe-O thin films.* Solid State Ionics, 2007. **178**(21-22): p. 1257-1261.
17. Smit, J. and H.P.J. Wijn, *Ferrite*. 1959, London: Cleaver-Hume Press. 156.
18. Healy, D.W. and R.A. Johnson, *Anisotropy Constants and g Value of Nickel Ferrite.* Physical Review, 1956. **104**: p. 634-636.
19. Uitert, L.G.V., *High Resistivity Nickel Ferrites-the Effect of Minor Additions of Manganese or Cobalt.* The Journal of Chemical Physics, 1956. **24**(2): p.

306-310.

20. Verma, A., et al., *High-resistivity nickel-zinc ferrites by the citrate precursor method.* Journal of Magnetism and Magnetic Materials, 1999. **192**(2): p. 271-276.
21. Kale, A., S. Gubbala, and R.D.K. Misra, *Magnetic behavior of nanocrystalline nickel ferrite synthesized by the reverse micelle technique.* Journal of Magnetism and Magnetic Materials, 2004. **277**(3): p. 350-358.
22. Landau, L.D. and E.M. Lifshitz, *Electrodynamics of continuous media*. 1960, Oxford: Pergamon. vii, 417 p.
23. Rado, G.T. and V.J. Folen, *Observation of the Magnetically Induced Magnetoelectric Effect and Evidence for Antiferromagnetic Domains.* Phys. Rev. Lett., 1961. **7**(8): p. 310.
24. Ascher, E., et al., *Some Properties of Ferromagnetoelectric Nickel-Iodine Boracite, $Ni_3B_7O_{13}I$.* Journal of Applied Physics, 1966. **37**(3): p. 1404-1405.
25. Khomskii, D.I., *Multiferroics: Different ways to combine magnetism and ferroelectricity.* J. Magn. Magn. Mater., 2006. **306**(1): p. 1-8.
26. Seshadri, R. and N.A. Hill, *Visualizing the Role of Bi 6s "Lone Pairs" in the Off-Center Distortion in Ferromagnetic $BiMnO_3$.* Chem. Mater., 2001. **13**(9): p. 2892-2899.
27. Wiegelmann, H., et al., *Magnetoelectric Phenomena in R_2CuO_4 Rare-Earth Cuprates.* Key Engineering Materials, 1998. **155-156**: p. 429.
28. Al'shin, B.I., D.N. Astrov, and R.V. Zorin, *Low-frequency magnetoelectric resonances in barium tetrafluoromanganate (BaMnF4).* Zhurnal Eksperimental'noi i Teoreticheskoi Fiziki, 1972. **63**(6): p. 2198-204.
29. Kubel, F. and H. Schmid, *Structure of a ferroelectric and ferroelastic monodomain crystal of the perovskite BiFeO3.* Acta Crystallogr. B, 1990. **46**(6): p. 698-702.
30. Bosak, A.A., et al., *Epitaxial phase stabilisation phenomena in rare earth manganites.* Thin Solid Films, 2001. **400**(1-2): p. 149-153.
31. Choi, K.-J., W.-C. Shin, and S.-G. Yoon, *Ferroelectric $YMnO_3$ thin films grown by metal-organic chemical vapor deposition for metal/ferroelectric/semiconductor field-effect transistors.* Thin Solid Films, 2001. **384**(1): p. 146-150.
32. Kaul, A.R. and B.V. Seleznev, *New principle of feeding for flash evaporation MOCVD devices.* Journal de Physique IV France, 1993. **3**(C3): p. 375.
33. Kim, D., et al., *Ferroelectric properties of $YMnO_3$ films deposited by metalorganic chemical vapor deposition on $Pt/Ti/SiO_2/Si$ substrates.* Mater. Lett., 2006. **60**(3): p. 295-297.
34. Thery, J., et al., *MOCVD of $BiFeO_3$ Thin Films on $SrTiO_3$.* Chemical Vapor Deposition, 2007. **13**(5): p. 232-238.
35. Gelard, I., et al., *Neutron diffraction study of hexagonal manganite $YMnO_3$, $HoMnO_3$, and $ErMnO_3$ epitaxial films.* Appl. Phys. Lett., 2008. **92**(23): p. 232506-3.
36. Nakamura, M., T. Higuchi, and T. Tsukamoto, *Effect of thermal treatment of*

undoped $Bi_4Ti_3O_{12}$ thin films prepared by metalorganic chemical vapor deposition. Japanese Journal of Applied Physics, Part 1: Regular Papers, Short Notes & Review Papers, 2003. **42**(9A): p. 5687-5691.

37. Tasaki, Y., et al., *Evaluation of Metalorganic Precursors for Preparing $BiFeO_3$ Thin Films by Liquid Delivery Chemical Vapor Deposition.* Integrated Ferroelectrics, 2006. **81**(1): p. 281-288.
38. Tasaki, Y., et al., *Evaluation of metalorganic precursors for preparing $BiFeO_3$ thin films by liquid delivery chemical vapor deposition.* Integrated Ferroelectrics, 2006. **81**: p. 281-288.
39. Ueno, R., et al., *Crystal Structure and Electrical Properties of Epitaxial $BiFeO_3$ Thin Films Grown by Metal Organic Chemical Vapor Deposition.* Jpn. J. Appl. Phys., Part 2, 2005. **44**(37-41): p. L1231-L1233.
40. Yang, S.Y., et al., *Metalorganic chemical vapor deposition of lead-free ferroelectric $BiFeO_3$ films for memory applications.* Applied Physics Letters, 2005. **87**(10): p. 102903-3.
41. Kartavtseva, M.S., et al., *$BiFeO_3$ thin films prepared using metalorganic chemical vapor deposition.* Thin Solid Films, 2007. **515**(16): p. 6416-6421.
42. Huang, H.-C., Y.-C. Chang, and T.-S. Sheu, *Physical properties in the Bi_2O_3-Fe_2O_3 system containing Y_2O_3 and CaO dopants.* Ceramic Engineering and Science Proceedings, 2007. **27**(4, Advances in Solid Oxide Fuel Cells II): p. 87-93.
43. Yang, C.H., et al., *Synthesis of nanoscale composites of exchange biased $MnFe_2O_4$ and Mn-doped $BiFeO_3$.* Applied Physics Letters, 2007. **90**(16): p. 163116-3.
44. Hongri, L., et al., *Effects of substitution of Ti for Fe in $BiFeO_3$ films prepared by sol-gel process.* Physica B: Condensed Matter, 2007. **400**(1-2): p. 252-256.
45. Hu, G.D., et al., *Low leakage current and enhanced ferroelectric properties of Ti and Zn codoped $BiFeO_3$ thin film.* Applied Physics Letters, 2008. **92**(19): p. 192905-3.
46. Singh, V.R., A. Garg, and D.C. Agrawal, *Structural changes in chemical solution deposited lanthanum doped bismuth ferrite thin films.* Applied Physics Letters, 2008. **92**(15): p. 152905-3.
47. Kartopu, G., et al., *Observation of structural transitions and Jahn-Teller distortion in $LaMnO_3$-doped $BiFeO_3$ thin films.* Applied Physics Letters, 2008. **92**(15): p. 151910-3.
48. Naganuma, H., et al. *Enhancement of ferroelectric and magnetic properties in $BiFeO_3$ films by small amount of cobalt addition*. in *Proceedings of the 52nd Annual Conference on Magnetism and Magnetic Materials*. 2008. Tampa, Florida (USA): AIP.
49. Yang, H., et al., *Rectifying current-voltage characteristics of $BiFeO_3$/Nb-doped $SrTiO_3$ heterojunction.* Applied Physics Letters, 2008. **92**(10): p. 102113-3.
50. Wang, Y. and C.-W. Nan, *Effect of Tb doping on electric and magnetic behavior of $BiFeO_3$ thin films.* Journal of Applied Physics, 2008. **103**(2): p.

024103-5.
51. Hu, G.D., et al., *Effects of Gd substitution on structure and ferroelectric properties of $BiFeO_3$ thin films prepared using metal organic decomposition.* Applied Physics Letters, 2007. **91**(23): p. 232909-3.
52. Gautreau, O., et al., *Structural and multiferroic properties of epitaxial γ-Fe_2O_3-$BiFeO_3$/$Bi_{3.25}La_{0.75}Ti_3O_{12}$ composite bi-layers.* Journal of Physics D: Applied Physics, 2008. **41**(11): p. 112002.
53. Kumar, M. and K.L. Yadav, *Synthesis of nanocrystalline $xCuFe_2O_4$-$(1-x)BiFeO_3$ magnetoelectric composite by chemical method.* Materials Letters, 2007. **61**(10): p. 2089-2092.
54. Kumar, M. and K.L. Yadav, *Magnetoelectric characterization of $xNi_{0.75}Co_{0.25}Fe_2O_4$-$(1-x)BiFeO_3$ nanocomposites.* Journal of Physics and Chemistry of Solids, 2007. **68**(9): p. 1791-1795.
55. Cheng, Z. and X. Wang, *Room temperature magnetic-field manipulation of electrical polarization in multiferroic thin film composite $BiFeO_3$/$La_{2/3}Ca_{1/3}MnO_3$.* Physical Review B (Condensed Matter and Materials Physics), 2007. **75**(17): p. 172406-4.
56. Wang, D.H. and C.K. Ong, *The phase formation and magnetodielectric property in $(1-x)Bi_2Fe_4O_9$-$xBaO$ composites.* Journal of Applied Physics, 2006. **100**(4): p. 044111-3.
57. Song, M.-K. and S.-W. Rhee, *Deposition of $Bi_{4-x}Nd_xTi_3O_{12}$ Films with Direct Liquid Injection Metallorganic Chemical Vapor Deposition and Characterization of Ferroelectric Properties.* Journal of The Electrochemical Society, 2006. **153**(11): p. G992-G995.
58. Kim, J.K., et al., *Enhanced ferroelectric properties of Cr-doped $BiFeO_3$ thin films grown by chemical solution deposition.* Appl. Phys. Lett., 2006. **88**(13): p. 132901.
59. Uchida, H., et al., *Crystal structure and ferroelectric properties of rare-earth substituted $BiFeO_3$ thin films.* J. Appl. Phys., 2006. **100**(1): p. 014106-9.
60. Qi, X., et al., *High-resolution x-ray diffraction and transmission electron microscopy of multiferroic $BiFeO_3$ films.* Applied Physics Letters, 2005. **86**(7): p. 071913-3.
61. Brinkman, K., et al., *The Influence of Acceptor Doping on the Structure and Electrical Properties of Sol-Gel Derived $BiFeO_3$ Thin Films.* Ferroelectrics, 2007. **357**(1): p. 35 - 40.
62. Van den Boomgaard, J., A.M.J.G. Van Run, and J. Van Suchtelen, *Magnetoelectricity in piezoelectric-magnetostrictive composites.* Ferroelectrics, 1976. **10**(1-4): p. 295-8.
63. Van den Boomgaard, J. and R.A.J. Born, *A sintered magnetoelectric composite material barium titanate-nickel(cobalt, manganese) ferrite.* J. Mater. Sci., 1978. **13**(7): p. 1538-48.
64. Ryu, J., et al., *Magnetoelectric effect in composites of magnetostrictive and piezoelectric materials.* J. Electroceram., 2002. **8**(2): p. 107-119.
65. Petrov, V.M., et al., Physical Review B (Condensed Matter and Materials

Physics), 2007. **75**: p. 224407.
66. Dorr, K., et al., *Approaches towards ferroelectric control of thin film magnetism.* Phil. Mag. Lett., 2007. **87**(3): p. 269 - 278.
67. Zhang, Y., et al., Chinese Physics B, 2008. **17**: p. 3910-3916.
68. Patil, D.R. and B.K. Chougule, Journal of Materials Science: Mater Electron, 2009. **20**: p. 398-402.
69. Stringfellow, G.B., *Organometallic Vapor-Phase Epitaxy: Theory and Practice*. 2 ed. 1999, San Diego, CA: Academic Press.
70. Rastogi, A.C., S. Dhara, and B.K. Das, *Kinetics, Growth, Structure, and Atmospheric Chemical Vapor Deposition of Ferrimagnetic Iron Oxide Thin Films from Metallorganic Acetyl Acetonate Precursor.* Journal of The Electrochemical Society, 1995. **142**(9): p. 3148-3156.
71. O'Brien, P., N.L. Pickett, and D.J. Otway, *Developments in CVD Delivery Systems: A Chemist's Perspective on the Chemical and Physical Interactions Between Precursors.* Chemical Vapor Deposition, 2002. **8**(6): p. 237-249.
72. Vahlas, C., et al., *A Delivery System for Precursor Vapors Based on Sublimation in a Fluidized Bed.* Chemical Vapor Deposition, 2007. **13**(2-3): p. 123-129.
73. Henn-Lecordier, L., J.J.N. Kidder, and G.W. Rubloff, *Real-time acoustic sensing and control of metalorganic chemical vapor deposition precursor concentrations delivered from solid phase sources.* Journal of Vacuum Science & Technology A: Vacuum, Surfaces, and Films, 2004. **22**(5): p. 1984-1991.
74. Williams, P.A., et al., *Development of improved precursors for the MOCVD of bismuth titanate.* Materials Research Society Symposium Proceedings, 2003. **748**(Ferroelectric Thin Films XI): p. 105-110.
75. J. P. Sénateur, et al., *Synthesis and characterisation of YBCO thin films grown by injection-MOCVD.* Journal of Alloys and Compounds, 1997. **251**: p. 288.
76. Bedoya, C., et al., *MOCVD of Bismuth Oxides: Transport Properties and Deposition Mechanisms of the $Bi(C_6H_5)_3$ Precursor.* Chemistry of Materials, 2004. **16**(16): p. 3176-3183.
77. Zhang, J.M., et al., *Preparation of high-T_c superconducting Bi-Sr-Ca-Cu-O films by organometallic chemical vapor deposition using second-generation fluorocarbon-based precursors.* Journal of Applied Physics, 1991. **69**(4): p. 2743-2745.
78. Si, J. and S.B. Desu, *Ferroelectric bismuth titanate films by hot wall metalorganic chemical vapor deposition.* Journal of Applied Physics, 1993. **73**(11): p. 7910-7913.
79. Wang, H., L.W. Fu, and S.X. Shang, *Preparation and properties of $Bi_4Ti_3O_{12}$ single-crystal thin films by atmospheric pressure metalorganic chemical vapor deposition.* Journal of Applied Physics, 1993. **73**(11): p. 7963-7965.
80. Shin, D.S., et al., *$SrBi_2Ta_2O_9$ thin films grown by MOCVD using a novel double metal alkoxide precursor.* Journal of Crystal Growth, 2000. **209**(4): p. 1009-1012.

81. Kang, S.-W. and S.-W. Rhee, *Evaluation of Precursors for DLI MOCVD of Ferroelectric BLT.* Journal of The Electrochemical Society, 2003. **150**(9): p. C573-C576.
82. Tasaki, Y., et al., *Low Temperature Preparation of $(Bi,Nd)_4Ti_3O_{12}$ Thin Films by Liquid-DElivery MOCVD using neodymium Precursors with High Deposition Efficiency.* Integrated Ferroelectrics, 2006. **81**(1): p. 271-279.
83. Kijima, T., M. Ushikubo, and H. Matsunaga, *New low-temperature processing of metalorganic chemical vapor deposition - $Bi_4Ti_3O_{12}$ thin films using BiO_x buffer layer.* Japanese Journal of Applied Physics, Part 1: Regular Papers, Short Notes & Review Papers, 1999. **38**(1A): p. 127-130.
84. Yoshimura, K., et al., *Preparation of ferroelectric $Bi_4Ti_3O_{12}$ thin films with c-axis orientation by atmospheric-pressure metal-organic chemical vapor deposition.* Japanese Journal of Applied Physics, Part 1: Regular Papers, Short Notes & Review Papers, 1995. **34**(5A): p. 2425-9.
85. Kang, S.W. and S.W. Rhee, *Growth of bismuth oxide films by direct liquid injection-metal organic chemical vapor deposition with $Bi(tmhd)_3$ (tmhd: 2,2,6,6-tetramethyl-3,5-heptanedione).* Thin Solid Films, 2004. **468**(1-2): p. 79-83.
86. Hintermaier, F., et al., *Properties of $SrBi_2Ta_2O_9$ thin films grown by MOCVD for high density FeRAM applications.* Integrated Ferroelectrics, 1998. **21**(1): p. 367-379.
87. Kartavtseva, M.S., et al., *$BiFeO_3$ thin films prepared by MOCVD.* Surface and Coatings Technology, 2007. **201**(22-23): p. 9149-9153.
88. K. Takahashi, M.S.T.O.T.K.T.W.H.F., *MOCVD of Single-Axis c-Oriented Strontium Bismuth Titanate Thin Films and Their Electrical Properties.* Chemical Vapor Deposition, 2006. **12**(2-3): p. 136-142.
89. P. A. Williams, A.C.J.M.J.C.P.J.W.J.F.B.A.S.H.O.D.T.J.L.G., *Crystal Structure of $Bi(OCMe_2CH_2OMe)_3$ and Its Use in the MOCVD of Bi_2O_3.* Chemical Vapor Deposition, 2001. **7**(5): p. 205-209.
90. Yasui, S., et al., *Crystal structure analysis of epitaxial $BiFeO_3$-$BiCoO_3$ solid solution films grown by metalorganic chemical vapor deposition.* Japanese Journal of Applied Physics, Part 1: Regular Papers, Brief Communications & Review Papers, 2007. **46**(10B): p. 6948-6951.
91. Furukawa, T., et al., *Properties of a Novel Bismuth Precursor for MOCVD.* Integrated Ferroelectrics, 2006. **84**(1): p. 197-202.
92. Kojima, Y., H. Kadokura, and e. al., Integrated Ferroelectrics, 1997. **18**: p. 183-195.
93. Fujii, E., et al., Jpn. J. Appl. Phys., 1996. **35**: p. L328.
94. Maruyama, T. and S. Arai, *The electrochromic properties of nickel oxide thin films prepared by chemical vapor deposition.* Solar Energy Materials and Solar Cells, 1993. **30**(3): p. 257-262.
95. Ben-dor, L., R. Druilhe, and P. Gibart, Journal of Crystal Growth, 1974. **24/25**: p. 172.
96. Sugimoto, K., et al., Journal of Electrochemical Society, 1993. **140**: p. 1586.

97. Yeh, W.-c. and M. Matsumura, *Chemical Vapor Deposition of Nickel Oxide Films from Bis-π-Cyclopentadienyl-Nickel.* Japanese Journal of Applied Physics, Part 1, 1997. **36**(11): p. 6884-6887.
98. Kang, J.-K. and S.-W. Rhee, Thin Solid Films, 2001. **391**: p. 57-61.
99. Lu, H.L., et al., *Atomic Layer Deposition of NiO Films on Si(100) Using Cyclopentadienyl-Type Compounds and Ozone as Precursors.* Journal of Electrochemical Society, 2008. **155**(10): p. H807-H811.
100. Brissonneau, L., Chemical Vapor Deposition, 1999. **5**: p. 135.
101. Kang, J.-K. and S.-W. Rhee, *Metalorganic chemical vapor deposition of nickel films from Ni(C5H5)2/H2.* Journal of Materials Research, 2000. **15**(8): p. 1828-1833.
102. Maruyama, T. and Y. Shinyashiki, *Iron-iron oxide composite thin films prepared by chemical vapor deposition from iron pentacarbonyl.* Thin Solid Films, 1998. **333**(1-2): p. 203-206.
103. Chai, C.C., J. Peng, and B.P. Yan, *Characterization of α-Fe_2O_3 thin films deposited by atmospheric pressure CVD onto alumina substrates.* Sensors and Actuators, B: Chemical, 1996. **B34**(1-3): p. 412-416.
104. Lee, E.T., et al., *Fabrication and gas sensing properties of α-Fe_2O_3 thin film prepared by plasma enhanced chemical vapor deposition (PECVD).* Sensors and Actuators, B: Chemical, 2001. **B77**(1-2): p. 221-227.
105. Yubero, F., et al., *Iron oxide thin films prepared by ion beam induced chemical vapor deposition: Structural characterization by infrared spectroscopy.* Journal of Vacuum Science & Technology, A: Vacuum, Surfaces, and Films, 2000. **18**(5): p. 2244-2248.
106. Gilbert, A.G. and K.G.P. Sulzmann, *The Vapor Pressure of Iron Pentacarbonyl.* Journal of The Electrochemical Society, 1974. **121**(6): p. 832-834.
107. Behrens, S., et al., *Air-stable Co-, Fe-, and Fe/Co-Nanoparticles and Ferrofluids.* Zeitschrift für Physikalische Chemie, 2006. **220**(1): p. 3-40.
108. Hardee, K.L. and A.J. Bard, *Semiconductor electrodes. V. The application of chemically vapor deposited iron oxide films to photosensitized electrolysis.* Journal of The Electrochemical Society, 1976. **123**(7): p. 1024-6.
109. Barreca, D., et al., *Chemical Vapor Deposited Fe_2O_3 Thin Films Analyzed by XPS.* Surface Science Spectra, 2001. **8**(3): p. 240-245.
110. Cheng, J. and Y. Zhang, *Preparation of oriented Fe_2O_3 film on glass/Si substrate by atmospheric MOCVD.* Materials Science Forum, 2005. **475-479**(Pt. 5, PRICM 5: The Fifth Pacific Rim International Conference on Advanced Materials and Processing, 2004): p. 3749-3752.
111. Kuribayashi, K. and R. Ueyama, *Effect of the substrate on the growth of spinel iron oxide thin films by metal-organic chemical vapor deposition.* Thin Solid Films, 1997. **295**(1-2): p. 16-18.
112. Maruyama, T. and T. Kanagawa, *Electrochromic Properties of Iron Oxide Thin Films Prepared by Chemical Vapor Deposition.* Journal of The Electrochemical Society, 1996. **143**(5): p. 1675-1677.

113. Fujii, E., et al., *(100) Preferred orientation of spinel-type iron oxide films prepared by plasma-enhanced metalorganic chemical vapor deposition.* Japanese Journal of Applied Physics, Part 1: Regular Papers, Short Notes & Review Papers, 1995. **34**(4A): p. 1937-41.
114. Wang, Y.-Y., et al., *Synthesis and characterization of MOCVD precursor $Fe(DPM)_3$.* Wuji Huaxue Xuebao, 2006. **22**(7): p. 1269-1274.
115. Dhara, S., et al., *Parametric investigation for direct chemical vapor deposition of magnetite films.* Journal of Magnetism and Magnetic Materials, 1994. **134**(1): p. 29-33.
116. Shalini, K., et al., *Thin films of iron oxide by low pressure MOCVD using a novel precursor tris(t-butyl-3-oxo-butanoato)iron(III).* Thin Solid Films, 2003. **424**(1): p. 56-60.
117. Ben-Dor, L., et al., *β–Fe_2O_3: Preparation of Thin Films by Chemical Vapor Deposition from Organometallic Chelates and Their Characterization.* Journal of The Electrochemical Society, 1977. **124**(3): p. 451-457.
118. Lie, M., H. Fjellvag, and A. Kjekshus, *Growth of Fe_2O_3 thin films by atomic layer deposition.* Thin Solid Films, 2005. **488**(1-2): p. 74-81.
119. Beech, G. and R.M. Lintonbon, *Thermal and kinetic studies of some complexes of 2,4-pentanedione.* Thermochimica Acta, 1971. **3**(2): p. 97-105.
120. Mathur, S., et al., *Nanostructured films of iron, tin and titanium oxides by chemical vapor deposition.* Thin Solid Films, 2006. **502**(1-2): p. 88-93.
121. Park, S., S. Lim, and H. Choi, *Chemical vapor deposition of iron and iron oxide thin films from Fe(II) dihydride complexes.* Chemistry of Materials, 2006. **18**(22): p. 5150-5152.
122. Pflitsch, C., et al., *Growth of Thin Iron Oxide Films on Si(100) by MOCVD.* Journal of The Electrochemical Society, 2006. **153**(8): p. C546-C550.
123. Singh, M.K., Y. Yang, and C.G. Takoudis, *Low-pressure metalorganic chemical vapor deposition of Fe_2O_3 thin films on Si(100) using n-butylferrocene and oxygen.* Journal of The Electrochemical Society, 2008. **155**(9): p. D618-D623.
124. Karyakin, N.V., et al., Zhurnal Fizicheskoi Khimii, 2003. **77**: p. 1375.
125. J. A. Woollam Co., I., *A Short Course in Ellipsometry*, in *Guide to Using WVASE32*. 1999. p. 7.
126. J. A. Woollam Co., I., *A Short Course in Ellipsometry*, in *Guide to Using WVASE 32*. 1999. p. 32.
127. Cornell, R.M. and U. Schwertmann, *The Iron Oxides: Structure, Properties, Reactions, Occurrences and Uses*. 2nd ed. 2003, Weinheim: Wiley-VCH.
128. Lee, E.T., G.E. Jang, and D.D. Lee, *Sensing properties of α-Fe_2O_3 thin film gas sensor to reducing gases.* Yoop Hakhoechi, 1999. **36**(5): p. 465-470.
129. Zhao, S.-y., et al., *Preparation of Fe2O3 thin film-based gas sensor using MOCVD technique.* Huaxue Chuanganqi, 1996. **16**(2): p. 112-115, 120.
130. Sarov, G. and V. Docheva, *Optical, mechanical, and chemical properties of CVD iron(III) oxide thin films.* Bulgarian Journal of Physics, 1975. **2**(4): p. 356-63.

131. MacChesney, J.B., P.B. O'Connor, and M.V. Sullivan, *Chemical vapor deposition of iron oxide films for use as semitransparent masks.* Journal of the Electrochemical Society, 1971. **118**(5): p. 776-81.
132. Ralph, J.M., C.C.R. Rossignol, and J.T. Vaughey, *Iron-based perovskite cathodes for solid oxide fuel cells*. 2005, (The University of Chicago, USA). US. p. 12 pp.
133. Suzuki, Y., et al., *Magnetic properties of epitaxial ferrite multilayer films.* Journal of Applied Physics, 1996. **79**: p. 5923-5925.
134. Spaldin, N.A. and M. Fiebig, *Materials science: The renaissance of magnetoelectric multiferroics.* Science, 2005. **309**(5733): p. 391-392.
135. Mason, D.R., *Chemically Vapor Deposited Fe_2O_3 Films.* Journal of The Electrochemical Society, 1976. **123**(4): p. 519-523.
136. Lin, Y.-H., et al., *Ferromagnetism and electrical transport in Fe-doped NiO.* Physical Review B: Condensed Matter and Materials Physics, 2006. **73**(19): p. 193308/1-193308/4.
137. Lin, Y.-H., et al., *Enhancement of ferromagnetic properties of NiO: Fe thin film by Li doping.* Applied Physics Letters, 2006. **89**(20): p. 202501/1-202501/3.
138. Lin, Y.-H., et al., *Ferromagnetism in antiferromagnetic NiO-based thin films.* Journal of Applied Physics, 2011. **110**: p. 043921.
139. McBreen, J., *The nickel oxide electrode.* Modern Aspects of Electrochemistry, 1990. **21**: p. 29-63.
140. Brenet, J.P., *Electrochemical behaviour of metallic oxides.* Journal of Power Sources, 1979. **4**: p. 183-190.
141. Soleimanpour, A.M., Y. Hou, and A.H. Jayatissa, *Evolution of hydrogen gas sensing properties of sol-gel derived nickel oxide thin film.* Sensors and Actuators, B: Chemical, 2013. **182**: p. 125-133.
142. Tyagi, M., M. Tomar, and V. Gupta, *P-N junction of NiO thin film for photonic devices.* IEEE Electron Device Letters, 2013. **34**(1): p. 81-83.
143. Sun, N. and Y. Ren, *Study on nickel oxide thin film as buffering layer in photovoltaic solar cells.* Advanced Materials Research (Durnten-Zurich, Switzerland), 2012. **546-547**: p. 38-41.
144. Hotovy, I., et al., *The influences of preparation parameters on NiO thin film properties for gas-sensing application.* Sensors and Actuators, B: Chemical, 2001. **78**(1-3): p. 126-132.
145. Hotovy, I., et al., *Preparation and characterization of NiO thin films for gas sensor applications.* Vacuum, 2000. **58**(2-3): p. 300-307.
146. Wang, Y. and Q.-Z. Qin, *A Nanocrystalline NiO Thin-Film Electrode Prepared by Pulsed Laser Ablation for Li-ion Batteries.* Journal of The Electrochemical Society, 2002. **149**(7): p. A873-A878.
147. Xia, X.H., et al., *Morphology effect on the electrochromic and electrochemical performances of NiO thin films.* Electrochimica Acta, 2008. **53**(18): p. 5721-5724.
148. Kadam, L.D. and P.S. Patil, *Studies on electrochromic properties of nickel*

oxide thin films prepared by spray pyrolysis technique. Solar Energy Materials and Solar Cells, 2001. **69**(4): p. 361-369.

149. Shuk, P., et al., *Oxide ion conducting solid electrolytes based on Bi2O3.* Solid State Ionics, 1996. **89**: p. 179-196.
150. Gujar, T.P., et al., *Bismuth oxide thin films prepared by chemical bath deposition (CBD) method: annealing effect.* Applied Surface Science, 2005. **250**(1-4): p. 161-167.
151. Bohannan, E.W., et al., *Low-temperature electrodeposition of the high-temperature cubic polymorph of bismuth(III) oxide.* Solid State Ionics, 2000. **131**(1,2): p. 97-107.
152. Takeyama, T., et al., *Growth of the Bi2O3 thin films under atmospheric pressure by means of halide CVD.* Journal of Physics and Chemistry of Solids, 2004. **65**(7): p. 1349-1352.
153. Park, Y.-B., et al., *Bismuth composition control of SrBi2TaNbO9 thin films by heat treating Bi2O3-inserted heterostructure.* Journal of Materials Research, 1999. **14**(7): p. 2986-2992.
154. Aronniemi, M., J. Lahtinen, and P. Hautojärvi, *Characterization of iron oxide thin films.* Surface and Interface Analysis, 2004. **36**(8): p. 1004-1006.
155. McIntyre, N.S. and D.G. Zetaruk, Analytical Chemistry, 1977. **49**: p. 1521.
156. Darken, L.S. and R.W. Gurry, *The System Iron--Oxygen. II. Equilibrium and Thermodynamics of Liquid Oxide and Other Phases.* Journal of the American Chemical Society, 1946. **68**(5): p. 798-816.
157. Zhang, L.M., et al., *Substrate temperature dependent morphology and resistivity of pulsed laser deposited iridium oxide thin films.* Thin Solid Films, 2006. **496**(2): p. 371-375.
158. Dupin, J.-C., et al., Physical Chemistry Chemical Physics, 2000. **2**: p. 1319-1324.
159. Wang, J., *Deposition and characterization of multiferroic bismuth ferrite thin films*. 2005, Univ. of Maryland: College Park,MD. p. 180 pp.
160. Eerenstein, W., et al., *Comment on "Epitaxial BiFeO3 Multiferroic Thin Film Heterostructures".* Science, 2005. **307**(5713): p. 1203a-.
161. Ueno, R., et al., *Crystal Structure and Electrical Properties of Epitaxial $BiFeO_3$ Thin Films Grown by Metal Organic Chemical Vapor Deposition.* Japanese Journal of Applied Physics. Part 2, Letters, 2005. **44**(37-41): p. L1231-L1233.
162. Jones, A.C., H.C. Aspinall, and P.R. Chalker, *Molecular design of improved precursors for the MOCVD of oxides used in microelectronics.* Surface and Coatings Technology, 2007. **201**(22-23): p. 9046-9054.
163. Singh, M.K., Y. Yang, and C. Takoudis, G., *Low-pressure metalorganic chemical vapor deposition of Fe_2O_3 thin films on Si(100) using n-butylferrocene and oxygen.* Journal of the Electrochemical Society, 2008. **155**(9): p. D618-D623.
164. Moulder, J.F., et al., *Handbook of X Ray Photoelectron Spectroscopy*. 1992, Eden Prairie, MN: Perkin-Elmer Corporation.

165. Lee, S.W. and C.S. Kim, *Growth of multiferroics $BiFeO_3$ thin films by sol-gel method.* Journal of Magnetism and Magnetic Materials, 2006. **304**(2): p. e772-e774.
166. Chen, L.F., et al., *Microwave Electronics: Measurement and Materials Characterization*. 2004: John Wiley & Sons, Hoboken, NJ.
167. Kimura, T., et al., Nature (London, United Kingdom), 2003. **426**(55).
168. Zavaliche, F., et al., *Multiferroic $BiFeO_3$ films: domain structure and polarization dynamics.* Phase Transitions, 2006. **79**(12): p. 991-1017.
169. Palkar, V.R., J. John, and R. Pinto, *Observation of saturated polarization and dielectric anomaly in magnetoelectric $BiFeO_3$ thin films.* Applied Physics Letters, 2002. **80**(9): p. 1628-1630.
170. Zurbuchen, M.A., et al., *Multiferroic composite ferroelectric-ferromagnetic films.* Applied Physics Letters, 2005. **87**(23): p. 232908-3.
171. Avellaneda, M. and G. Harshe, *Magnetoelectric effect in piezoelectric/magnetostrictive multilayer (2-2) composites.* Journal of Intelligent Material Systems and Structures 1994. **5**: p. 501-513.
172. Vaz, C.A.F., et al., *Magnetoelectric Coupling Effects in Multiferroic Complex Oxide Composite Structures.* Advanced Materials, 2010. **22**(26-27): p. 2900-2918.
173. Petrov, V.M., et al., Physical Review B 2007. **75**: p. 224407.
174. Zhang, Y., et al., Chinese Physics B, 2008. **17**(10): p. 3910.
175. Patil, D.R. and B.K. Chougule, J. Mater. Sci.: Mater Electron, 2009. **20**: p. 398-402.
176. S.P.Crane, et al., Journal of Magnetism and Magnetic Materials, 2009. **321**: p. L5-L9.
177. Fitzgerald, A.G. and R. Engin, Thin Solid Films, 1974. **20**: p. 317-327.
178. Ito, S., H. Miyashita, and N. Yoneda, Journal of Crystal Growth, 1985. **73**: p. 167-174.
179. Itoh, H., et al., JOURNAL OF MATERIALS SCIENCE, 1989. **24**: p. 3549-3552.
180. Lane, P.A., et al., Journal of Crystal Growth, 1998. **192**: p. 423-429.
181. Datta, R., et al., *Structural features of epitaxial NiFe2O4thin films grown on different substrates by direct liquid injection chemical vapor deposition.* Journal of Crystal Growth, 2012. **345**(1): p. 44-50.
182. Li, N., et al., *Growth of Atomically Smooth Epitaxial Nickel Ferrite Films by Direct Liquid Injection CVD.* Chemical Vapor Deposition, 2011. **17**: p. 261-269.
183. Singh, M., et al., Electrochemical and Solid-State Letters, 2009. **12**: p. H161-H164.
184. Franssila, S., *Introduction to Microfabrication*. Second Edition ed. 2010: John Wiley & Sons.
185. Crist, B.V., *Handbook of monochromatic XPS spectra*. Vol. The Elements and Native Oxides. 2000.
186. Oswald, S. and W. Bruckner, Surface and Interface Analysis, 2004. **36**: p.

17-22.
187. McIntyre, N.S. and M.G. Cook, Analytical Chemistry, 1975. **47**(13): p. 2208-2213.
188. Biesinger, M.C., et al., *Resolving surface chemical states in XPS analysis of first row transition metals, oxides and hydroxides: Cr, Mn, Fe, Co and Ni.* Applied Surface Science, 2011. **257**: p. 2717-2730.
189. Dixit, G., et al., *Annealing effect on the structural and magnetic properties of nickel ferrite thin films.* Surface and Interface Analysis, 2010. **42**(3): p. 151-156.
190. Singh, M., et al., *Metallorganic Chemical-Vapor-Deposited BiFeO3 Films for Tunable High-Frequency Devices.* Electrochemical and Solid-State Letters, 2009. **12**(5): p. H161-H164.
191. Dixit, G., et al., *Structural, magnetic and optical studies of nickel ferrite thin films.* Advanced Materials Letters, 2012. **3**(1): p. 21-28.
192. Tao, Q., et al., *Atomic Layer Deposition of HfO2, TiO2, and HfxTi1-xO2 Using Metal (Diethylamino) Precursors and H2O.* Journal of The Electrochemical Society, 2011. **158**(2): p. G27-G33.
193. Shafi, K.V.P., et al., Journal of Physics and Chemistry B, 1997. **101**: p. 6409.
194. Kinemuchi, Y., et al., Thin Solid Films, 2002. **407**: p. 109.
195. Mohallem, N.D.S. and L.M. Seara, *Magnetic nanocomposite thin films of NiFe2O4/SiO2 prepared by sol-gel process.* Applied Surface Science, 2003. **214**(1-4): p. 143-150.
196. Morrish, A.H. and K. Haneda, Journal of Applied Physics, 1981. **52**: p. 2496.
197. Prasad, S. and N.S. Gajbhiye, *Magnetic studies of nanosized nickel ferrite particles synthesized by the citrate precursor technique.* Journal of Alloys and Compounds, 1998. **265**: p. 87-92.
198. Batlle, X. and A. Labarta, *Finite-size effects in fine particles: magnetic and transport properties.* Journal of Physics D: Applied Physics, 2002. **35**: p. R15-R42.

APPENDICES

In this appendix, the permissions to reproduce or re-publish my earlier papers from The Electrochemical Society and ELSEVIER are included.

Request for Permission to Reproduce or Re-Publish ECS Material

Please fax this form to: The Electrochemical Society (ECS), Attn: Permissions Requests, 1.609.730.0629. You may also e-mail your request to: copyright@electrochem.org. Include all the information as required on this form. Please allow 3-7 days for your request to be processed.

I am preparing a (choose one): ☐ paper ☐ chapter ☐ book ☒ thesis

entitled: Fabrication of Ferrite Thin Film using Low Pressure Metalorganic Chemical Vapor Deposition

to be published by: May 30, 2014

in an upcoming publication entitled: _____

I request permission to use the following material in the publication noted above, and request nonexclusive rights for all subsequent editions and in all foreign language translations for distribution throughout the world.

Description of material to be used—Indicate what material you wish to use (figures, tables, text, etc.) and give the full bibliographic reference for the source publication. You may attach a separate list, organized by ECS title.

I'd like to use Figure 4, 6, 7 in a paper published in 2008.
Journal of The Electrochemical Society, 155 (9) D618-D623 (2008).
Title: Low-Pressure Metallorganic Chemical Vapor Deposition of Fe_2O_3 Thin Films on Si(100) Using n-Butylferrocene and Oxygen.
Authors: M. K. Singh, Y. Yang, and C. G. Takoudis

Signature: Y. Yang Date: 4/10/2014

Name: Yi Yang

Address: 1621 Westminster Drive, Apt 206
Naperville, IL 60563

Telephone: (312)823-0436 Fax: _____

E-mail: pagyy26@gmail.com

Permission is granted to reproduce the above-referenced material. Please acknowledge the author(s) and publication data of the original material, and include the words: "Reproduced by permission of The Electrochemical Society."

4/18/14
Date

John Lewis, Associate Director of Publications

Request for Permission to Reproduce or Re-Publish ECS Material

Please fax this form to: The Electrochemical Society (ECS), Attn: Permissions Requests, 1.609.730.0629. You may also e-mail your request to: copyright@electrochem.org. Include all the information as required on this form. Please allow 3-7 days for your request to be processed.

I am preparing a (choose one): ☐ paper ☐ chapter ☐ book ☒ thesis

entitled: Fabrication of Ferrite Thin Film using Low Pressure Metalorganic Chemical Vapor Deposition

to be published by: May 30, 2014

in an upcoming publication entitled: _____

I request permission to use the following material in the publication noted above, and request nonexclusive rights for all subsequent editions and in all foreign language translations for distribution throughout the world.

Description of material to be used—Indicate what material you wish to use (figures, tables, text, etc.) and give the full bibliographic reference for the source publication. You may attach a separate list, organized by ECS title.

I'd like to use Figure 1, 2, 4, 5, 6 in paper which published in 2009. Electrochemical and Solid-State Letters, 12(5), H161-H164 (2009).

Title: Metallorganic Chemical-Vapor-Deposited $BiFeO_3$ Films for Tunable High-Frequency Devices.

Authors: M. Singh, Y. Yang, C. G. Takoudis, A. Tatarenko, G. Srinivasan, P. Khare, and G. Lawes

Signature: Yi Yang Date: 4/10/2014

Name: Yi Yang

Address: 1621 Westminster Drive, Apt 206

Naperville, IL 60563

Telephone: (312) 823-0436 Fax: _____

E-mail: pagyy26@gmail.com

Permission is granted to reproduce the above-referenced material. Please acknowledge the author(s) and publication data of the original material, and include the words: "Reproduced by permission of The Electrochemical Society."

4/18/14
Date

John Lewis, Associate Director of Publications

ELSEVIER LICENSE
TERMS AND CONDITIONS

Apr 10, 2014

This is a License Agreement between Yi Yang ("You") and Elsevier ("Elsevier") provided by Copyright Clearance Center ("CCC"). The license consists of your order details, the terms and conditions provided by Elsevier, and the payment terms and conditions.

All payments must be made in full to CCC. For payment instructions, please see information listed at the bottom of this form.

Supplier	Elsevier Limited The Boulevard,Langford Lane Kidlington,Oxford,OX5 1GB,UK
Registered Company Number	1982084
Customer name	Yi Yang
Customer address	1621 Westminster Dr Naperville, IL 60563
License number	3365570133755
License date	Apr 10, 2014
Licensed content publisher	Elsevier
Licensed content publication	Coordination Chemistry Reviews
Licensed content title	Synthesis of multifunctional multiferroic materials from metalorganics
Licensed content author	Manish K. Singh,Yi Yang,Christos G. Takoudis
Licensed content date	December 2009
Licensed content volume number	253
Licensed content issue number	23–24
Number of pages	15
Start Page	2920
End Page	2934
Type of Use	reuse in a thesis/dissertation
Portion	full article
Format	both print and electronic
Are you the author of this Elsevier article?	Yes
Will you be translating?	No
Title of your	Fabrication of Ferrite Thin Film using Low Pressure Metalorganic

thesis/dissertation	Chemical Vapor Deposition
Expected completion date	May 2014
Estimated size (number of pages)	115
Elsevier VAT number	GB 494 6272 12
Permissions price	0.00 USD
VAT/Local Sales Tax	0.00 USD / 0.00 GBP
Total	0.00 USD
Terms and Conditions	

INTRODUCTION

1. The publisher for this copyrighted material is Elsevier. Byclicking "accept" in connection with completing this licensingtransaction, you agree that the following terms and conditions apply to thistransaction (along with the Billing and Payment terms and conditionsestablished by Copyright Clearance Center, Inc. ("CCC"), at the timethat you opened your Rightslink account and that are available at any time at http://myaccount.copyright.com).

GENERAL TERMS

2. Elsevier hereby grants you permission to reproduce the aforementionedmaterial subject to the terms and conditions indicated.

3. Acknowledgement: If any part of the material to be used (for example,figures) has appeared in our publication with credit or acknowledgement toanother source, permission must also be sought from that source. If suchpermission is not obtained then that material may not be included in yourpublication/copies. Suitable acknowledgement to the source must be made, eitheras a footnote or in a reference list at the end of your publication, asfollows:

"Reprinted from Publication title, Vol /edition number, Author(s), Title ofarticle / title of chapter, Pages No., Copyright (Year), with permission fromElsevier [OR APPLICABLE SOCIETY COPYRIGHT OWNER]." Also Lancet special credit -"Reprinted from The Lancet, Vol. number, Author(s), Title of article, PagesNo., Copyright (Year), with permission from Elsevier."

4. Reproduction of this material is confined to the purpose and/or media forwhich permission is hereby given.

5. Altering/Modifying Material: Not Permitted. However figures andillustrations may be altered/adapted minimally to serve your work. Any otherabbreviations, additions, deletions and/or any other alterations shall be madeonly with prior written authorization of Elsevier Ltd. (Please contact Elsevierat permissions@elsevier.com)

6. If the permission fee for the requested use of our material is waived inthis instance, please be advised that your future requests for Elseviermaterials may attract a fee.

7. Reservation of Rights: Publisher reserves all rights not specificallygranted in the combination of (i) the license details provided by you andaccepted in the course of this licensing transaction, (ii) these

terms andconditions and (iii) CCC's Billing and Payment terms and conditions.

8. License Contingent Upon Payment: While you may exercise the rightslicensed immediately upon issuance of the license at the end of the licensingprocess for the transaction, provided that you have disclosed complete andaccurate details of your proposed use, no license is finally effective unlessand until full payment is received from you (either by publisher or by CCC) asprovided in CCC's Billing and Payment terms and conditions. If fullpayment is not received on a timely basis, then any license preliminarilygranted shall be deemed automatically revoked and shall be void as if nevergranted. Further, in the event that you breach any of these terms andconditions or any of CCC's Billing and Payment terms and conditions, thelicense is automatically revoked and shall be void as if never granted. Use of materials as described in a revoked license, as well as any use of thematerials beyond the scope of an unrevoked license, may constitute copyrightinfringement and publisher reserves the right to take any and all action toprotect its copyright in the materials.

9. Warranties: Publisher makes no representations or warranties with respectto the licensed material.

10. Indemnity: You hereby indemnify and agree to hold harmless publisher andCCC, and their respective officers, directors, employees and agents, from andagainst any and all claims arising out of your use of the licensed materialother than as specifically authorized pursuant to this license.

11. No Transfer of License: This license is personal to you and may not besublicensed, assigned, or transferred by you to any other person withoutpublisher's written permission.

12. No Amendment Except in Writing: This license may not be amended exceptin a writing signed by both parties (or, in the case of publisher, by CCC onpublisher's behalf).

13. Objection to Contrary Terms: Publisher hereby objects to any termscontained in any purchase order, acknowledgment, check endorsement or otherwriting prepared by you, which terms are inconsistent with these terms andconditions or CCC's Billing and Payment terms and conditions. These termsand conditions, together with CCC's Billing and Payment terms and conditions(which are incorporated herein), comprise the entire agreement between you andpublisher (and CCC) concerning this licensing transaction. In the eventof any conflict between your obligations established by these terms andconditions and those established by CCC's Billing and Payment terms andconditions, these terms and conditions shall control.

14. Revocation: Elsevier or Copyright Clearance Center may deny thepermissions described in this License at their sole discretion, for any reasonor no reason, with a full refund payable to you. Notice of such denialwill be made using the contact information provided by you. Failure toreceive such notice will not alter or invalidate the denial. In no eventwill Elsevier or Copyright Clearance Center be responsible or liable for anycosts, expenses or damage incurred by you as a result of a denial of yourpermission request, other than a refund of the amount(s) paid by you toElsevier and/or Copyright Clearance Center for denied permissions.

LIMITED LICENSE

The following terms and conditions apply only to specific license types:

15. **Translation**: This permission is granted fornon-exclusive world **English** rights only unless yourlicense was granted for translation rights. If you licensed translation rightsyou may only translate this content into the languages you requested. Aprofessional translator must perform all translations and reproduce the contentword for word preserving the integrity of the article. If this license is tore-use 1 or 2 figures then permission is granted for non-exclusive world rightsin all languages.

16. **Posting licensed content on any Website**: The followingterms and conditions apply as follows: Licensing material from an Elsevierjournal: All content posted to the web site must maintain the copyright informationline on the bottom of each image; A hyper-text must be included to the Homepageof the journal from which you are licensing at http://www.sciencedirect.com/science/journal/xxxxx orthe Elsevier homepage for books at http://www.elsevier.com; CentralStorage: This license does not include permission for a scanned version of thematerial to be stored in a central repository such as that provided byHeron/XanEdu.

Licensing material from an Elsevier book: A hyper-text link must be includedto the Elsevier homepage at http://www.elsevier.com . Allcontent posted to the web site must maintain the copyright information line onthe bottom of each image.

Posting licensed content on Electronic reserve: In addition to the above the following clausesare applicable: The web site must be password-protected and made available onlyto bona fide students registered on a relevant course. This permission isgranted for 1 year only. You may obtain a new license for future websiteposting.

For journal authors: the following clauses are applicable inaddition to the above: Permission granted is limited to the author acceptedmanuscript version* of your paper.

***Accepted Author Manuscript (AAM) Definition:** An accepted authormanuscript (AAM) is the author's version of the manuscript of an article thathas been accepted for publication and which may include any author-incorporatedchanges suggested through the processes of submission processing, peer review,and editor-author communications. AAMs do not include other publishervalue-added contributions such as copy-editing, formatting, technicalenhancements and (if relevant) pagination.

You are not allowed to download and post the published journal article (whetherPDF or HTML, proof or final version), nor may you scan the printed edition tocreate an electronic version. A hyper-text must be included to the Homepage ofthe journal from which you are licensing at http://www.sciencedirect.com/science/journal/xxxxx. As part of our normal production process, you will receive an e-mail noticewhen your article appears on Elsevier's online service ScienceDirect(www.sciencedirect.com). That e-mail will include the article's Digital ObjectIdentifier (DOI). This number provides the electronic link to the publishedarticle and should be included in the posting of your personal version. We askthat you wait until you receive this e-mail and have the DOI to do any posting.

Posting to a repository: Authorsmay post their AAM immediately to their employer's institutional repository forinternal use only and may make their manuscript publically available after thejournal-specific embargo period has ended.

Please also refer to Elsevier'sArticle Posting Policy for further information.

18. **For book authors** the following clauses are applicable in addition tothe above: Authors are permitted to place a briefsummary of their work online only.. You are notallowed to download and post the published electronic version of your chapter,nor may you scan the printed edition to create an electronic version. Posting to a repository: Authors arepermitted to post a summary of their chapter only in their institution'srepository.

20. **Thesis/Dissertation**: If your license is for use in athesis/dissertation your thesis may be submitted to your institution in eitherprint or electronic form. Should your thesis be published commercially, pleasereapply for permission. These requirements include permission for the Libraryand Archives of Canada to supply single copies, on demand, of the completethesis and include permission for UMI to supply single copies, on demand, ofthe complete thesis. Should your thesis be published commercially, pleasereapply for permission.

Elsevier Open Access Terms andConditions

Elsevier publishes Open Access articles in both its Open Access journals andvia its Open Access articles option in subscription journals.

Authors publishing in an Open Access journal or who choose to make theirarticle Open Access in an Elsevier subscription journal select one of thefollowing Creative Commons user licenses, which define how a reader may reusetheir work: Creative Commons Attribution License (CC BY), Creative CommonsAttribution – Non Commercial - ShareAlike (CC BY NCSA) and Creative Commons Attribution – Non Commercial – No Derivatives (CC BYNC ND)

Terms & Conditions applicable toall Elsevier Open Access articles:

Any reuse of the article must not represent the author as endorsing theadaptation of the article nor should the article be modified in such a way asto damage the author's honour or reputation.

The author(s) must be appropriately credited.

If any part of the material to be used (for example, figures) has appearedin our publication with credit or acknowledgement to another source it is theresponsibility of the user to ensure their reuse complies with the terms andconditions determined by the rights holder.

Additional Terms & Conditionsapplicable to each Creative Commons user license:

CC BY: You may distribute andcopy the article, create extracts, abstracts, and other revised versions,adaptations or derivative works of or from an article (such as a translation),to include in a collective work (such as an anthology), to text or data minethe article, including for commercial purposes without permission from Elsevier

CC BY NC SA: For non-commercialpurposes you may distribute and copy the article, create extracts, abstractsand other revised versions, adaptations or derivative works of or from anarticle

(such as a translation), to include in a collective work (such as ananthology), to text and data mine the article and license new adaptations or creationsunder identical terms without permission from Elsevier

CC BY NC ND: For non-commercialpurposes you may distribute and copy the article and include it in a collectivework (such as an anthology), provided you do not alter or modify the article,without permission from Elsevier

Any commercial reuse of Open Access articles published with a CC BY NC SA or CC BY NC NDlicense requires permission from Elsevier and will be subject to a fee.

Commercial reuse includes:

- Promotional purposes (advertising or marketing)
- Commercial exploitation (e.g. a product forsale or loan)
- Systematic distribution (for a fee or free ofcharge)

Please refer to Elsevier'sOpen Access Policy for further information.

21. **Other Conditions**:

v1.7

If you would like to pay for this license now, please remit this license along with your payment made payable to "COPYRIGHT CLEARANCE CENTER" otherwise you will be invoiced within 48 hours of the license date. Payment should be in the form of a check or money order referencing your account number and this invoice number RLNK501275450. Once you receive your invoice for this order, you may pay your invoice by credit card. Please follow instructions provided at that time.

Make Payment To:
Copyright Clearance Center
Dept 001
P.O. Box 843006
Boston, MA 02284-3006

For suggestions or comments regarding this order, contact RightsLink Customer Support: customercare@copyright.com or +1-877-622-5543 (toll free in the US) or +1-978-646-2777.

Gratis licenses (referencing $0 in the Total field) are free. Please retain this printable license for your reference. No payment is required.

VITA

YI YANG

EDUCATION

Ph. D., Chemical Engineering, University of Illinois, Chicago, Illinois, USA, 2014

B. S., Chemical Engineering, Nanjing University, Nanjing, China, 2005

PUBLICATIONS

1. Y. Yang, Q. Tao and C. G. Takoudis, "Cyclic Chemical Vapor Deposition of nickel ferrite thin films using novel metalorganic precursor combination", manuscript in preparation.
2. Runshen Xu, Qian Tao, Yi Yang, Christos G. Takoudis, "Atomic Layer Deposition and Characterization of Stoichiometric Erbium Oxide Thin Dielectrics on Si (100) Using $(CpMe)_3Er$ Precursor and Ozone", *Applied Surface Science*, **258**, 8514-8520 (2012).
3. M. Singh, Y. Yang, C. G. Takoudis, A. Tatarenko, G. Srinivasan, P. Kharel and G. Lawes, "Multiferroic BiFeO3 Thin Films for Multifunctional Devices", *Journal of Nanoscience and Nanotechnology*, **10**, 6195-6199 (2010).
4. M. Singh, Y. Yang, and C. G. Takoudis, "Synthesis of Multifunctional Multiferroic Materials from Metalorganics", *Coordination Chemistry Reviews*, **253**, 2920-2934 (2009).
5. M. Singh, Y. Yang, C. G. Takoudis, A. Tatarenko, G. Srinivasan, P. Kharel, and G. Lawes, "Metalorganic Chemical-Vapor-Deposited BiFeO3 Films for Tunable High-Frequency Devices", *Electrochemical and Solid-State Letters*, **12**, H161-H164

(2009).

6. M. Singh., Y. Yang, and C. G. Takoudis, "Low-Pressure Metalorganic Chemical Vapor Deposition of Fe2O3 Thin Films on Si(100) Using n-Butylferrocene and Oxygen", *Journal of the Electrochemical Society*, **155**, D618-D623 (2008).

PRESENTATIONS

1. Y. Yang, M. Singh, and C. G. Takoudis, "Low-Pressure Metalorganic Chemical Vapor Deposition of Nickel Ferrite Thin Films on Ferroelectric Substrates", Nov. 12th, 2009 *AIChE*, Nashville, TN.
2. M. Singh, Y. Yang, and C. G. Takoudis, "Deposition and Characterization of Low-pressure Metalorganic Chemical Vapor Deposited Epitaxial BiFeO3 Thin Films", Dec. 1st, 2008 *MRS Fall Meeting*, Boston, MA.
3. M. Singh, Y. Yang, and C. G. Takoudis, "Multiferroic BiFeO3 Thin Films Deposited by MOCVD Method", Nov. 1st, 2008 *AIChE*, Philadelphia, PA.
4. M. Singh, Y. Yang, and C. G. Takoudis, "Multiferroic BiFeO3 Thin Films for Multifunctional Devices", June, 2008 *International Conference from Nanoparticles and Nanomaterials to Nanodevices and Nanosystems (IC4N)*, Halkidiki, Greece.
5. Y. Yang, M. Singh, and C. G. Takoudis, "Iron Oxide Thin Film Deposited by MOCVD method", Jan. 7th, 2008 *NSF CMMI Engineering Research and Innovation Conference*, Knoxville, TN.

PROFESSIONAL AFFLIATIONS

- Member, Materials Research Society
- Member, American Institute of Chemical Engineers

HONORS

- Honored by Illinois Math and Science Academy for mentoring high-school students.
- Awarded National Science Foundation (NSF) Student Travel Grant at Knoxville, Tennessee
- Awarded Women in Science and Engineering (WISE) Travel Grant at University of Illinois, Chicago
- Awarded Graduate Student Presenter Award at University of Illinois, Chicago
- Awarded Graduate Student Council Travel Award at University of Illinois, Chicago
- People's Scholarship, Nanjing University